

A Summary of Radiation-Induced Transient Absorption and Recovery in Fiber Optic Waveguides

C. D. Skoog

Prepared by Sandia Laboratories, Albuquerque New Mexico 87115
and Livermore, California 94550 for the United States Energy Research
and Development Administration under Contract AT (29-1)-789

Printed November 1976

***When printing a copy of any digitized SAND
Report, you are required to update the
markings to current standards.***



Sandia Laboratories

Issued by Sandia Laboratories, operated for the United States Energy Research and Development Administration by Sandia Corporation.

NOTICE

This report was prepared as an account of work sponsored by the United States Government. Neither the United States nor the United States Energy Research and Development Administration, nor any of their employees, nor any of their contractors, subcontractors, or their employees, makes any warranty, express or implied, or assumes any legal liability or responsibility for the accuracy, completeness or usefulness of any information, apparatus, product or process disclosed, or represents that its use would not infringe privately owned rights.

Printed in the United States of America
Available from
National Technical Information Service
U. S. Department of Commerce
5285 Port Royal Road
Springfield, VA 22151
Price: Printed Copy \$7.00; Microfiche \$3.00

SAND76-8056
Unlimited Release
Printed November 1976

A SUMMARY OF RADIATION-INDUCED TRANSIENT
ABSORPTION AND RECOVERY IN FIBER OPTIC WAVEGUIDES*

Clifford D. Skoog
Device Studies Division 8342
Sandia Laboratories, Livermore

ABSTRACT

The absorption induced in fiber optic waveguides by pulsed electron and X-ray radiation has been measured as a function of optical wavelength from 450 to 950 nm, irradiation temperature from -54 to 71°C, and dose from 1 to 500 krads. The fibers studied are Ge-doped silica core fibers (Corning Low Loss), "pure" vitreous silica core fibers (Schott, Bell Laboratories, Fiberoptic Cable Corp., and Valtec Fiberoptics), polymethylmethacrylate core fibers (DuPont CROFON and PFX), and polystyrene core fibers (International Fiber Optics and Polyoptics). Models that have been developed to account for the observed absorption recovery are also summarized.

* This work was supported by the United States Energy Research and Development Administration, Contract Number AT-(29-1)-789, and the U. S. Air Force Weapons Laboratory.

ACKNOWLEDGMENTS

The author is indebted to S. J. Vasey for assistance with the measurements and data reduction, and to E. H. Barsis for direction and many useful discussions. The author is also indebted to P. L. Mattern, L. M. Watkins, J. R. Brandon, Lt. K. Soda, Capt. J. Tucker, Jake Tausch, and Carl F. Porter, who participated in the overall fiber program.

A SUMMARY OF RADIATION-INDUCED TRANSIENT ABSORPTION AND RECOVERY IN FIBER OPTIC WAVEGUIDES

Introduction

Recent studies¹⁻⁵ have shown that the operation of optical waveguides can be impaired in radiation environments. In particular, false signals can be generated by luminescence, and signal strengths can be lowered by radiation-induced absorption (Figure 1). These effects occur with both continuous and pulsed radiation sources; however, the loss of signal strength following pulsed irradiation is particularly serious when the duration of the pulse is shorter than the lifetime of the induced absorption centers. This situation occurs in many applications and produces large values of absorption, even in systems employing short fiber lengths. Thus adequate system design requires knowledge of the time-dependence of absorption values as a function of optical wavelength, irradiation dose, irradiation temperature, and the environment surrounding the fiber.

In the last few years, extensive investigations have been performed at Sandia Laboratories on the transient absorption that results from pulsed radiation. These investigations have produced many new results which supplement the extensive permanent absorption data collected in Reference 1. The results of these new transient investigations are presented here for several fibers which have been identified as the most radiation-resistant, that is, the most promising for use in pulsed radiation environments. For the sake of completeness, the previously unpublished data presented here are supplemented by data already reported elsewhere.

In general, this document contains the absorption and the absorption recovery data necessary for designing fiber optic data links that will be exposed to pulsed electrons, X rays, and gamma rays. Data are given for radiation doses up to 500 krads, for irradiation temperatures from -54 to 71°C, and for operating wavelengths from 450 to 950 nm. Although neutron-induced absorption data are not included here, the effect is determined by the neutron ionizing dose⁴ and is generally small compared with the absorption induced by ionizing radiation in many practical environments. Data are also included on the significant effects of atmospheric oxygen on the recovery of plastic fiber waveguides. Fiber recovery models which are useful for extrapolating the measured values are also summarized here.

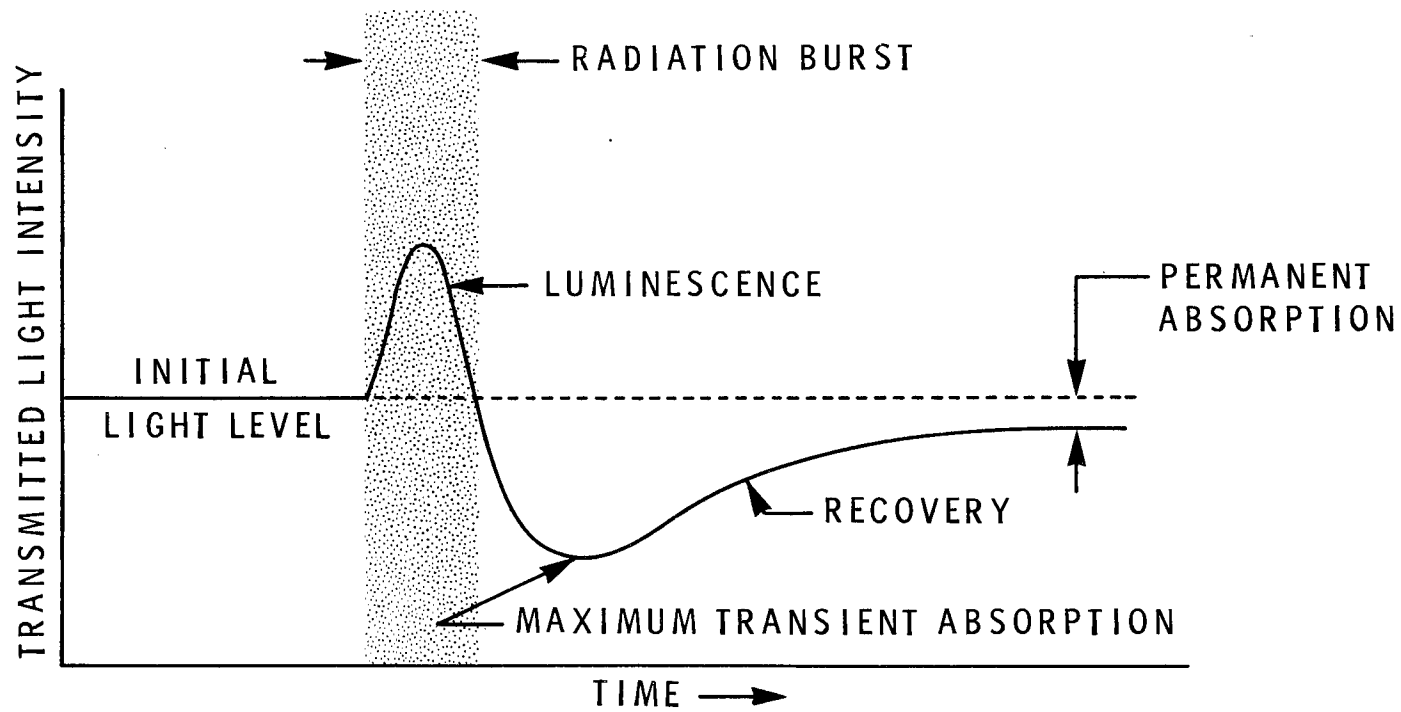


Figure 1. Schematic Representation of the Response of Glass and Plastic Fiberoptic Waveguides to Pulsed Irradiation. The signal level increases as a result of luminescence during the radiation pulse and reaches a minimum at the end of the pulse because of the induced absorption.

Experimental Technique

Previous studies¹⁻⁴ have shown the transient absorption to be independent of the type of ionizing irradiation, a result to be expected from considerations of energy loss mechanisms in solids (ionization versus displacement). Thus for most of the experiments, an electron beam machine was used since it offered the advantages of high dose capability and simple shielding to define exposure length accurately, and since machines were readily available. Unless the data reported here are specifically labeled "X ray," the fibers were exposed to electrons from a 600 keV Febetron 750 in conjunction with a Model 5237 electron beam tube. With this machine-tube combination, there is very little self-pinching of the beam and the exposure dose is controlled by varying the anode-to-fiber spacing. Doses of from 10 to 500 krads per shot were obtained with spacing variations of 25 cm.

Because the range of the electrons was short, the fiber bundles were stripped of their protective sheaths and the individual fibers fanned out across the exposure aperture. The fiber length from light source to detector was typically three metres. The routing of the fiber bundle into and out of the exposure chamber contained several bends to ensure that the waveguide properties were measured. The length and routing of the bundles also minimized signal transmission through the cladding, and photo-optical measurements confirmed that such transmissions were negligible.

Dose measurements for the electron beam irradiations were made with 0.05 mm thick, nylon-base radiochromic film supplied by Far West Technology. Pretest and posttest film densities were measured with a Far West Technology Model FWT-90 film reader. The film reader system calibration was verified by making known irradiations in the Sandia gamma irradiation facility.

Data which are labeled "X ray" were collected from specimens irradiated by a 2 MeV Febetron 705 operated in the bremsstrahlung mode. The beam was directed into a tungsten bremsstrahlung converter backed with an aluminum plate to stop all electrons passing through the converter. Dose measurements for the X-ray irradiations were made with TLD-400 dosimeters.

In all experiments, the light source, fiber, and detector were arranged as shown in Figure 2. A flash lamp was used for making peak transient absorption measurements and for recovery measurements over times up to five microseconds after the radiation pulse. For longer-time recovery (up to ten seconds), a continuous-source quartz lamp powered from a well-regulated dc power supply was used. The value of absorption obtained using the quartz lamp was normalized to the data obtained with the pulse source.

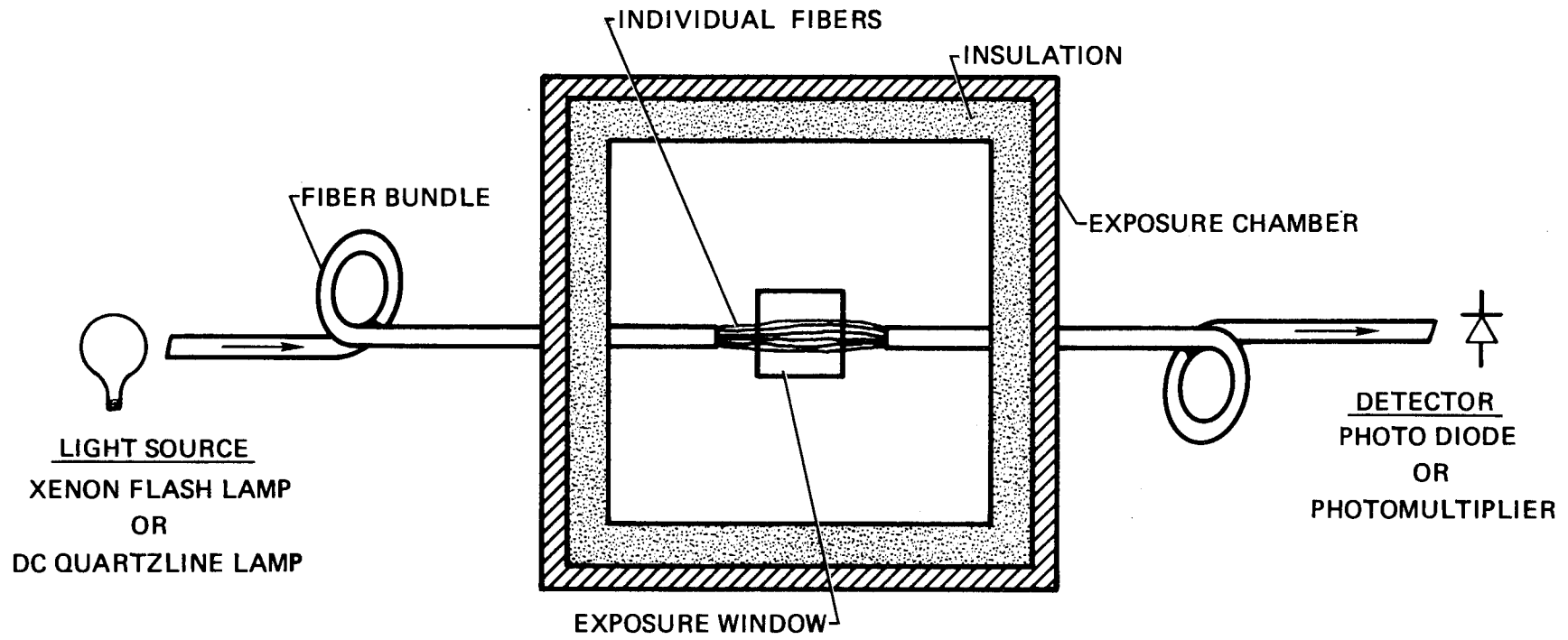


Figure 2. The Lamp, Fiber, and Detector Configuration Used in the Transient Absorption Measurements. The fiber length from source to detector was typically three metres, and the exposure length ranged from 1 to 10 cm.

Two different photodetectors were used. A C70042K photomultiplier* tube (RCA) was used to detect very low signal levels (involving a few fibers) and to ensure that the larger signal levels were not masking other phenomena. For most measurements, however, an SGD-100A photodiode (EG&G) with a traceable calibration was employed. The photodiode has good long-term stability and is linear over a much wider range of signal levels than is the PM tube. Both qualities simplify data reduction.

Luminescence measurements were made on experimental configurations identical with those used for the absorption measurements, except that the light source was not energized.

Wavelength discrimination was accomplished with nine individual notch filters ranging from 450 to 950 nm. Each filter has a band pass of approximately 100 nm. The precise bandwidth of each filter was determined using a Cary 14 spectrometer and is reported in the appendix. Some transient absorption measurements were also made with a spectrometer to ensure that significant fine structure was not masked by the wider bandwidth of the notch filters.

Transient Absorption Defined

The peak transient absorption $\alpha(0)$ has been defined as follows:

$$\alpha(0) = 10 \log_{10} \frac{I_0}{I_{\min}} Lx \text{ dB/m} \quad (1)$$

where Lx is the exposure length in meters, I_0 is the pre-irradiation signal level, and I_{\min} is the minimum signal level that occurs following the radiation pulse (see Figure 3).

The fractional recovery is defined as the absorption remaining at time t divided by the peak absorption $\alpha(t)/\alpha(0)$. Values of $\alpha(0)$ and $\alpha(t)/\alpha(0)$ are presented as a function of wavelength, dose, and temperature in following sections. The absorption at any time after irradiation can be determined by multiplying the fractional recovery by the peak absorption: $\alpha(t) = \alpha(t)/\alpha(0) \times \alpha(0)$.

* Extended-red multialkali photocathodes.

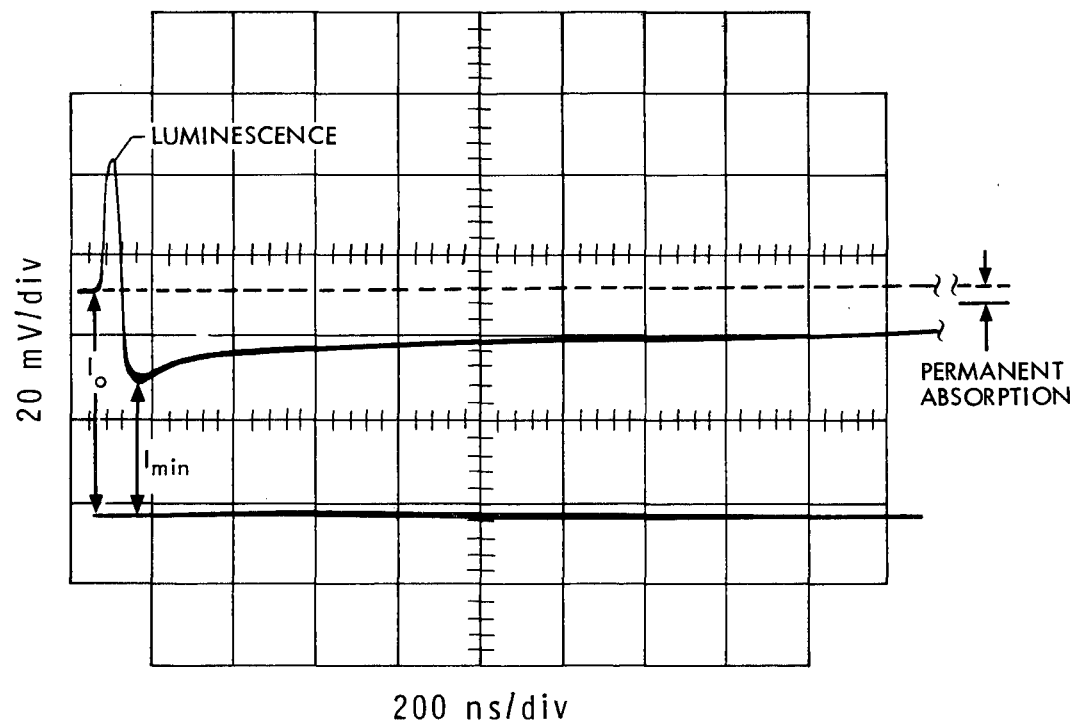


Figure 3. An Oscilloscope Record Indicating Radiation-Induced Absorption and Luminescence in a Polystyrene Fiber Bundle. The lower trace shows the zero-voltage (no-detected-signal) level. With the light source energized, the unirradiated transmission is given by the amplitude of the upper trace for the first 75 ns. The sharp increase in detected intensity, which peaks at 100 ns, is caused by luminescence in the fiber during a 1 krad, 50 ns X-ray pulse. A minimum in detected intensity occurs near 170 ns shortly after the termination of the irradiation and indicates the maximum transient absorption. For the remainder of the trace, the recorded intensity gradually increases toward the value shown prior to irradiation. The amount of absorption remaining after approximately 24 hours is considered permanent.

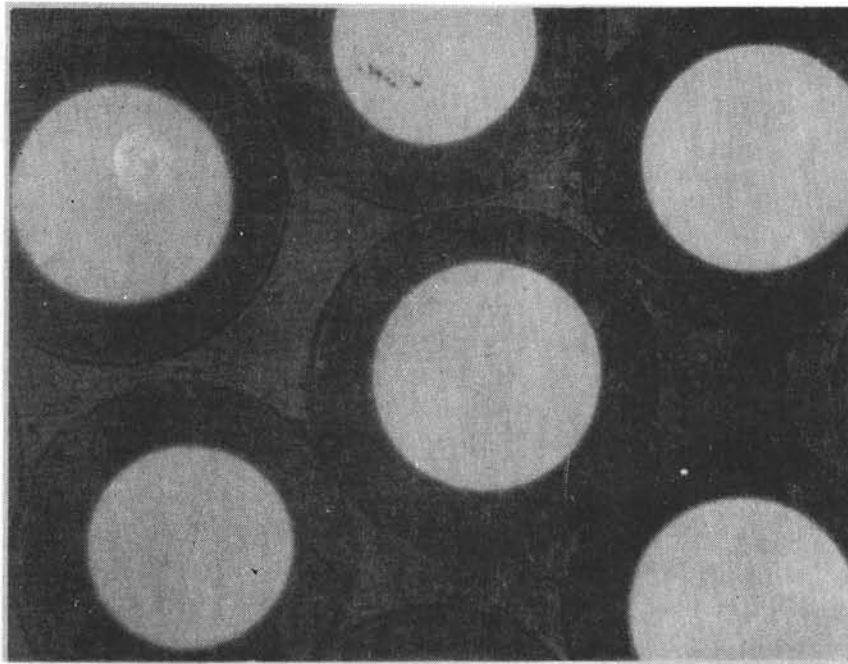
I. CORNING LOW LOSS FIBERS

Manufacturer: Corning Glass Works
Telecommunications Products Department
Corning, NY 14830

Core: Ge-Doped Silica

Cladding: Silica

Fiber Diameter: 0.09 mm



→ 0.05 mm ←

The Ge-doped silica fibers from the Corning Glass Works show peak transient absorptions which are approximately two orders of magnitude larger than those of "pure" vitreous silica fibers.

The spectral dependence of the peak transient absorptions for 70 and 9 krad electron doses are shown in Figures 4 and 5, while similar data for X-ray doses of 900 and 240 rads are presented in Figures 6 and 7. Maximum absorption occurs at wavelengths from 500 to 550 nm, a result common to all the silica core fibers studied. The spectral dependence of absorption in the Corning fibers, however, is more pronounced than in other silica core fibers.

Peak transient absorption as a function of dose is shown in Figure 8 for wavelengths of 500 and 800 nm; the insert shows similar data for low X-ray doses. The data in Figure 8 were recorded on fibers purchased in 1973, while the data in Figures 9 and 10 were recorded on fibers procured more recently (1975-76). The effect of temperature on the peak transient absorption is also shown in Figures 9 and 10. The absorptions measured at room temperature for the newer material are slightly larger than those for the "old" material (Figure 8). Microprobe analysis suggests that this difference in induced absorption is probably related to variations in dopant concentration; however, no effort has been made to establish the dependence quantitatively.

The recovery of the transient absorption for Ge-doped Corning fibers is shown in Figure 11. The most striking feature of these data is the large temperature dependence of the recovery, a trait not generally observed in "pure" vitreous silica fibers. For example, the data in Figure 11 show that a system which is "off-the-air" until the absorption diminishes to 0.1 of the peak value will recover in 0.1 ms at 71°C, but will require 0.15 second to recover at -54°C, a difference of three orders of magnitude in time. Two other features of the data in Figure 11 are also noteworthy: first, the recovery is independent of dose and wavelength within the accuracy limits of the measurements; and second, the 21 and 71°C recovery curves show a $t^{-1/2}$ dependence, while the lower-temperature curves approach a $t^{-1/2}$ dependence at longer times. The data suggest a geminate recombination process wherein defects created by irradiation recombine by diffusion under the influence of a mutual electrostatic field.

A model for geminate recombination taken from the literature on pulsed radiolysis of liquids^{6,7} and glasses^{8,9} explains the observed data. In this model,

$$\frac{n(t)}{n(0)} = \exp(\lambda t) \operatorname{erfc}(\lambda t)^{1/2} \quad (2)$$

where $\frac{n(t)}{n(0)}$ is the fraction of electron-ion pairs remaining at time t , λ is the recombination rate, and $\operatorname{erfc}(x)$ is the complement of the error function. Equation (2) reduces to

$$\frac{n(t)}{n(0)} \approx (1/\pi \lambda t)^{1/2} \quad (3)$$

for $\lambda t \gg 1$, yielding the $t^{-1/2}$ dependence observed in the data at long times and for large values of λ .

The data of Figure 11 are shown again in Figure 12 normalized to the peak transient absorption at -54°C . The average values of the data collected at each temperature are given by the symbols, while the solid lines were calculated from expression (2), varying only the parameter λ to achieve the best fit. The curves calculated in this fashion are in excellent agreement with the data. The values of λ used to produce the fit shown in Figure 12 are plotted semilogarithmically against T^{-1} in Figure 13. The near linear curve over five orders of magnitude in λ is further evidence for a thermally activated diffusion process for recombination which is characterized by

$$\lambda = \lambda_0 \exp(-E/KT) \quad (4)$$

where E is approximately 0.45 eV. A similar range of recovery rates has been observed as a function of temperature in other inorganic glasses. ⁸

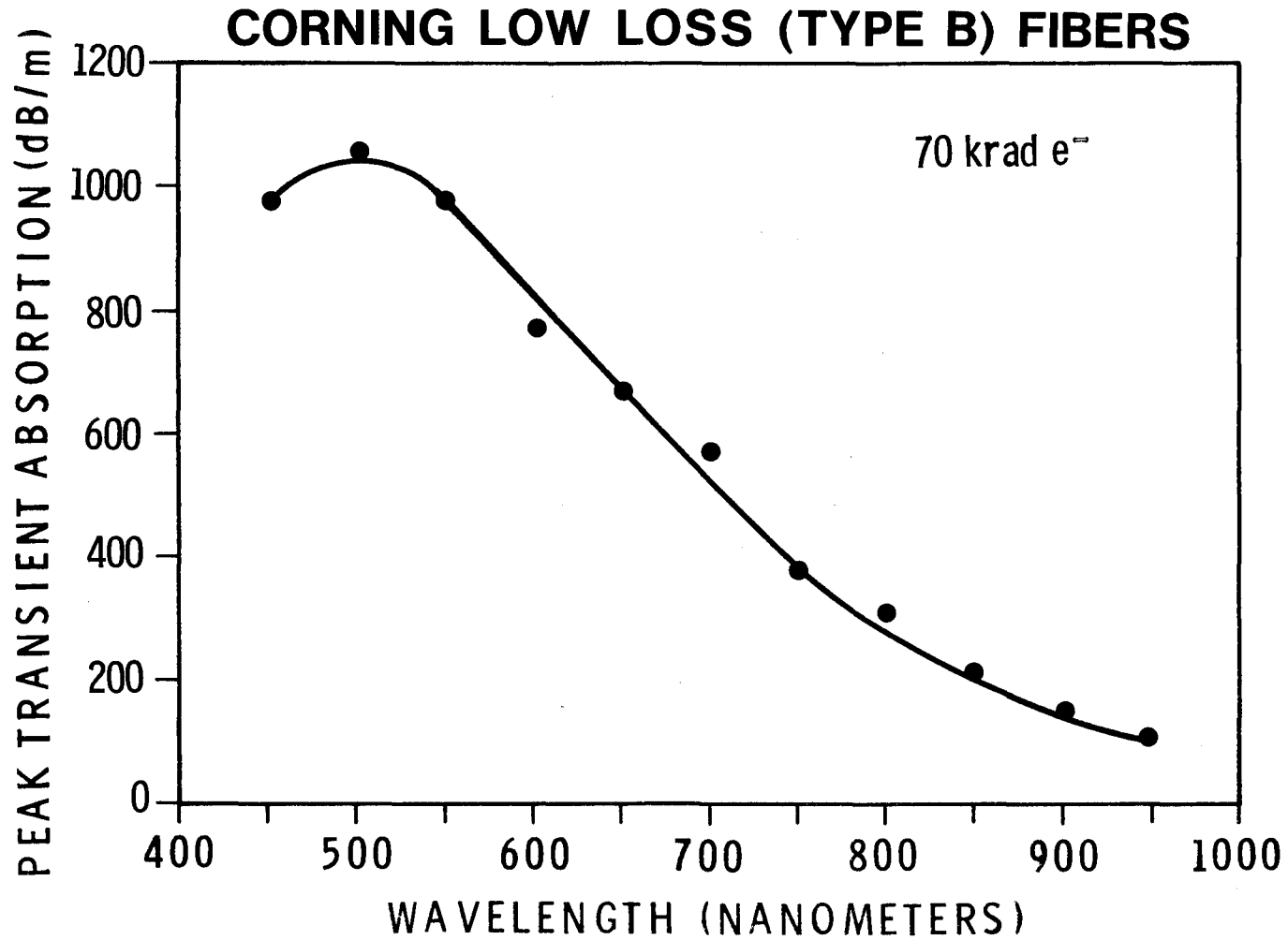


Figure 4. Peak Transient Absorption Spectrum for Corning Low Loss Fibers Exposed to a 70 krad Electron Dose. (Measurement error is estimated to be less than 10 percent of values plotted.)

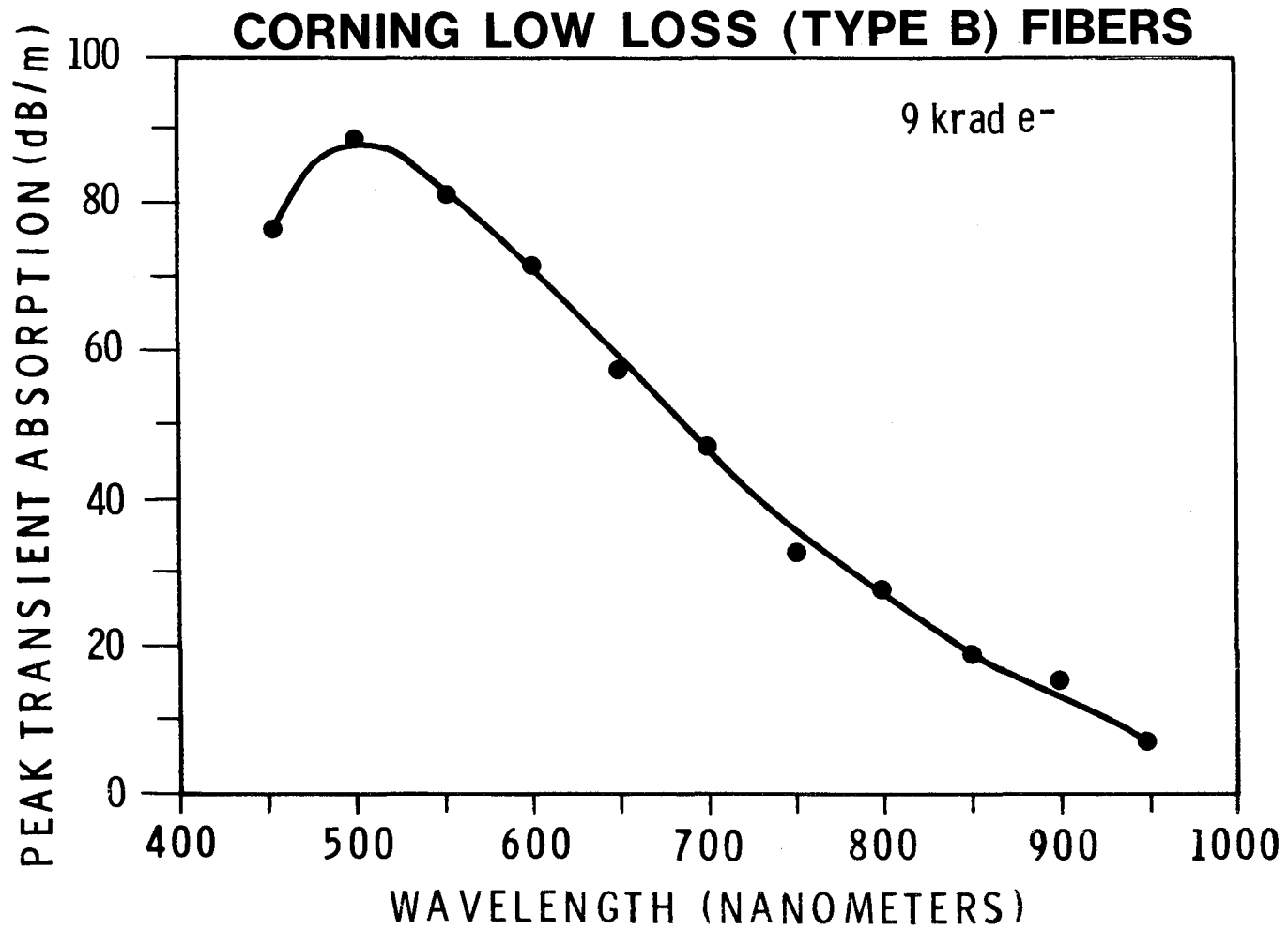


Figure 5. Peak Transient Absorption Spectrum for Corning Low Loss Fibers Exposed to a 9 krad Electron Dose. (Measurement error is estimated to be less than 10 percent of values plotted.)

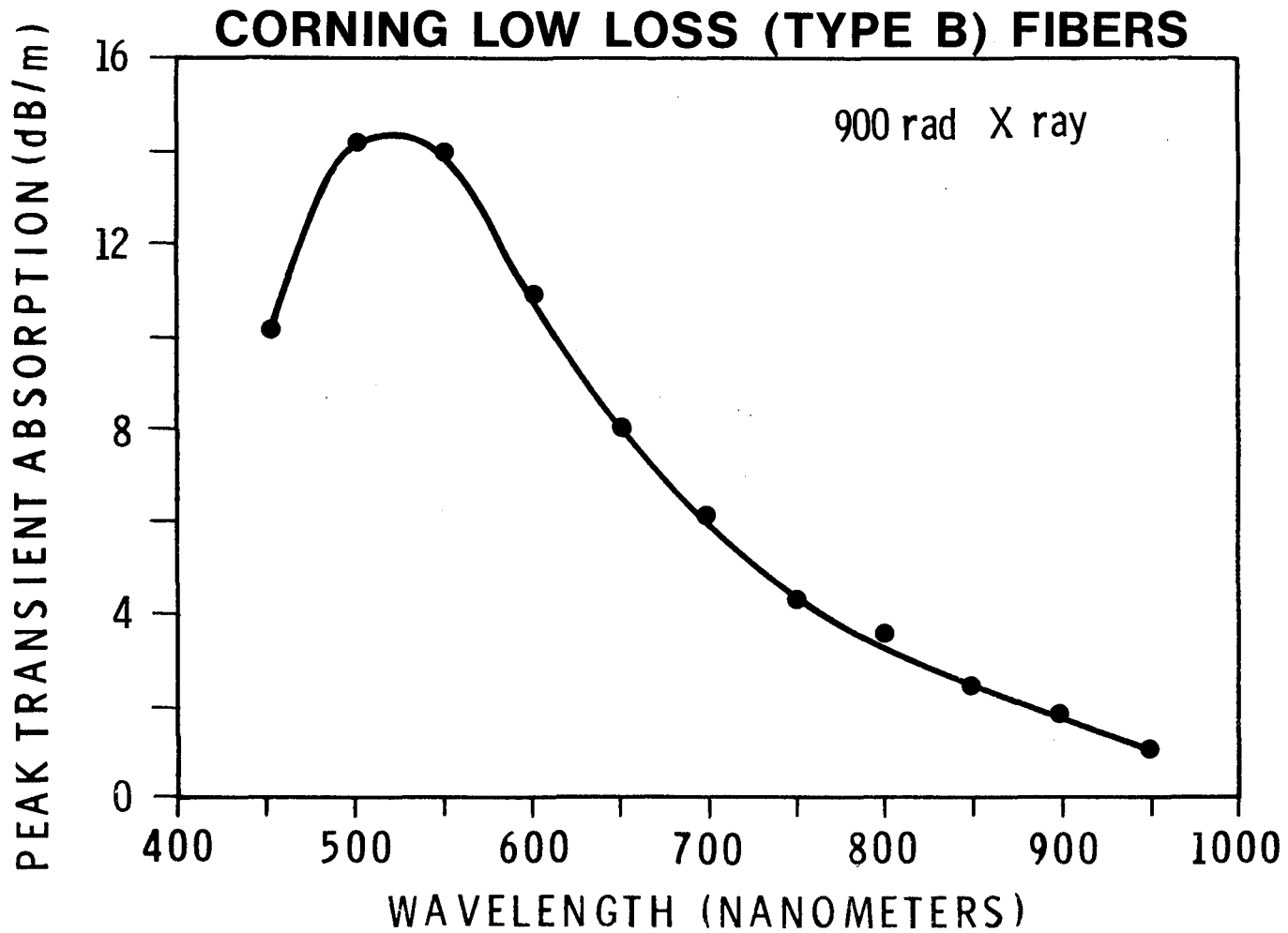


Figure 6. Peak Transient Absorption Spectrum for Corning Low Loss Fibers Exposed to a 900 rad X-ray Dose. (Measurement error is estimated to be less than 10 percent of values plotted.)

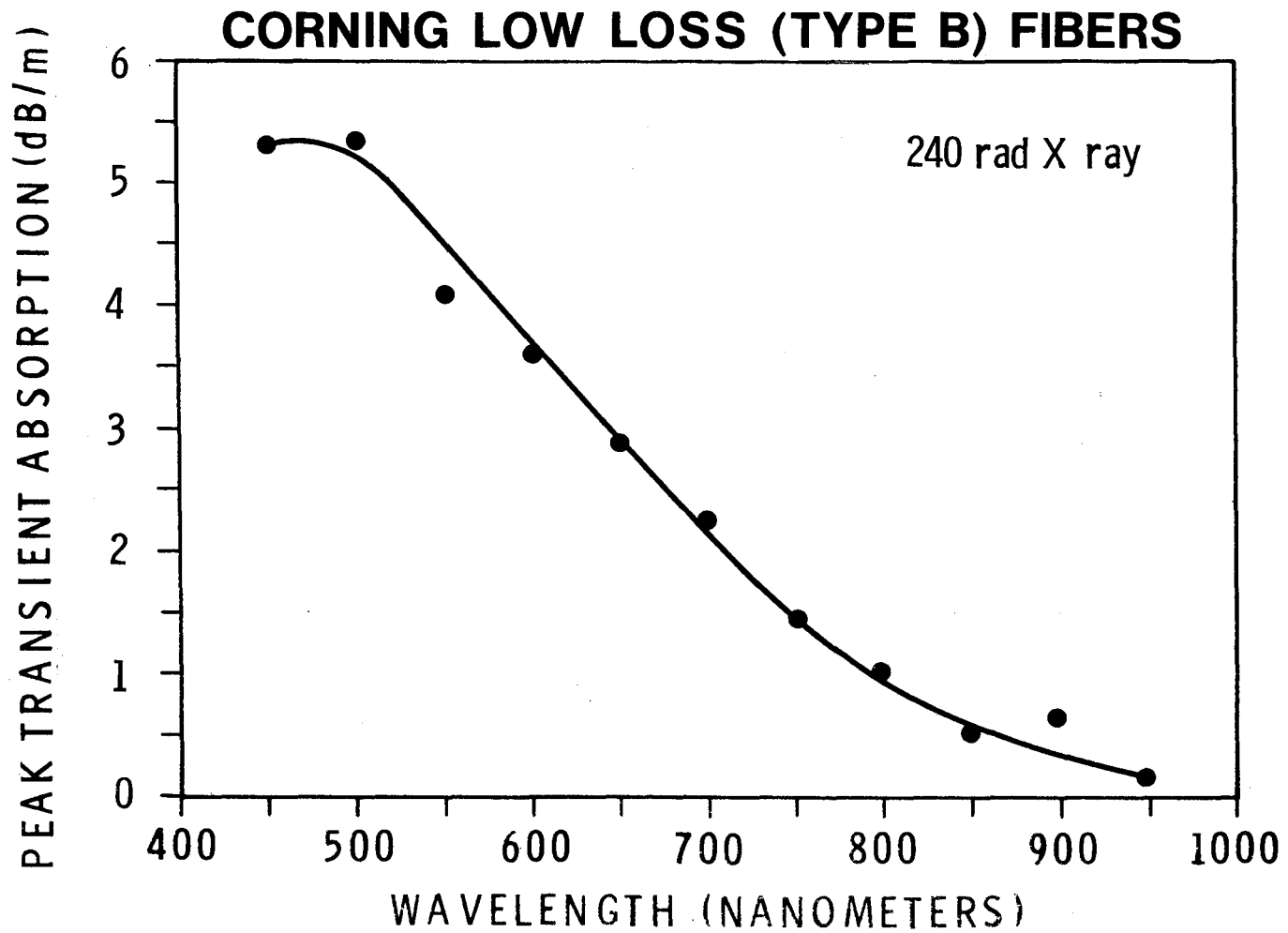


Figure 7. Peak Transient Absorption Spectrum for Corning Low Loss Fibers Exposed to a 240 rad X-ray Dose. (Measurement error is estimated to be less than 10 percent of values plotted.)

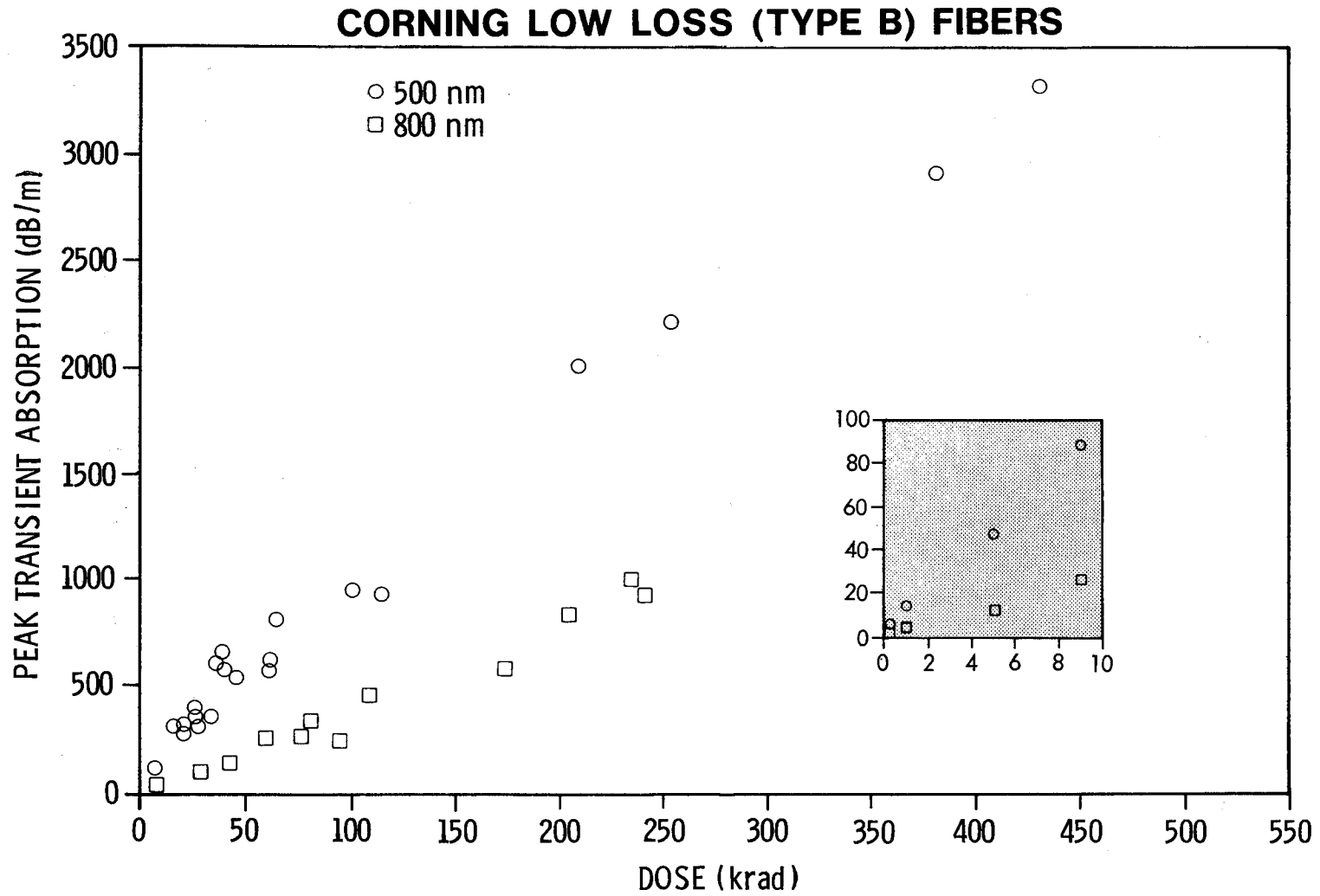


Figure 8. Peak Induced Absorption as a Function of Dose in Corning Low Loss Fibers for Wavelengths of 500 and 800 nm. The insert provides an expanded scale for the low X-ray doses. (Measurement error is less than 10 percent of values plotted.)

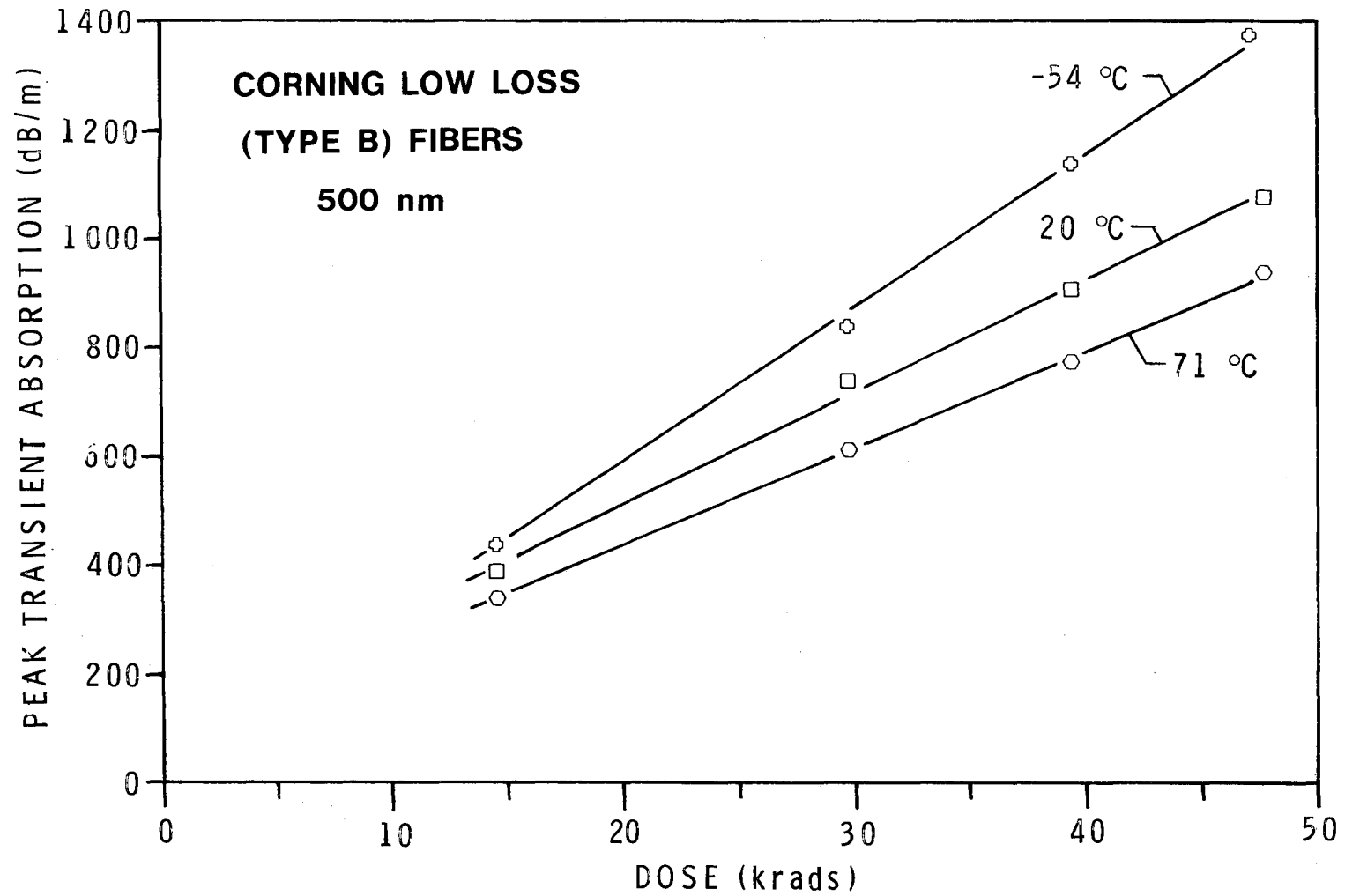


Figure 9. Peak Transient Absorption at 500 nm as a Function of Dose for Temperatures of -54, 20, and 71°C in Corning Low Loss Fibers. (Measurement error is less than 10 percent of values plotted.)

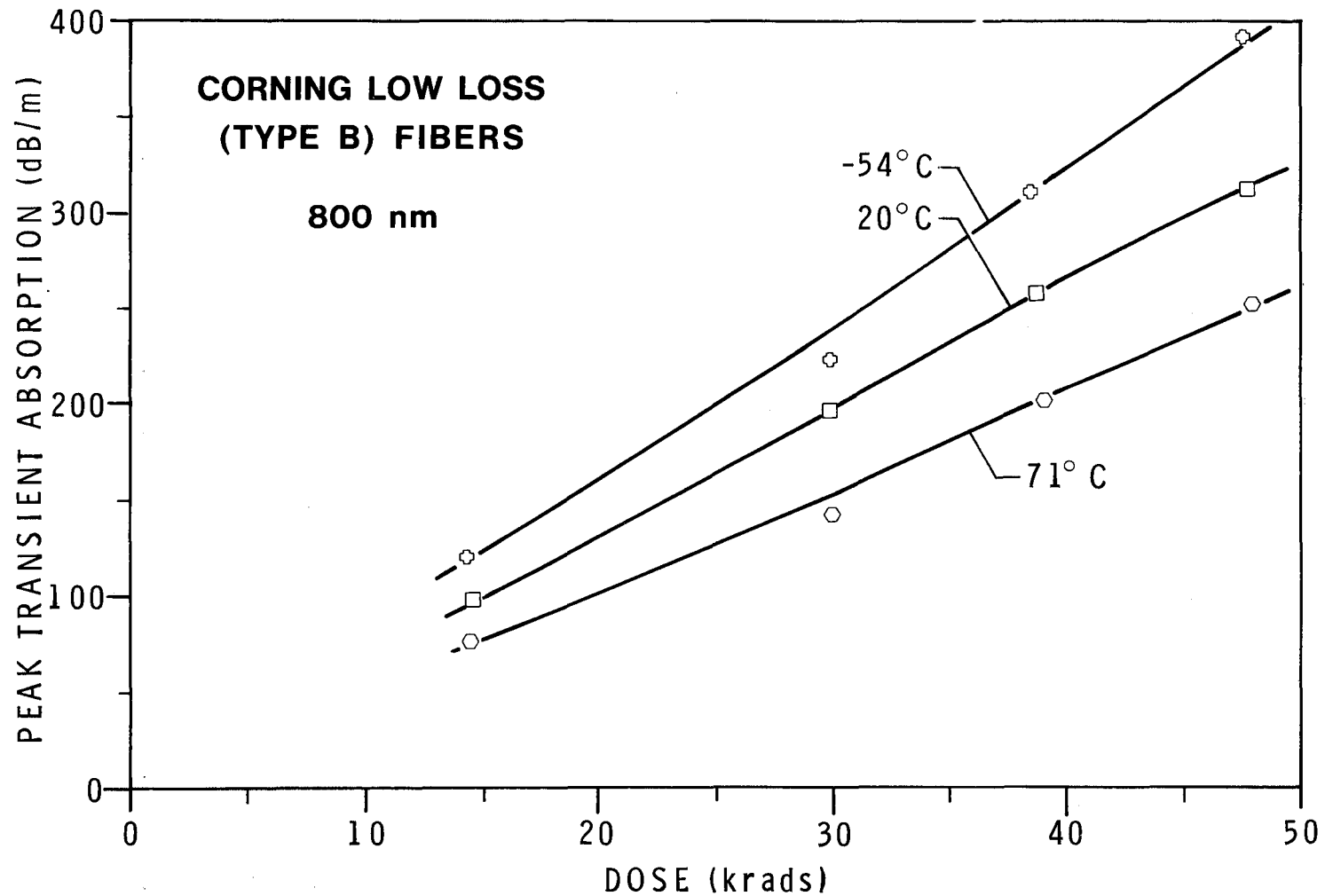


Figure 10. Peak Transient Absorption at 800 nm as a Function of Dose for Temperatures of -54, 20, and 71°C in Corning Low Loss Fibers. (Measurement error is less than 10 percent of values plotted.)

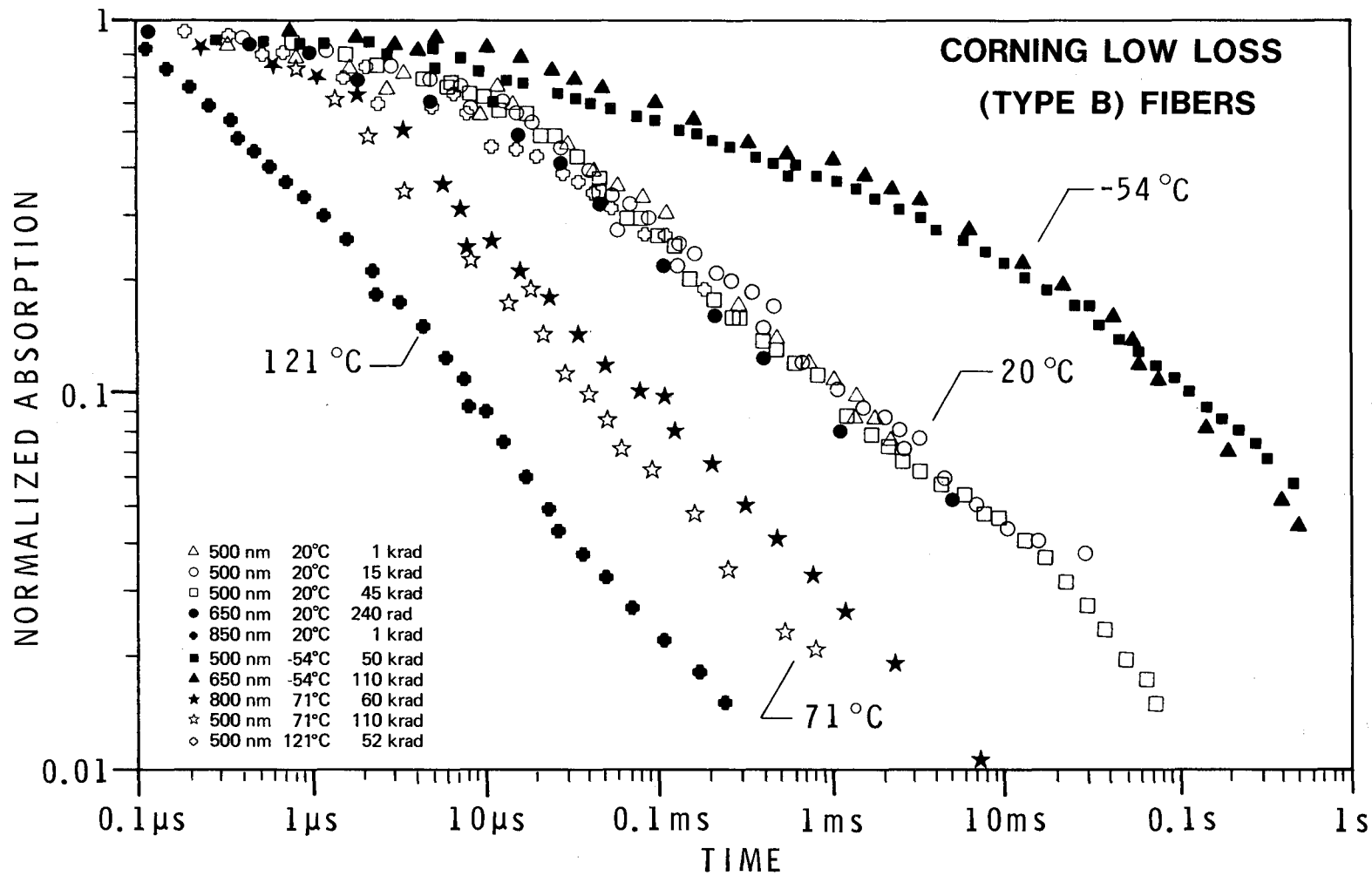


Figure 11. Transient Absorption Recovery in Corning Low Loss Fibers Plotted as the Fraction of the Absorption Remaining at Time t , as a Function of Time. Measurement error is less than 10 percent of the values shown for short times (0.1 ms) and less than 20 percent at longer times.

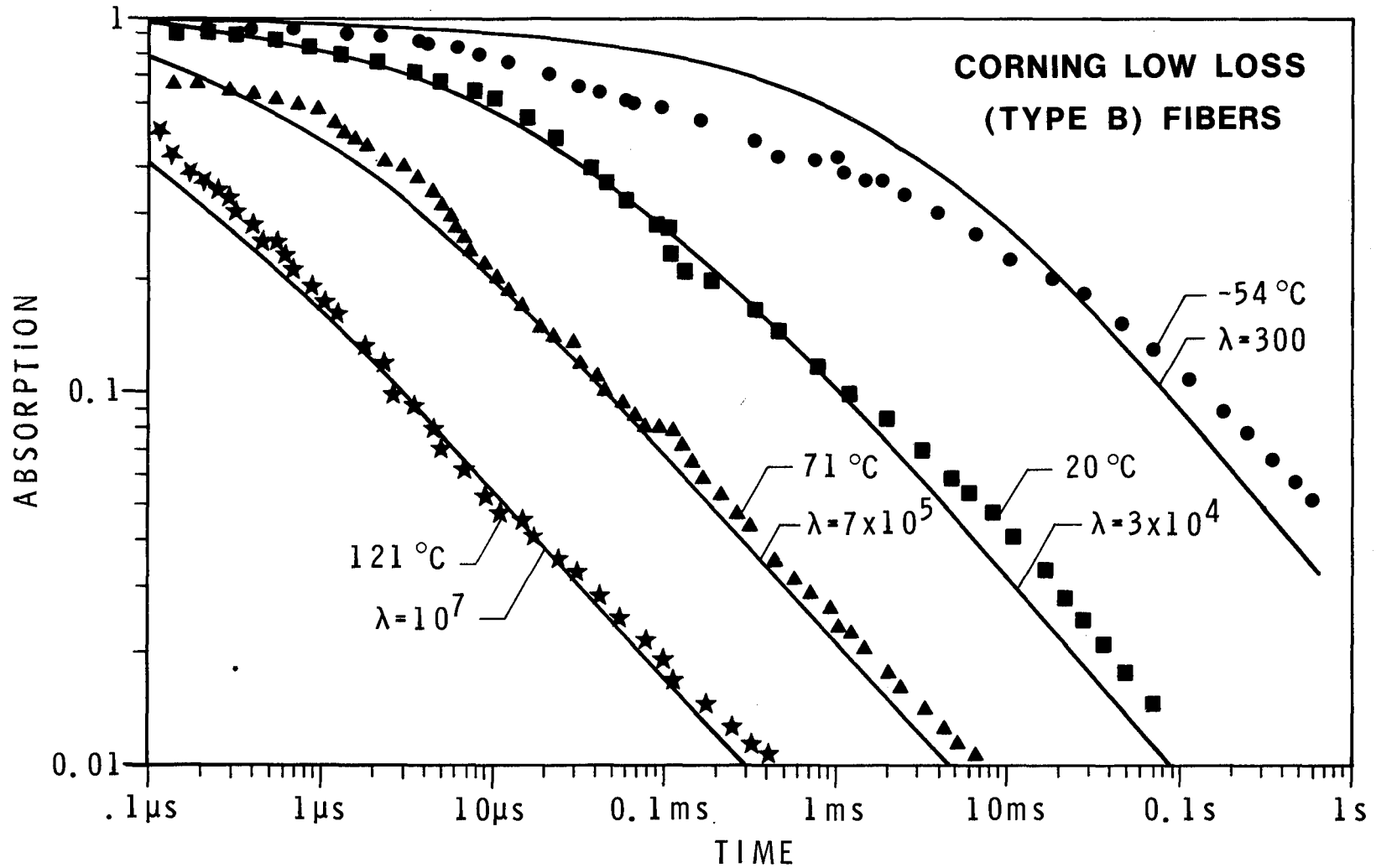


Figure 12. Absorption Recovery as a Function of Time for Corning Low Loss Fibers Where the Data Has Been Normalized to the Peak Absorption at -54°C . The solid lines represent values calculated by varying λ in the geminate recombination model expressed in Eq. (2) of the text.

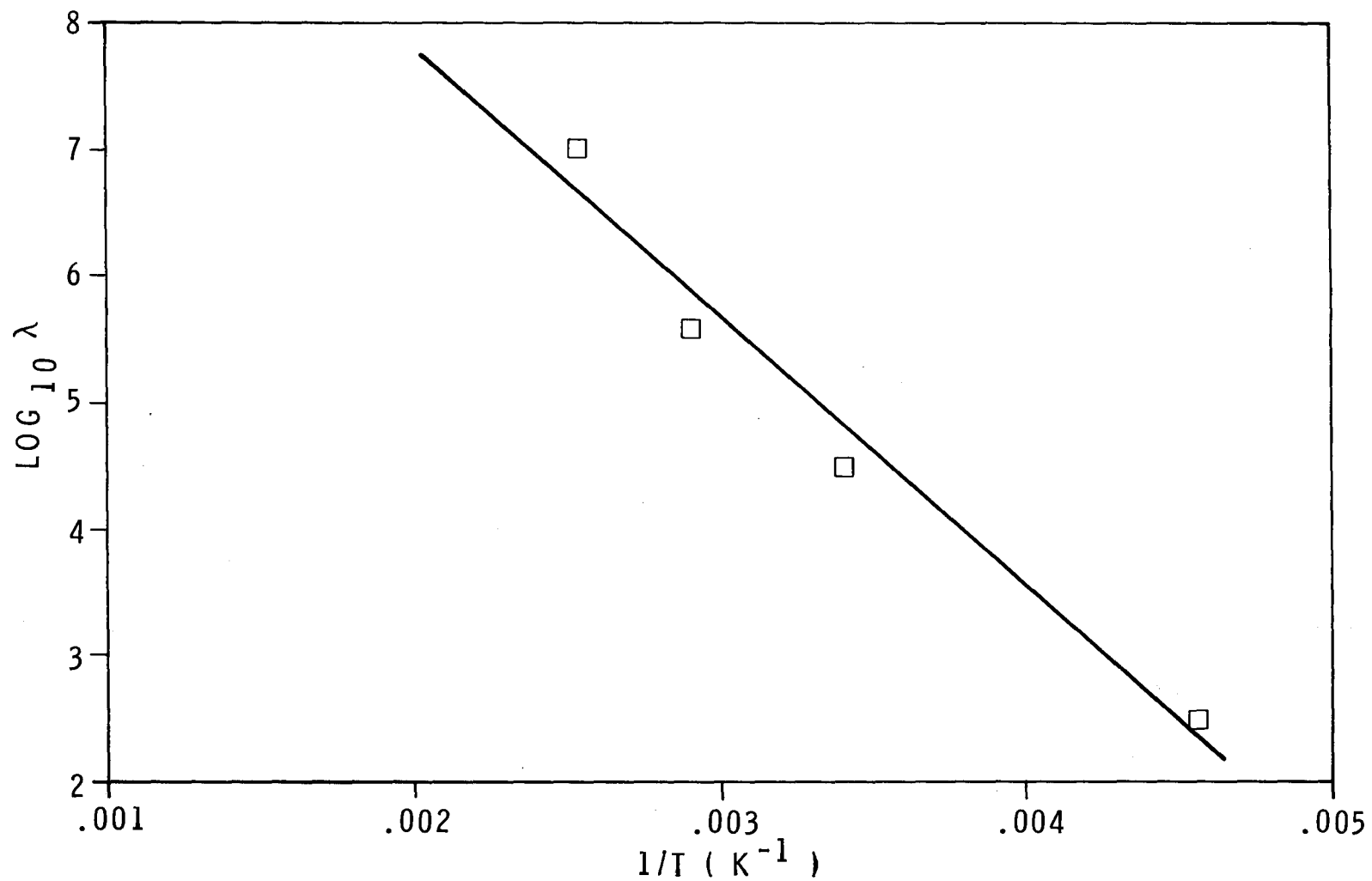


Figure 13. Plot of $\log_{10}(\lambda)$ (see Figure 12) as a Function of $1/T$. Approximate straight line indicates a thermally activated process with an activation energy of 0.5 eV.

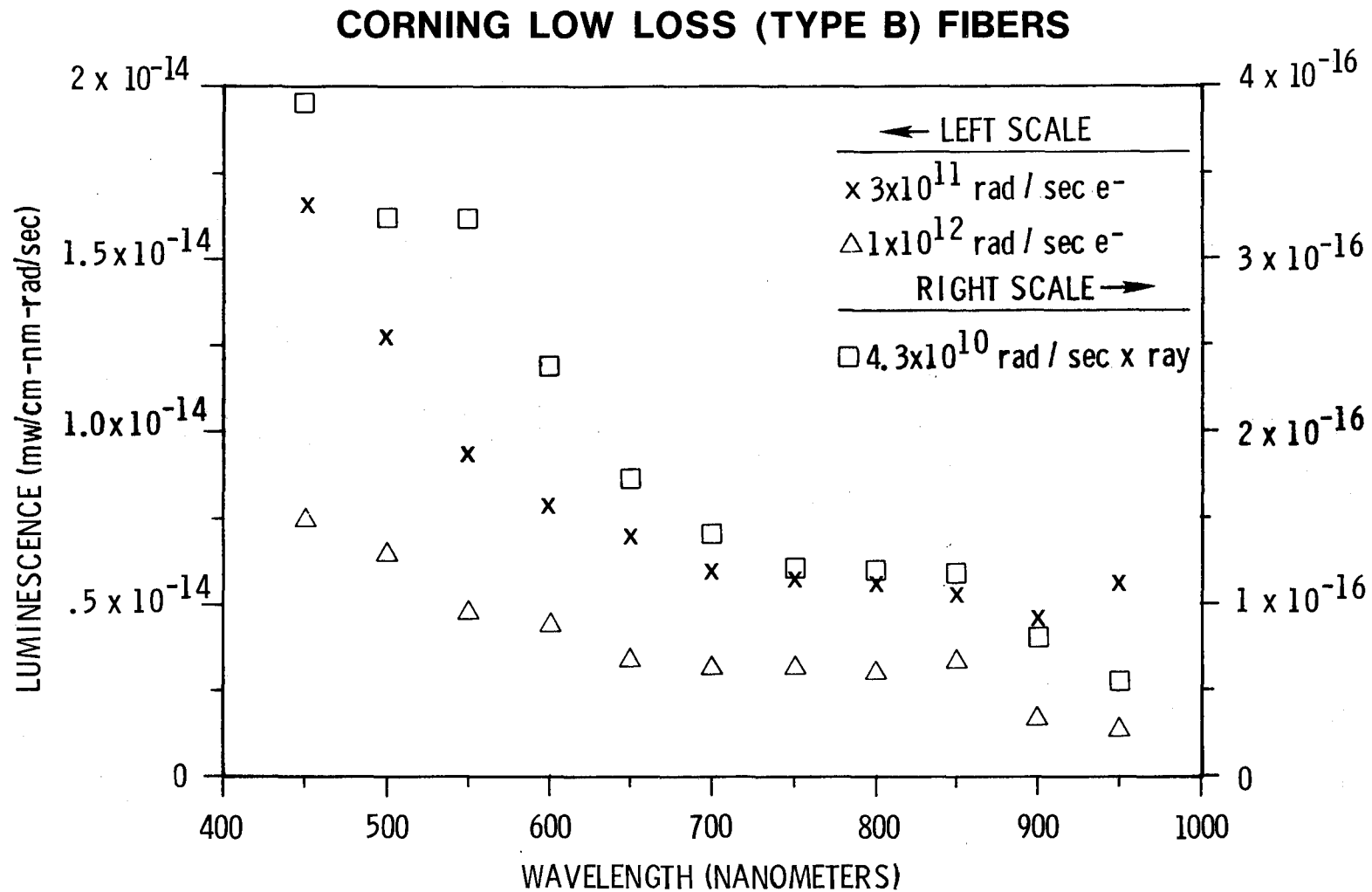


Figure 14. Transient Luminescence Spectra Induced in Corning Low Loss Fibers During Electron and X-ray Irradiation. The ordinate is proportional to the detected power in milliwatts per exposed centimeter of fiber, per nanometer of effective detector bandwidth, per unit dose rate. Data were corrected for detector response, unirradiated fiber attenuation, and filter bandwidth. The right-hand scale is for X-ray irradiations. The data shown are for 64 Corning Low Loss fibers with a diameter of 0.25 mm.

SCHOTT

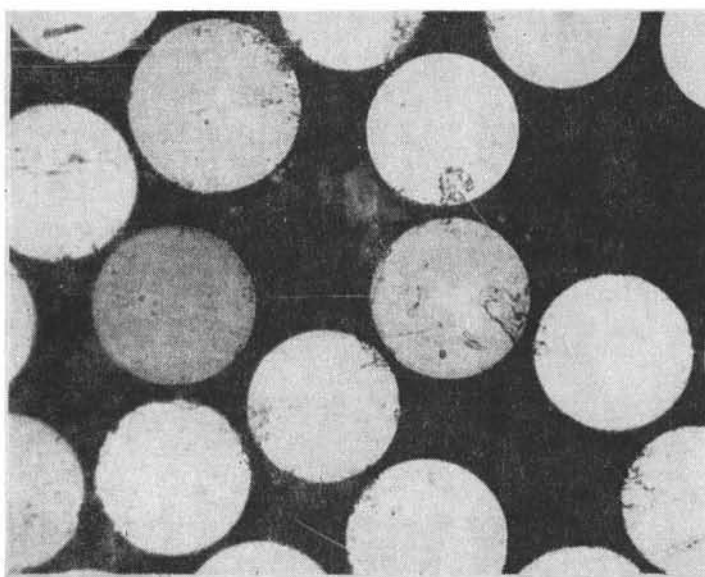
II. SCHOTT PURE FUSED SILICA FIBERS

Manufacturer: Schott Optical Glass
400 York Avenue
Duryea, PA 18642

Core: Vitreous Silica

Cladding: Plastic

Fiber Diameter: 0.1 mm



→ 0.1 mm ←

The "UV transmitting" fibers from Schott Optical Glass are one of the several commercially available plastic-clad fibers with a nominally pure vitreous silica core. Fibers of this type are among the most radiation-resistant studied.

The peak transient absorption spectra are shown in Figures 15 through 18 for several irradiation doses. At 550 nm, the spectra show a peak which

is not seen in the bulk material from which the fibers were drawn, thus indicating that impurities were introduced in the drawing process.

The peak transient absorption is plotted as a function of dose in Figure 19 for wavelengths of 500 and 800 nm and for an irradiation temperature of 20°C. The insert shows the results for low X-ray doses. Figure 20 shows the transient absorption versus dose at 500 nm for temperatures of -54, 20, and 71°C, and similar results are shown in Figure 21 for a wavelength of 800 nm.

The room-temperature data in Figures 20 and 21 differ significantly from those in Figure 19. The data in Figure 19 were obtained after the fibers had been pre-irradiated to a high dose (~100 krads) before the peak transient absorption measurements were made. The data in Figures 20 and 21, on the other hand, were obtained by exposing a "fresh" section of fiber for each datum. Comparison of the data shows that pre-irradiation increases the transient absorption. Further, the change to higher absorption values appears not to occur gradually with increasing pre-dose, but to increase abruptly at about 100 krads and 20°C. The increase occurs at lower pre-dose levels (~20 krads) for lower-temperature irradiations. The pre-dose phenomenon is not understood at this time.

The recovery data for several exposure doses and temperatures (Figure 22) show the recovery to be independent of dose, wavelength, and temperature within experimental error limits over the temperature range of interest. The recovery was also found to be independent of pre-dose.

The recovery behavior is consistent with a tunneling model^{2,10} developed to explain the recombination kinetics of irradiated organic glasses. In this model,

$$\log_{10} n(t) = a_1 \left(r_0 + \frac{15 + \log_{10} t}{0.443(V_0 - E_0)^{1/2}} \right)^3 \quad (5)$$

where $n(t)$ is the fraction of trapped electrons remaining at time t , a_1 is proportional to the concentration of acceptors that recombine with the trapped charges via a tunneling process, V_0 (eV) and E_0 (eV) are the potential height and zero-point energy respectively, and r_0 corrects for the finite radius of the trapped electron. Equation (5), which was fitted to the data of Figure 22 by varying a_1 and using estimates for r_0 , V_0 , and E_0 , adequately describes the data over five orders of magnitude in time as shown by the solid line.

The data also show that at very low temperatures (-172°C) there is a significant reduction in the recovery rate. This behavior can be explained qualitatively by summing an exponential recovery (0.6 relative amplitude)

and the tunneling mechanism (0.4 relative amplitude). The quality of the fit indicates that the tunneling process remains active for only 0.4 of the recombining species, while the remainder are described by

$$N_e(t) = 0.6 \exp(-t/\tau_e) \quad (6)$$

where N_e is the fraction recovering exponentially and τ_e is the recovery time ≈ 0.1 second.

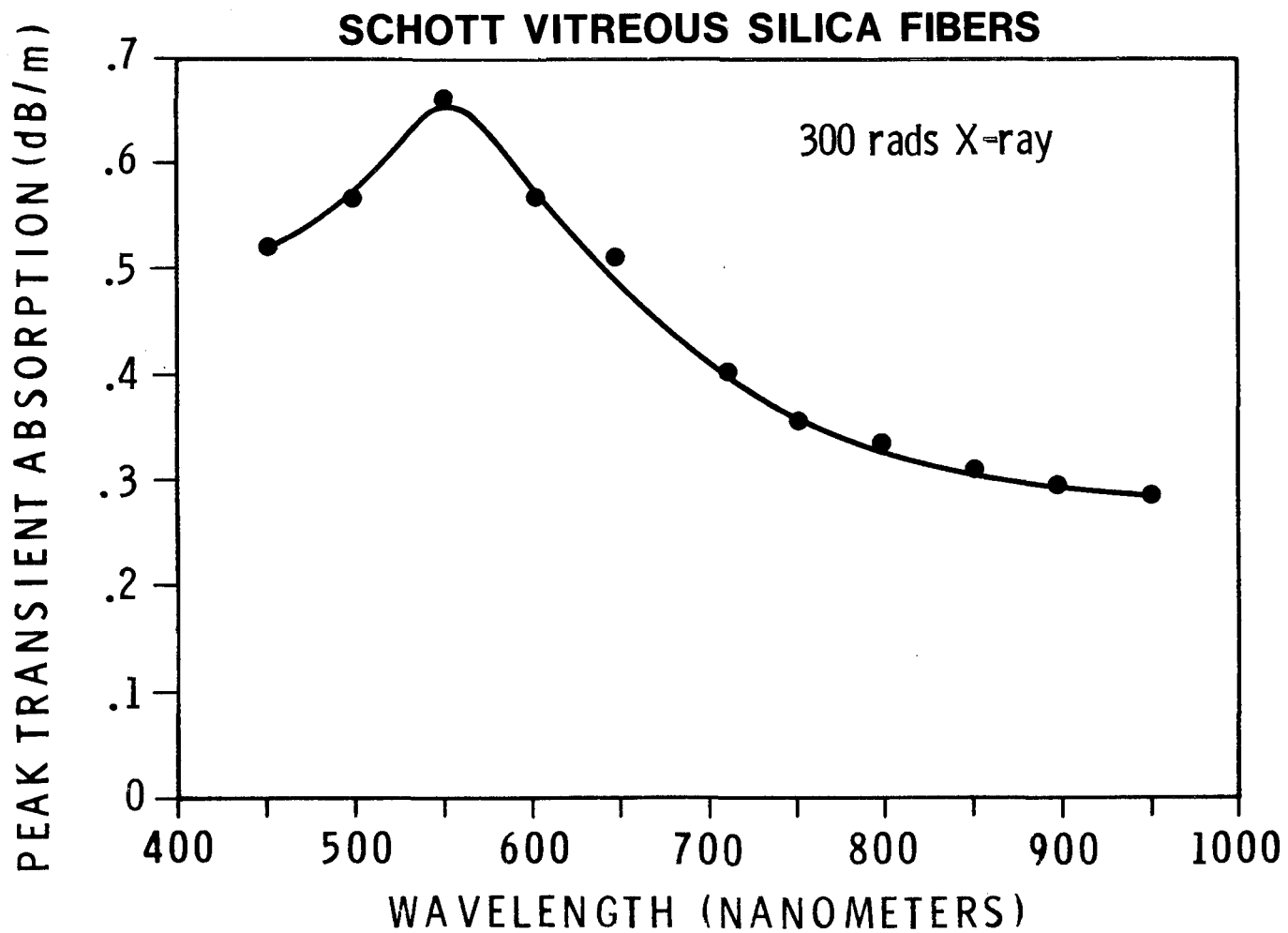


Figure 15. Peak Transient Absorption Spectrum in the Schott Vitreous Silica Fibers for an X-ray Dose of 300 rads. (Measurement error is less than 10 percent of values plotted.)

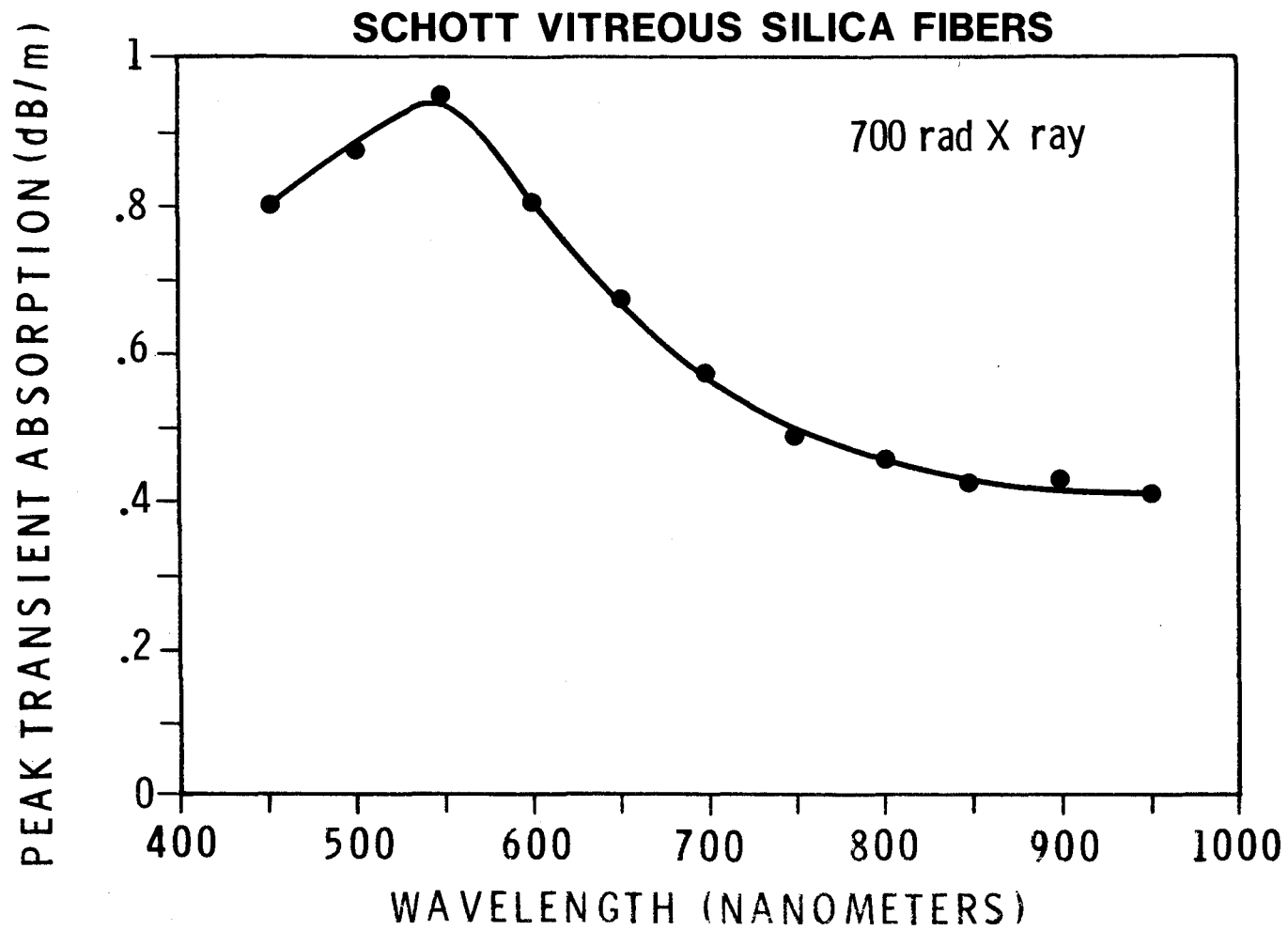


Figure 16. Peak Transient Absorption Spectrum in the Schott Vitreous Silica Fibers for an X-ray Dose of 700 rads. (Measurement error is less than 10 percent of the values plotted.)

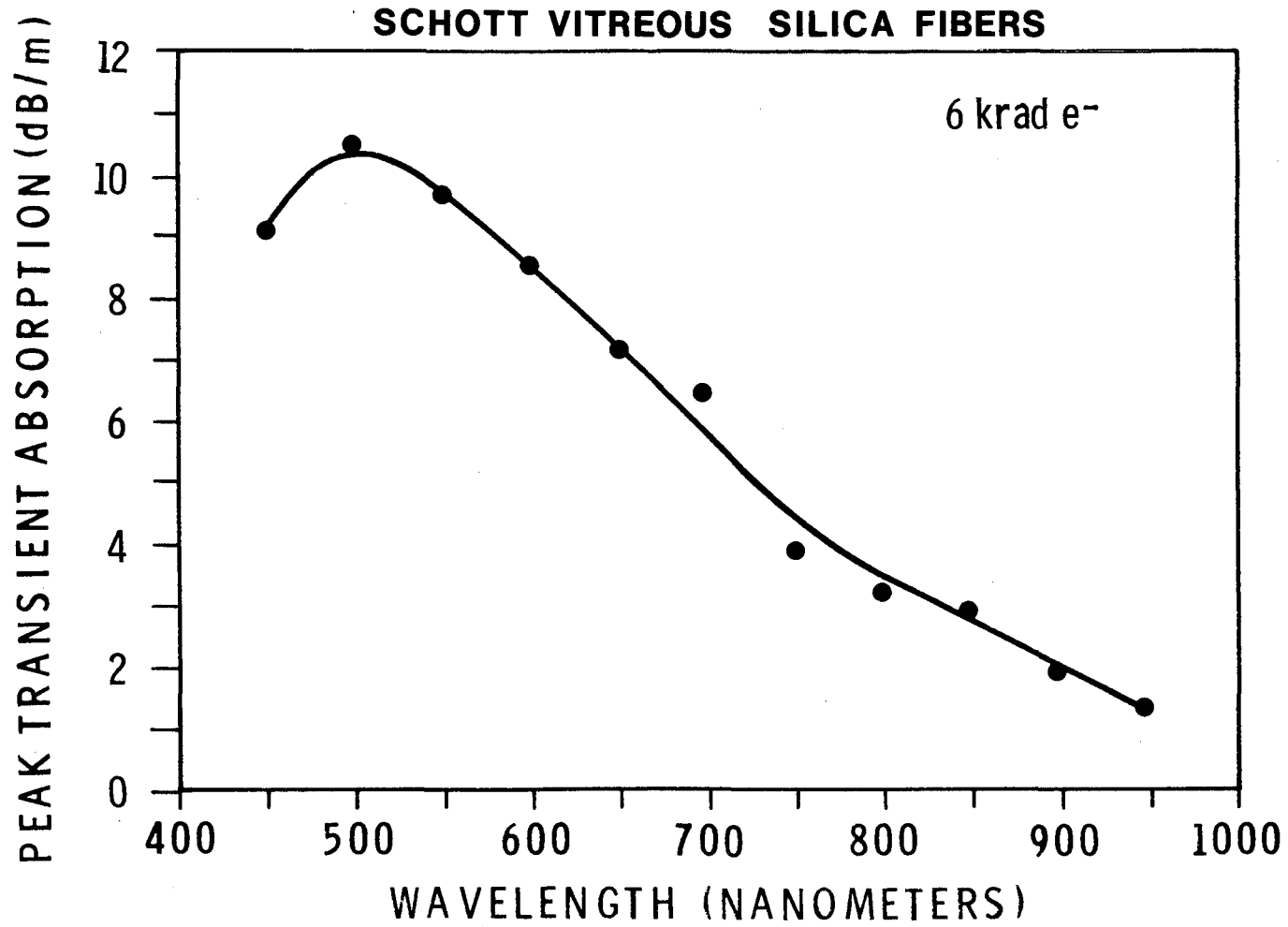


Figure 17. Peak Transient Absorption Spectrum in the Schott Vitreous Silica Fibers for an Electron Dose of 6 krad. (Measurement error is less than 10 percent of the values plotted.)

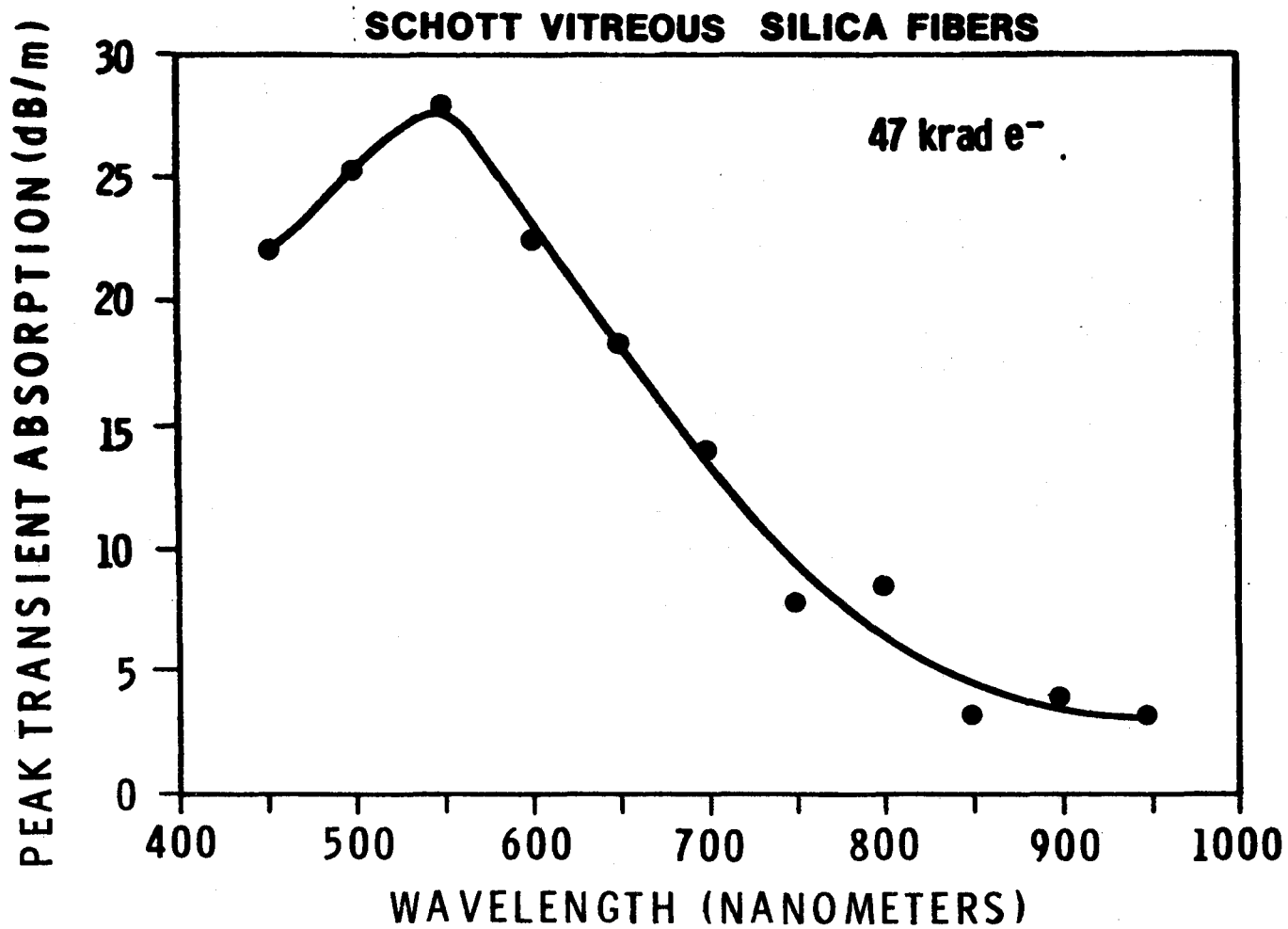


Figure 18. Peak Transient Absorption Spectrum in the Schott Vitreous Silica Fibers for an Electron Dose of 47 krads. (Measurement error is less than 10 percent of the values plotted.)

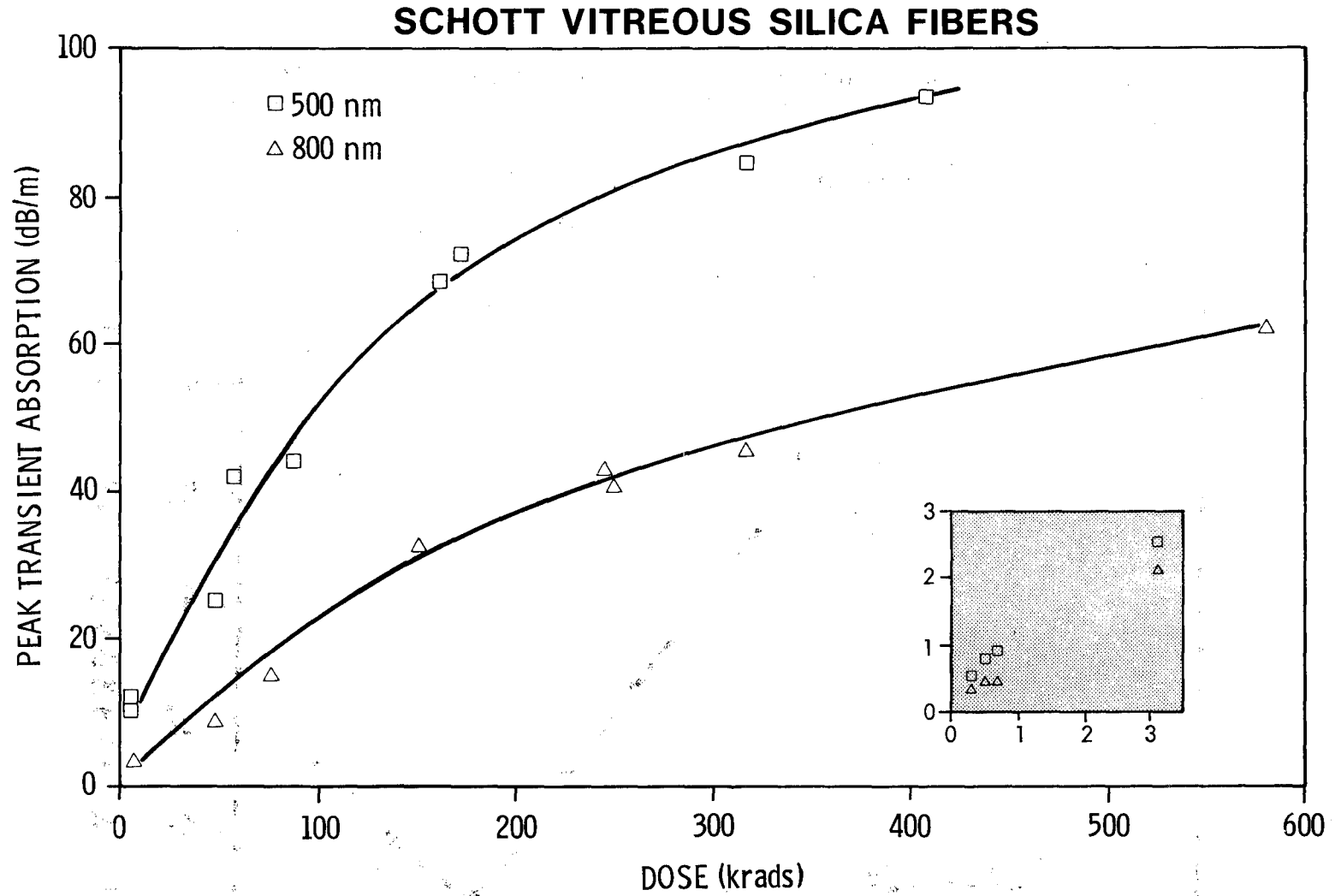


Figure 19. Peak Induced Absorption as a Function of Dose in Schott Vitreous Silica Fibers for Wavelengths of 500 and 800 nm. The insert provides an expanded scale for the low X-ray doses. (Measurement error is less than 10 percent of values plotted.)

SCHOTT VITREOUS SILICA FIBERS

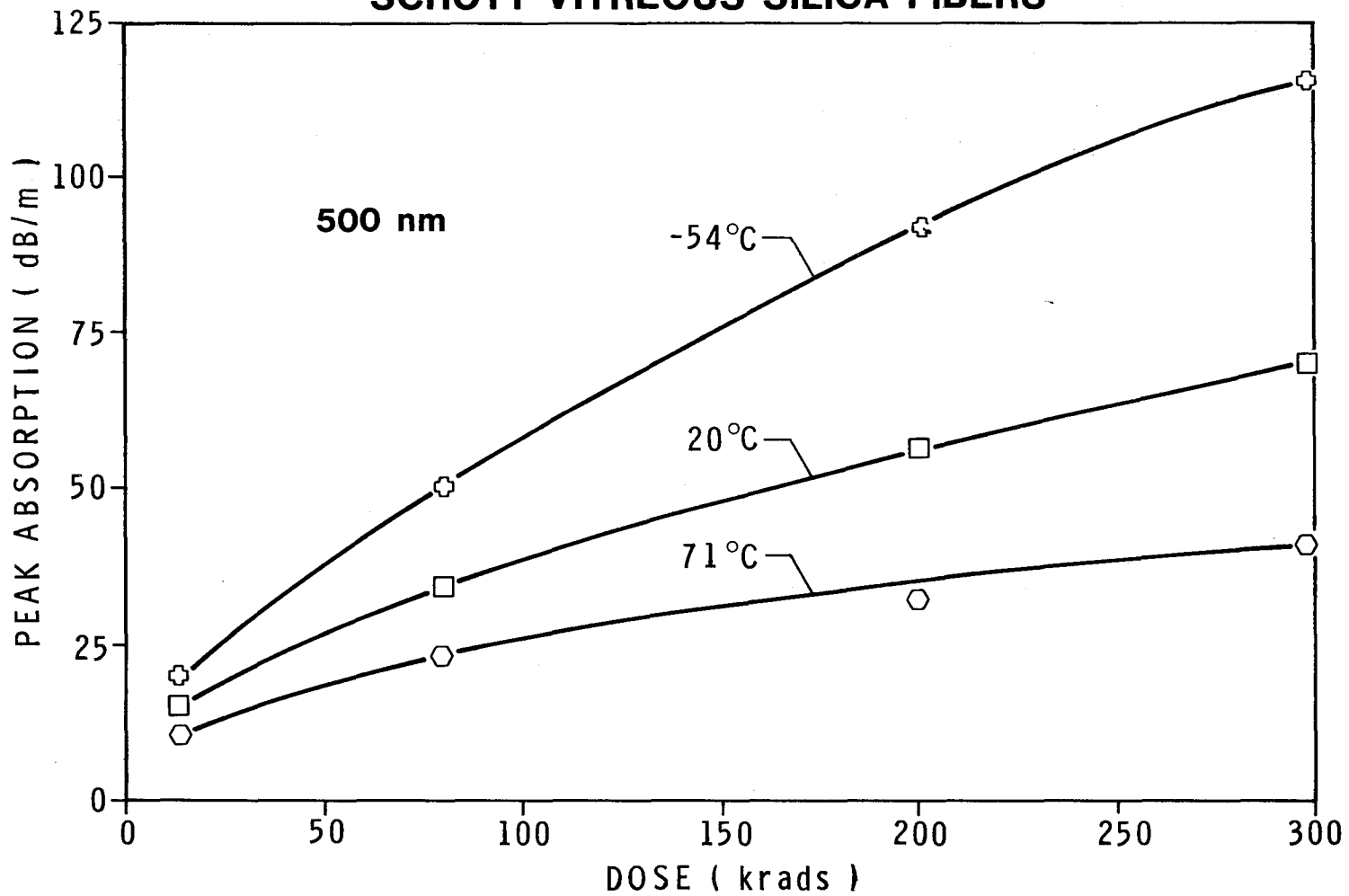


Figure 20. Peak Transient Absorption at 500 nm as a Function of Dose for Temperatures of -54, 20, and 71°C in Schott Vitreous Silica Fibers. (Measurement error is less than 10 percent of values plotted.)

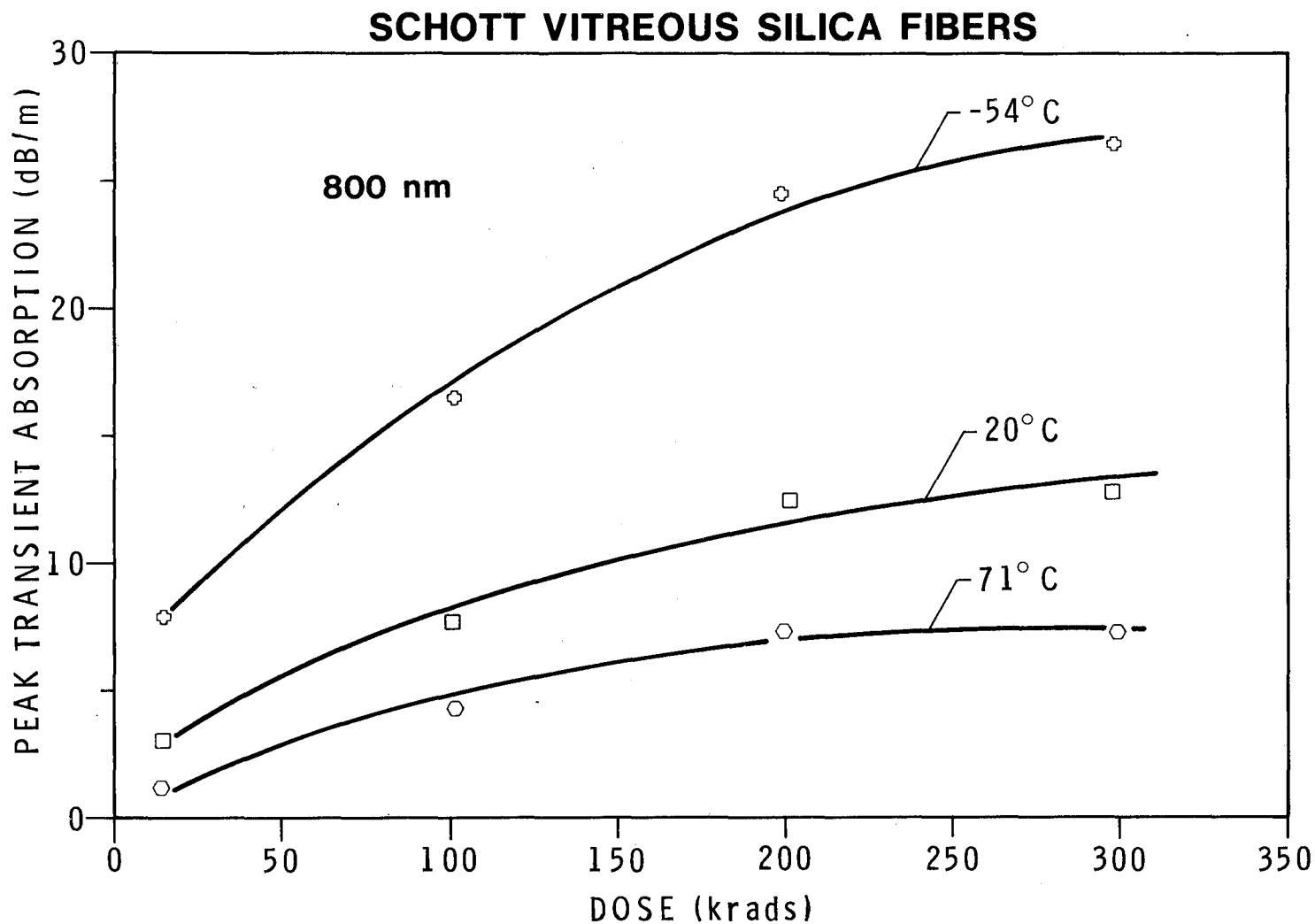


Figure 21. Peak Transient Absorption at 800 nm as a Function of Dose for Temperatures of -54, 20, and 71°C in Schott Vitreous Silica Fibers. (Measurement error is less than 10 percent of values plotted.)

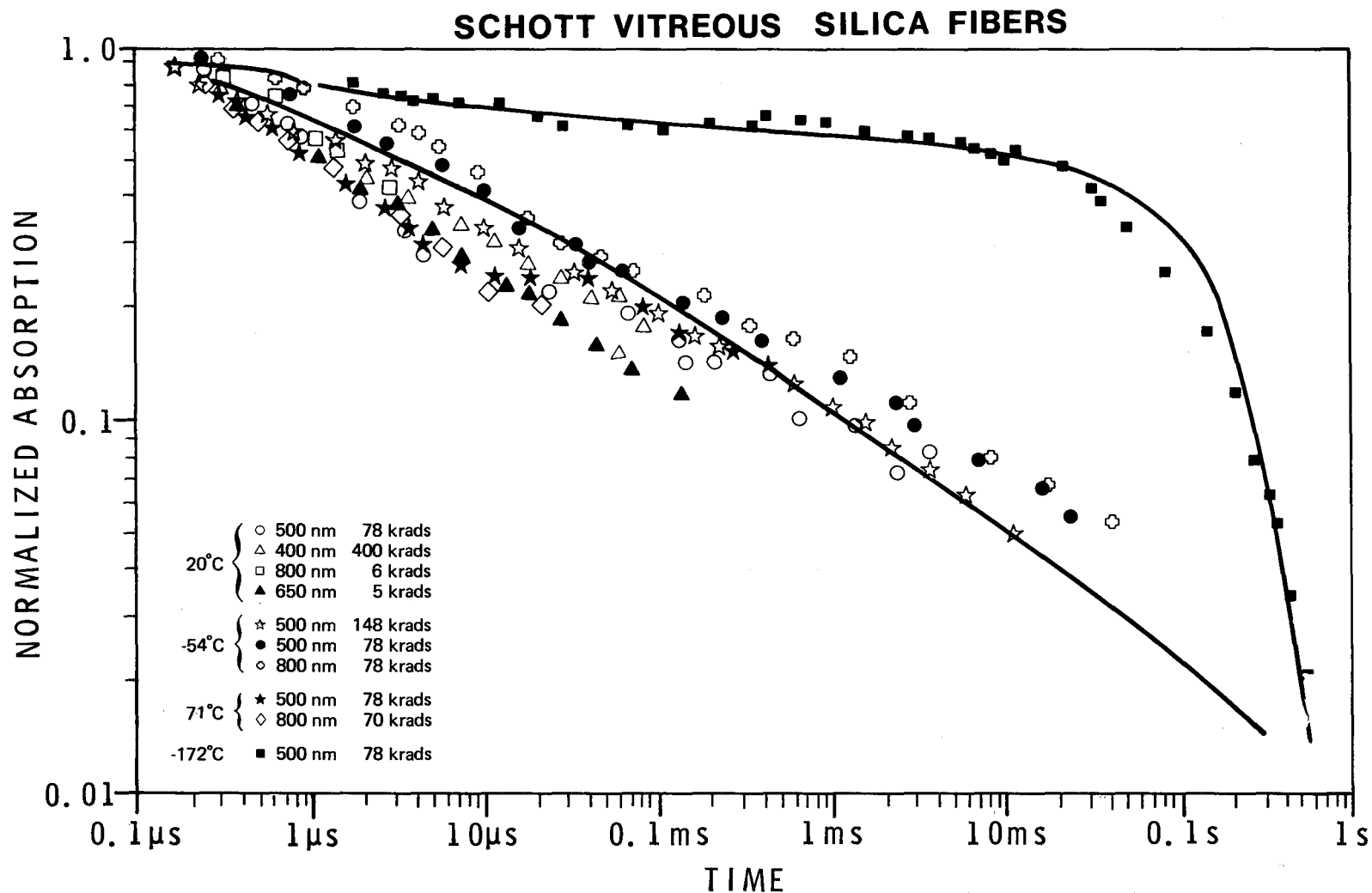


Figure 22. Recovery of Absorption in Schott Vitreous Silica Fibers. At all temperatures, recovery is independent of dose and wavelength. For temperatures greater than -54°C , recovery is independent of temperature and is accurately described by a tunneling model as shown by the solid line. At -170°C , the data are described by the superposition of the tunneling process and an exponential (see text). Measurement error is less than 10 percent at times less than 0.1 ms, and less than 20 percent at longer times.

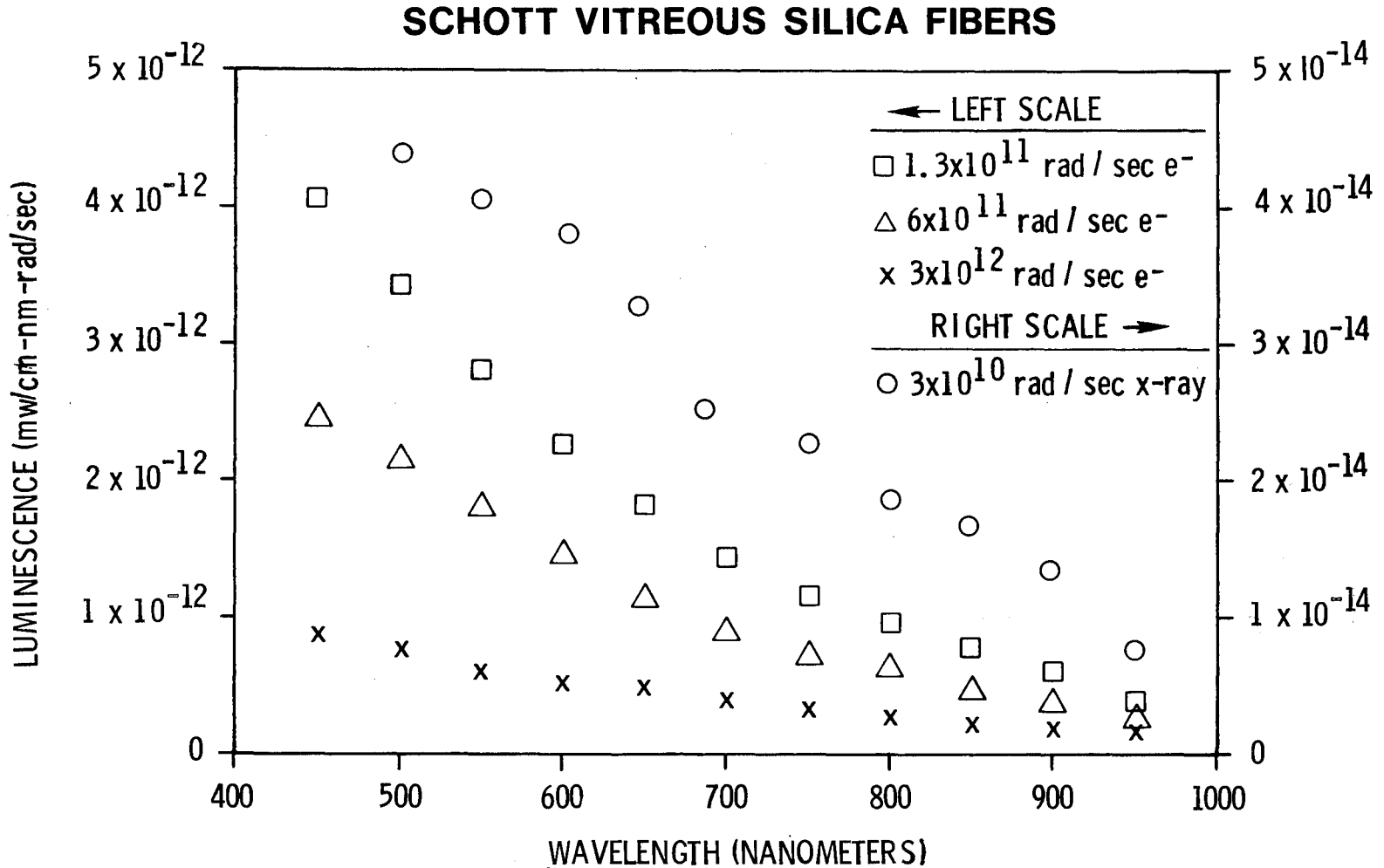


Figure 23. Transient Luminescence Spectra Induced in Corning Low Loss Fibers During Electron and X-ray Irradiation. The ordinate is proportional to the detected power in milliwatts per exposed cm of fiber, per nanometer of effective detector bandwidth, per unit dose rate. Data were corrected for detector response, unirradiated fiber attenuation, and filter bandwidth. The left-hand scale is for electron data and the right-hand scale for X-ray irradiations. The data shown are for 120 Schott fibers with a diameter of 0.1 mm.

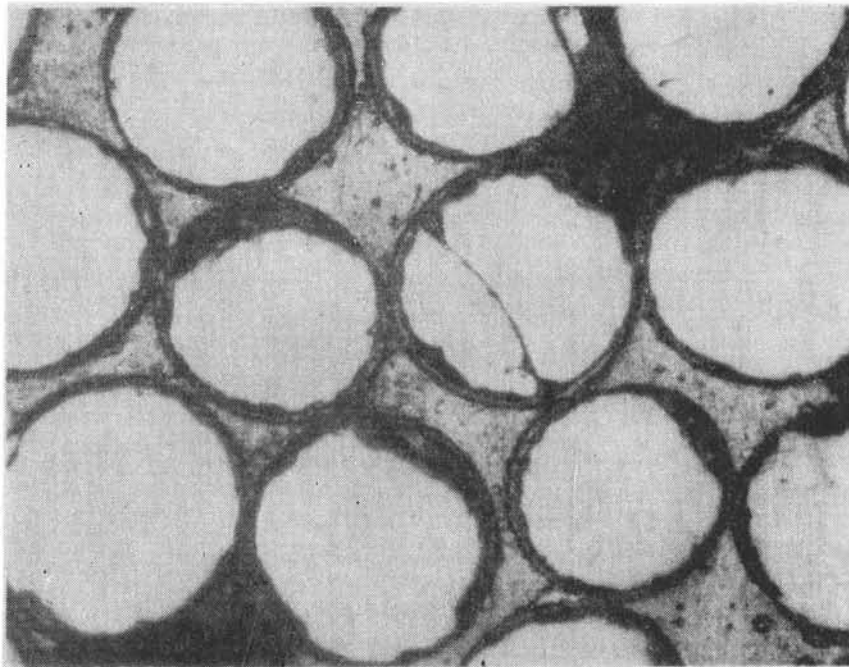
III. VALTEC PURE FUSED SILICA FIBERS

Manufacturer: Valtec Fiberoptics*
West Boylston, MA 01583

Core: Pure Fused Silica

Cladding: Plastic

Fiber Diameter: 0.12 mm



*Formerly Electro Fiberoptics Division, VALTEC Corporation

The transient absorption response of the plastic-clad, "pure" vitreous silica core fibers from Valtec Fiberoptics is similar to that of the Schott fibers. The spectral dependence of the peak transient absorption is shown in Figures 24 and 25, and the peak transient absorption versus dose for wavelengths of 500 and 800 nm are shown in Figure 26. These data were obtained by exposing a previously unirradiated section of fiber, and they compare very closely with the Schott data (Figures 20 and 21) obtained under similar conditions. The effect of temperature on the peak transient absorption is shown in Figures 27 and 28 for wavelengths of 500 and 800 nm, respectively. For these fibers, the peak absorption increases with decreasing temperature, as it does for the other fibers. At 500 nm after a dose of 150 krads, the absorption doubles as the irradiation temperature varies from 71 to -54°C.

The recovery data for the Valtec Fiberoptics material (Figure 29) are independent of dose and wavelength, as are the data for the other "pure" vitreous silica core fibers, within the limits of experimental error. For practical purposes, the recovery may also be considered independent of temperature over the range of interest. The recovery closely follows that of the Schott fibers at short times (< 0.1 ms), but occurs more slowly at longer times.

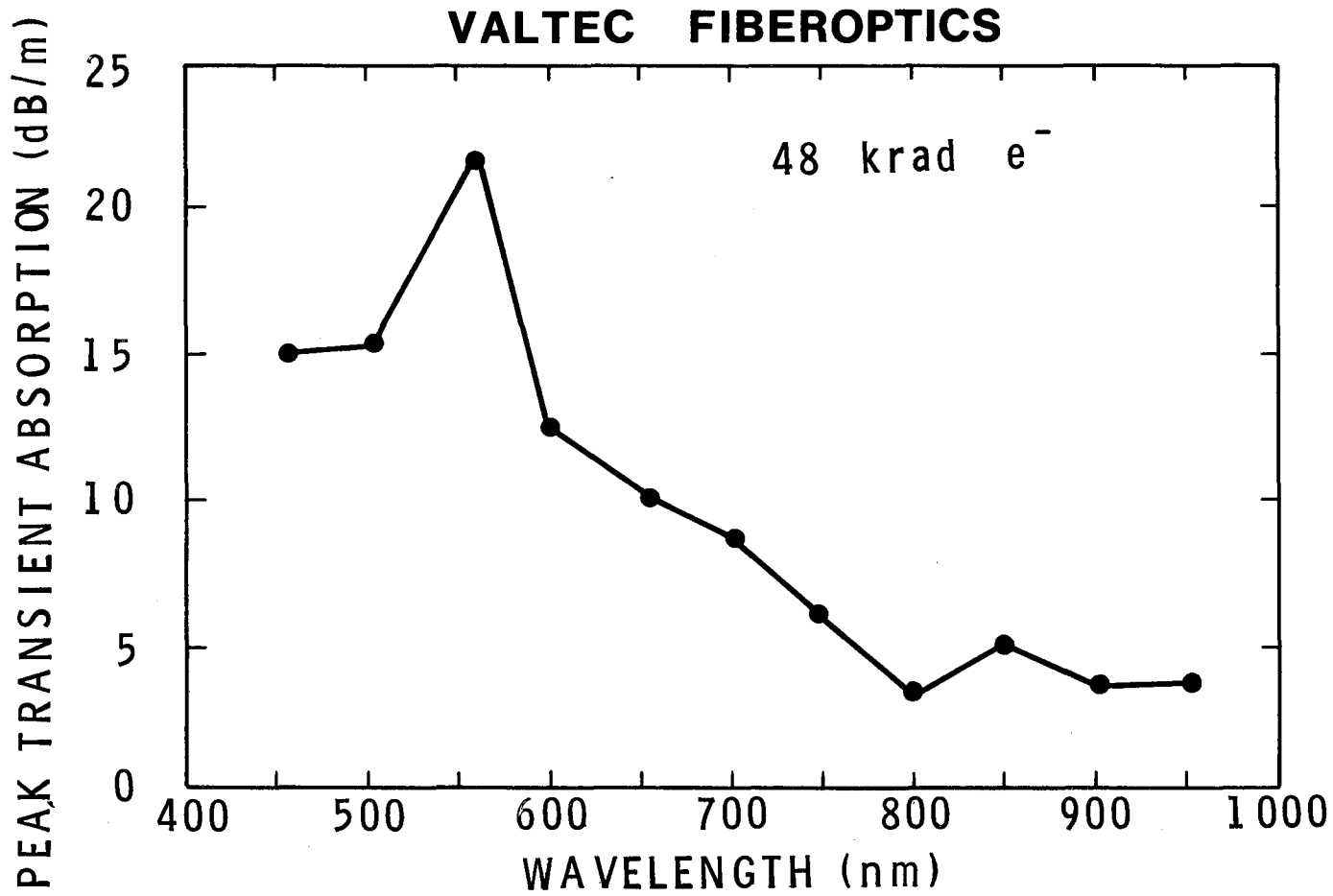


Figure 24. Peak Transient Absorption Spectrum for Valtec Fiberoptics Pure Fused Silica Fibers Exposed to a 48 krad Electron Dose. (Measurement error is less than 10 percent of values plotted.)

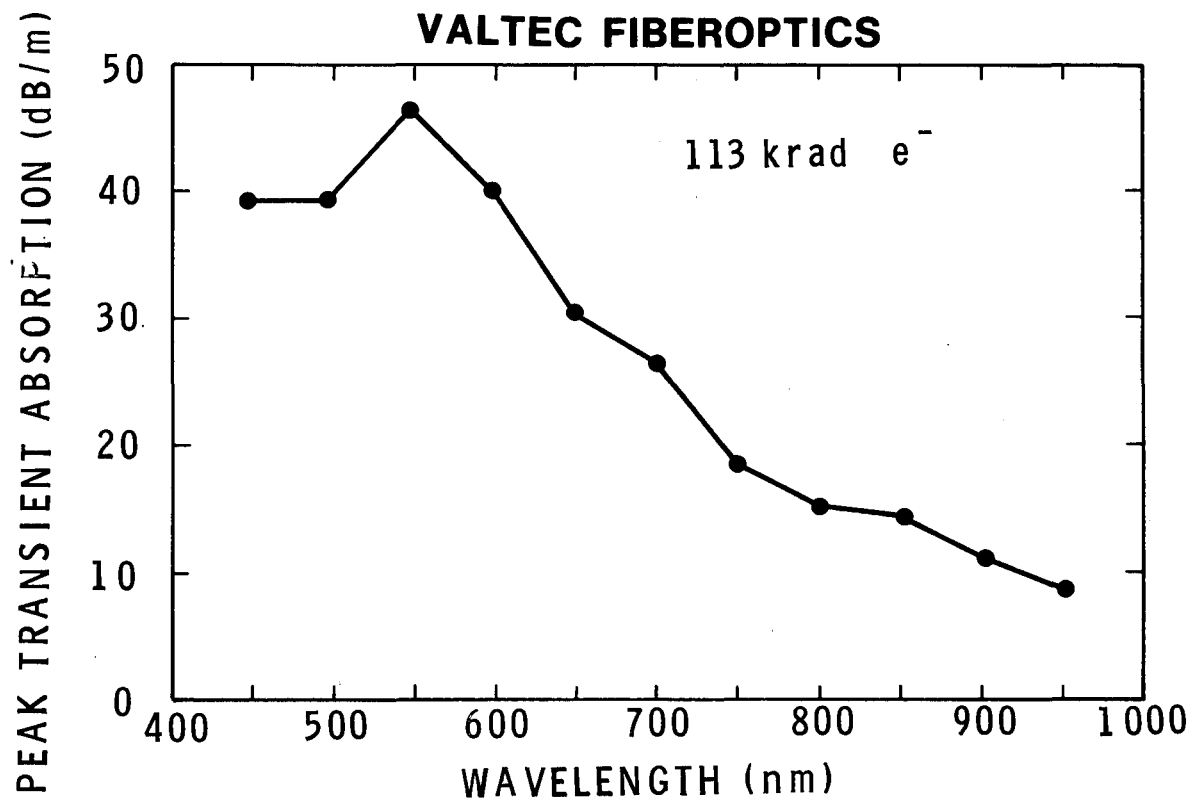


Figure 25. Peak Transient Absorption Spectrum for Valtec Fiberoptics Pure Fused Silica Fibers Exposed to a 113 krad Electron Dose. (Measurement error is less than 10 percent of values plotted.)

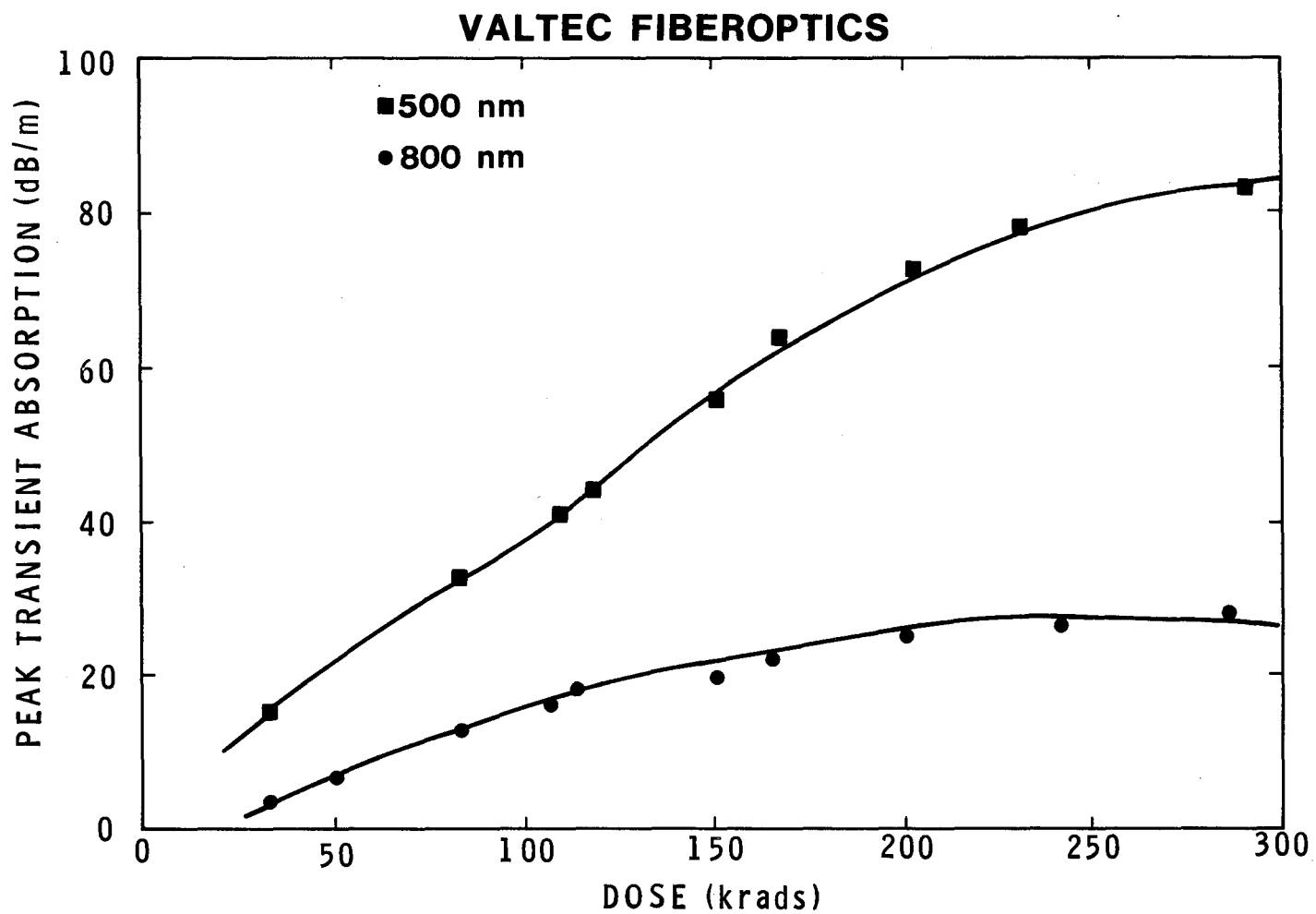


Figure 26. Peak Transient Absorption as a Function of Dose in the Valtec Fiberoptics Fibers for Wavelengths of 500 and 800 nm. (Measurement error is less than 10 percent of values plotted.)

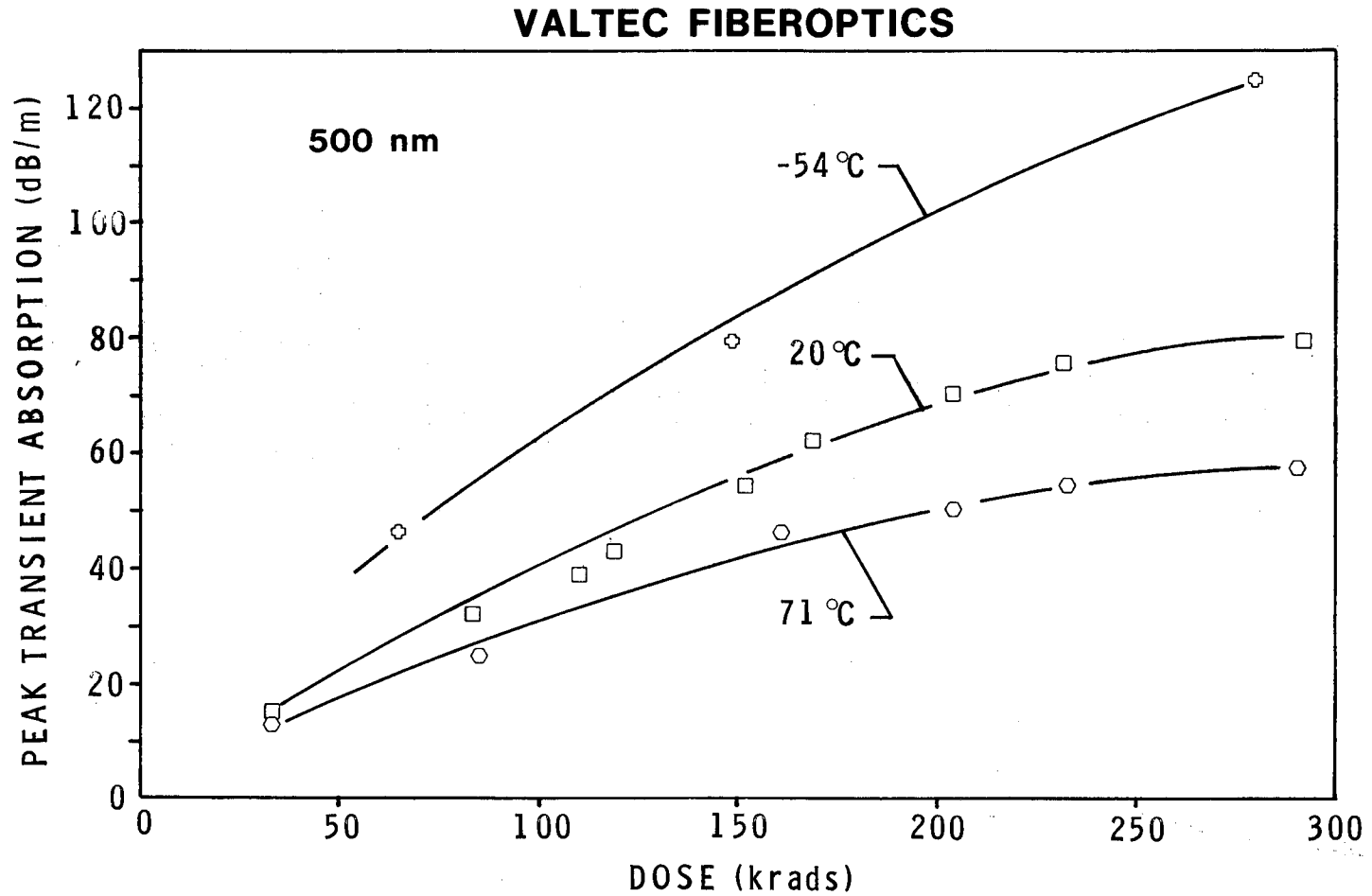


Figure 27. Peak Transient Absorption Versus Dose at 500 nm for Temperatures of -54, 20, and 71°C in Valtec Fiberoptics Fibers. (Measurement error is less than 10 percent of values plotted.)

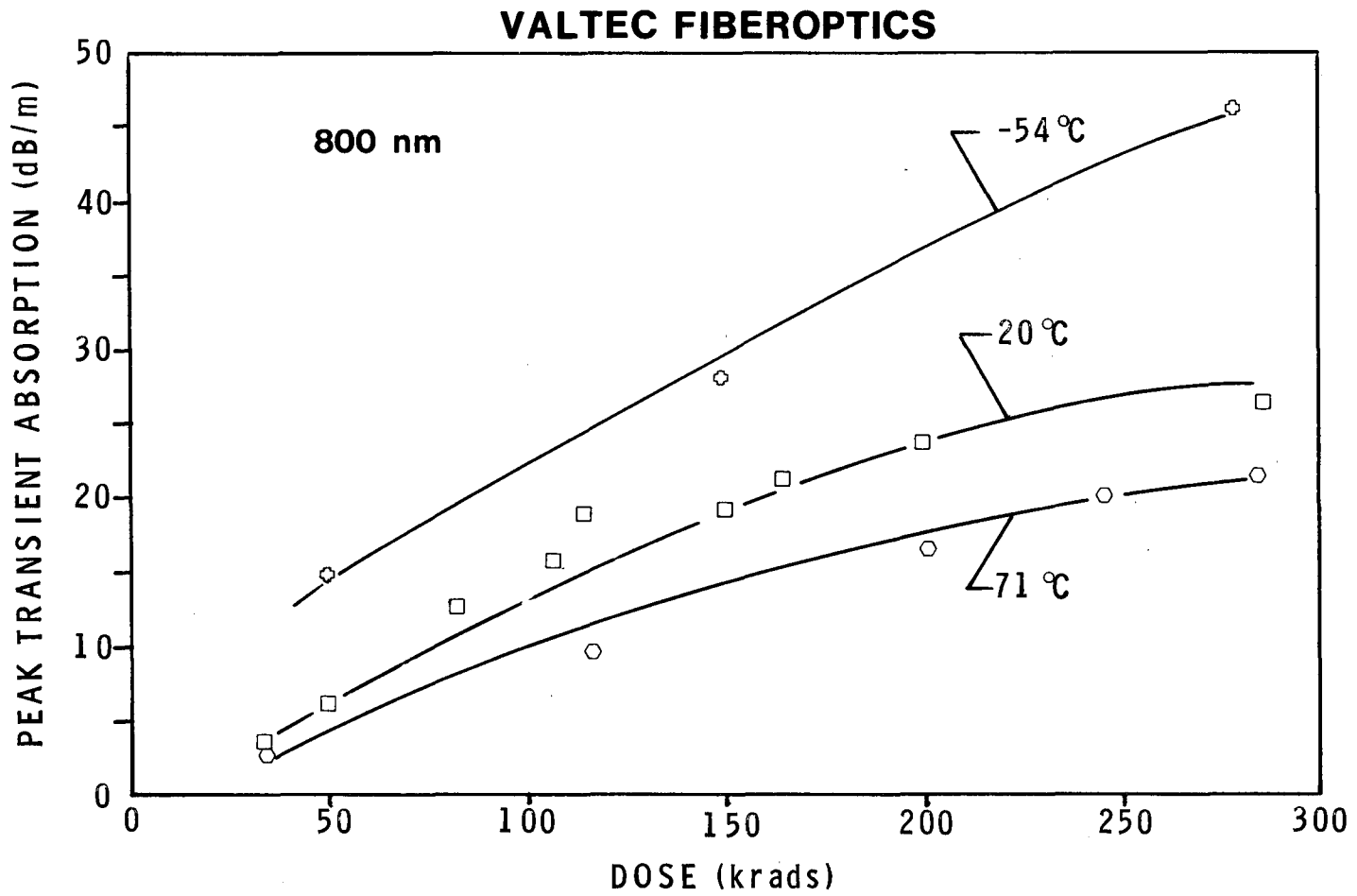


Figure 28. Peak Transient Absorption as a Function of Dose at 800 nm for Temperatures of -54, 20, and 71°C in Valtec Fiberoptics Fibers. (Measurement error is less than 10 percent of values plotted.)

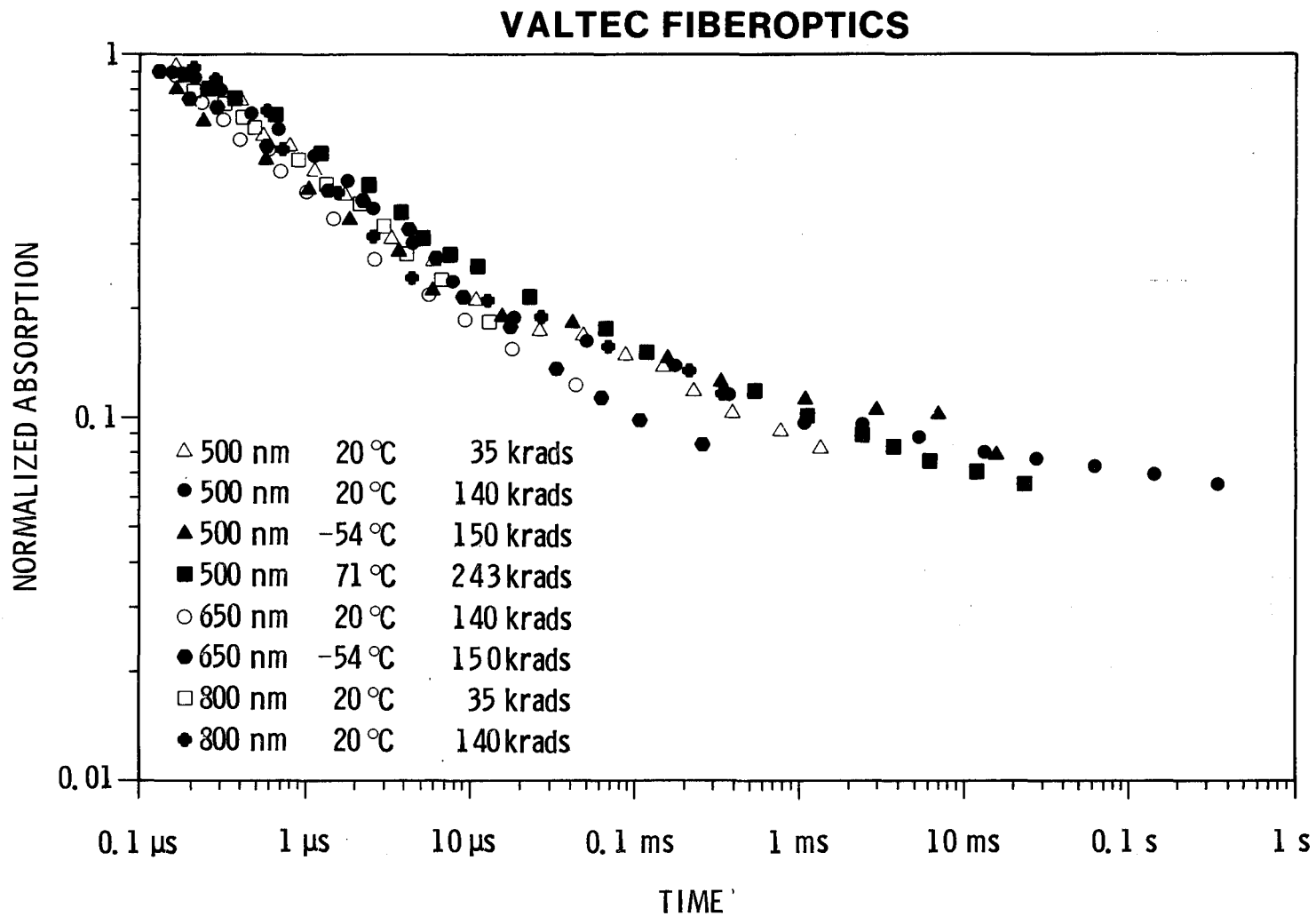


Figure 29. Transient Absorption Recovery in the Valtec Fiberoptic Fibers for Several Doses and Temperatures. The recovery is independent of dose, temperature, and wavelength. (Measurement error is less than 10 percent for times less than 0.1 ms, and less than 20 percent at longer times.)

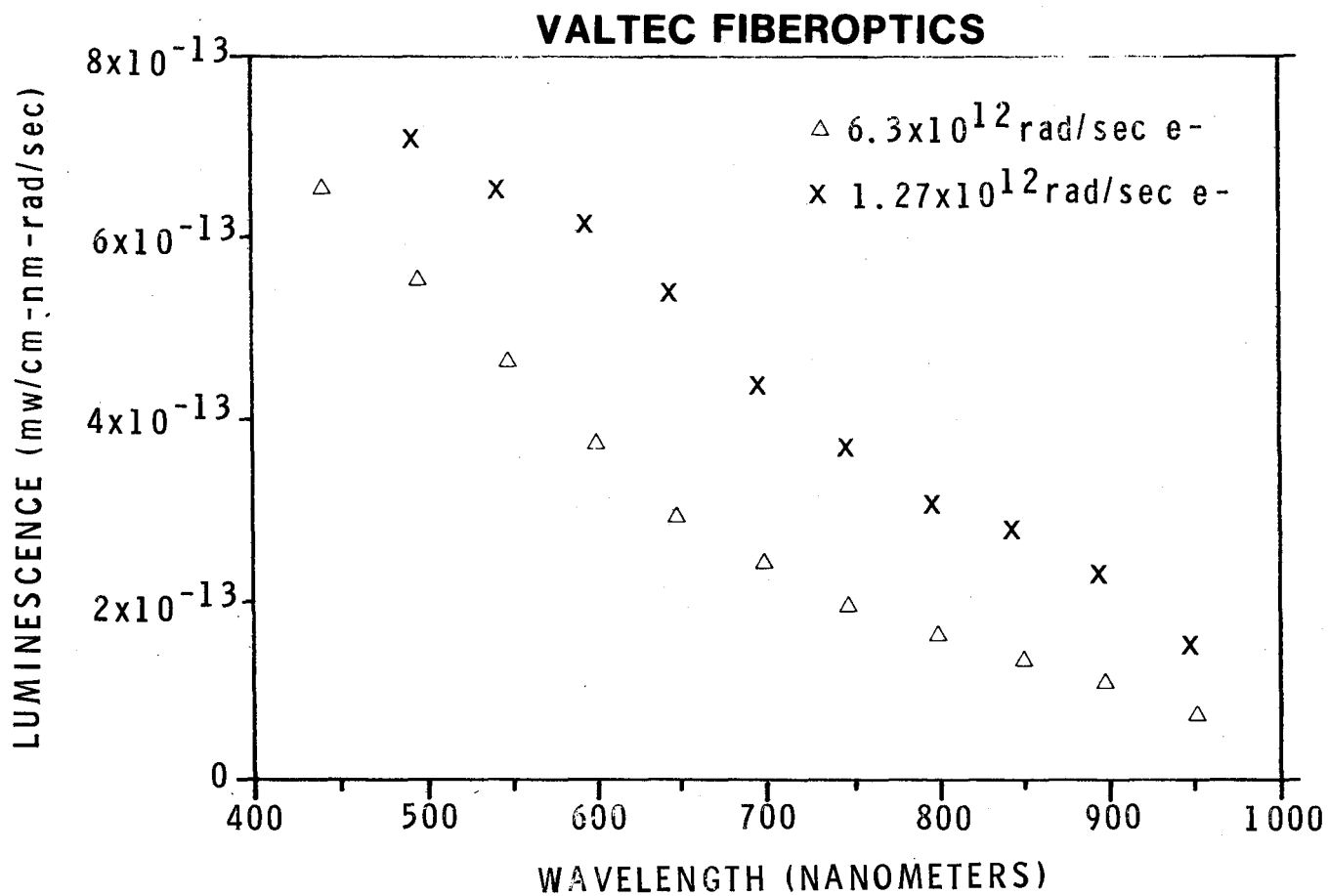


Figure 30. Transient Luminescence Spectra Induced in Valtec Fibers During Electron Irradiation. The ordinate is proportional to the detected power in milliwatts per exposed cm of fiber, per nanometer of effective detector bandwidth, per unit dose rate. Data were corrected for detector response, unirradiated fiber attenuation, and filter bandwidth. The data shown are for 17 Valtec fibers with a diameter of 0.12 mm.

BELL LABS

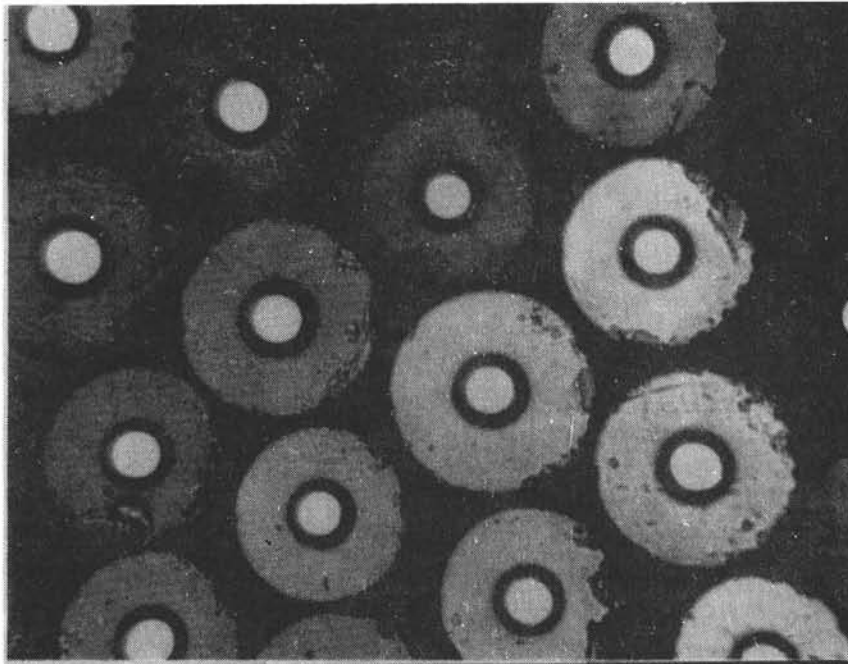
IV. BELL LABORATORIES PURE FUSED SILICA FIBERS

Manufacturer: Bell Laboratories
600 Mountain Avenue
Murray Hill, NJ 07974

Core: Pure Fused Silica

Cladding: $B_2O_3 - SiO_2$

Fiber Diameter: 0.125 mm



→ 0.1 mm ←

These research grade "pure" vitreous silica core fibers with glass cladding and glass sheath from Bell Telephone Laboratories (BTL) are also among the most radiation-resistant studied, showing results very similar to the Schott and Electro Fiberoptics data. The peak transient absorption is shown as a function of wavelength in Figures 31 and 32 for electron doses

of 70 and 230 krads, respectively. The peak in absorption at about 550 nm, which appears to be characteristic of the silica core fibers, again occurs.

The peak transient absorption as a function of dose is plotted in Figure 33 for wavelengths of 500 and 800 nm. Because of the small amount of fiber available, these data were obtained for several radiation exposures on the same section of fiber. The results are similar to those for the Schott data recorded on pre-irradiated fibers. The commercially available form of this fiber (with a plastic cladding) is now manufactured by Fiber-optic Cable Corporation, and additional data are reported in the following section.

The effect of temperature on the peak transient absorption is shown in Figures 34 and 35 as a function of dose at temperatures of -54, 20, and 71°C and for wavelengths of 500 and 800 nm.

The recovery data for the BTL fibers (Figure 36) differ from that for the "pure" vitreous silica fibers manufactured by Schott and by Valtec Fiberoptics in that the recovery of BTL fibers is not independent of temperature over the range from -54 to 71°C. The fact that the recovery rate increases with increasing temperature may indicate the presence of a thermally activated untrapping process. Moreover, it is tempting to surmise that the thermally activated process is similar to that observed in Schott fibers at -172°C, but with a lower temperature of onset.

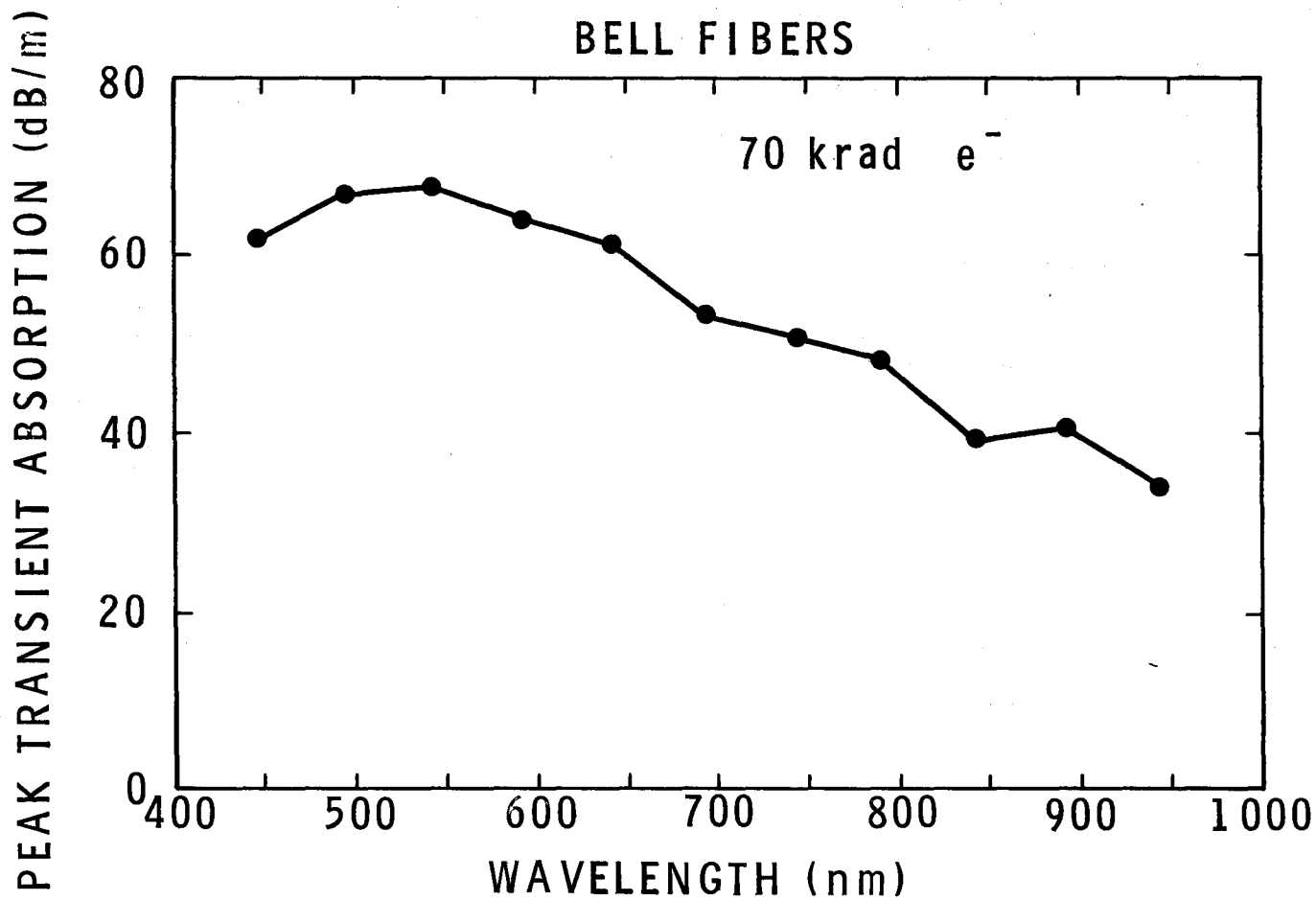


Figure 31. Peak Transient Absorption Spectrum for Bell Telephone Laboratories Pure Fused Silica Fibers Exposed to a 70 krad Electron Dose. (Measurement error is less than 10 percent of values plotted.)

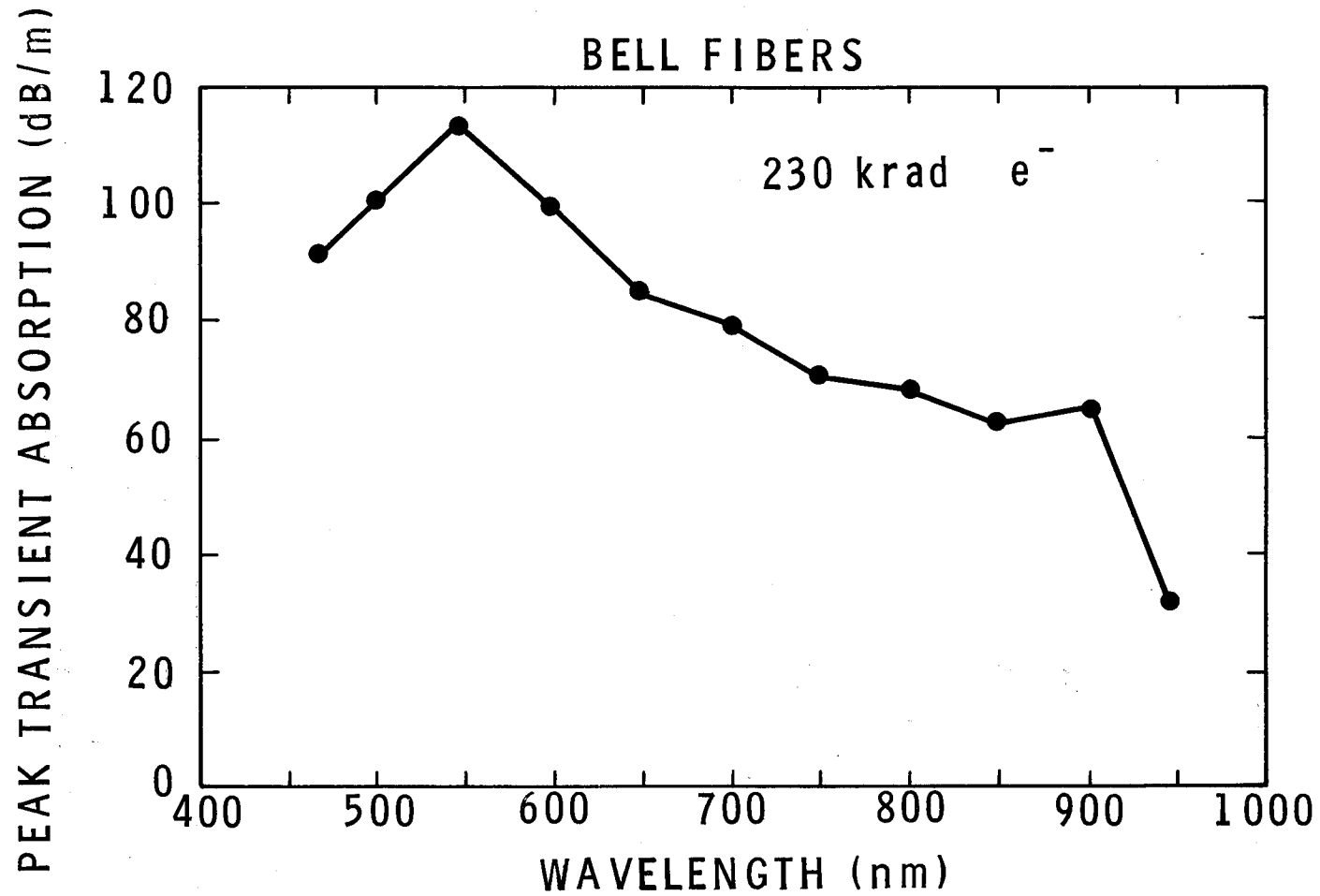


Figure 32. Peak Transient Absorption Spectrum for Bell Telephone Laboratories Pure Fused Silica Fibers Exposed to a 230 krad Electron Dose. (Measurement error is less than 10 percent of values plotted.)

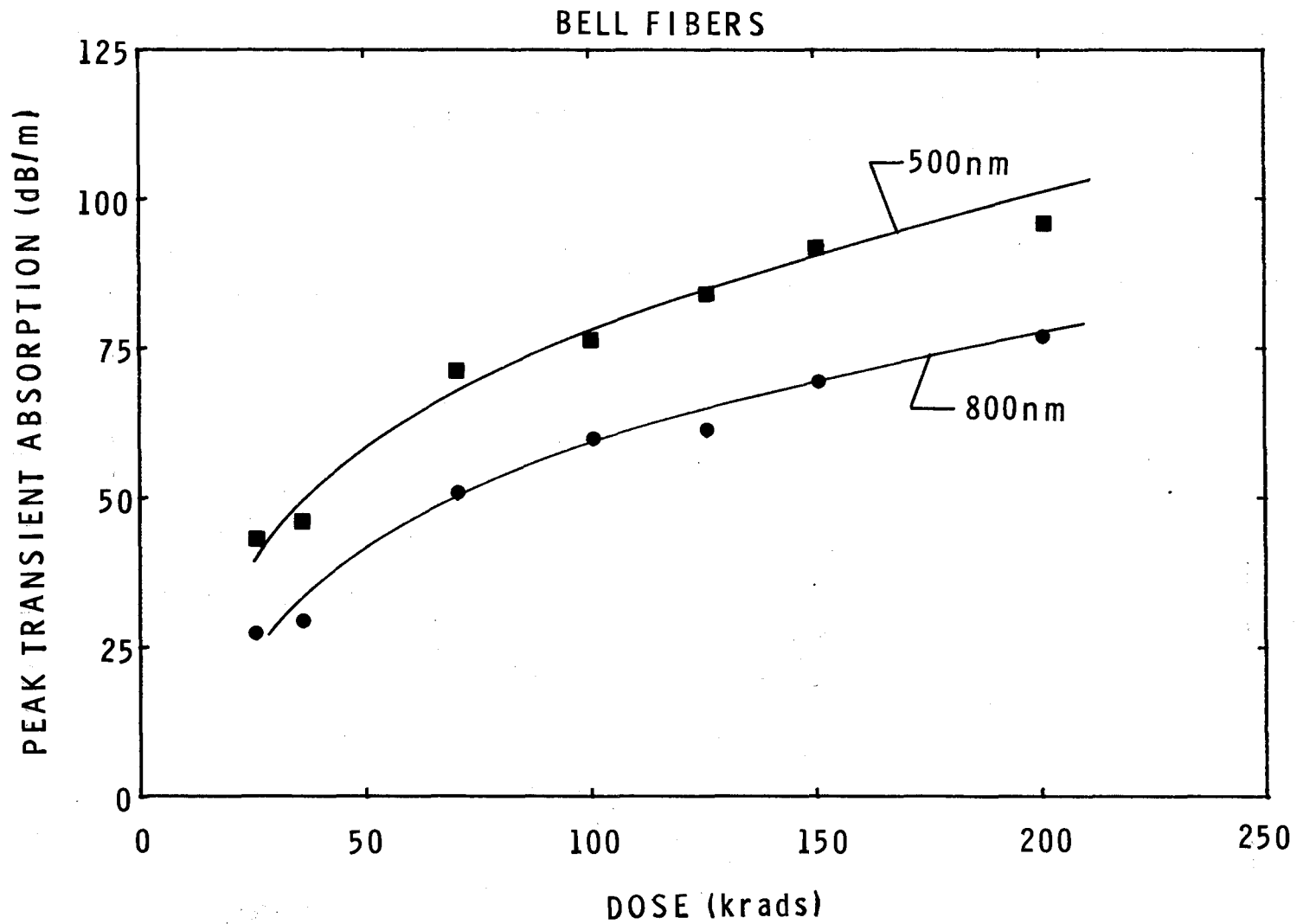


Figure 33. Peak Transient Absorption as a Function of Dose in the Bell Telephone Laboratories Fibers for Wavelengths of 500 and 800 nm. (Measurement error is less than 10 percent of values plotted.)

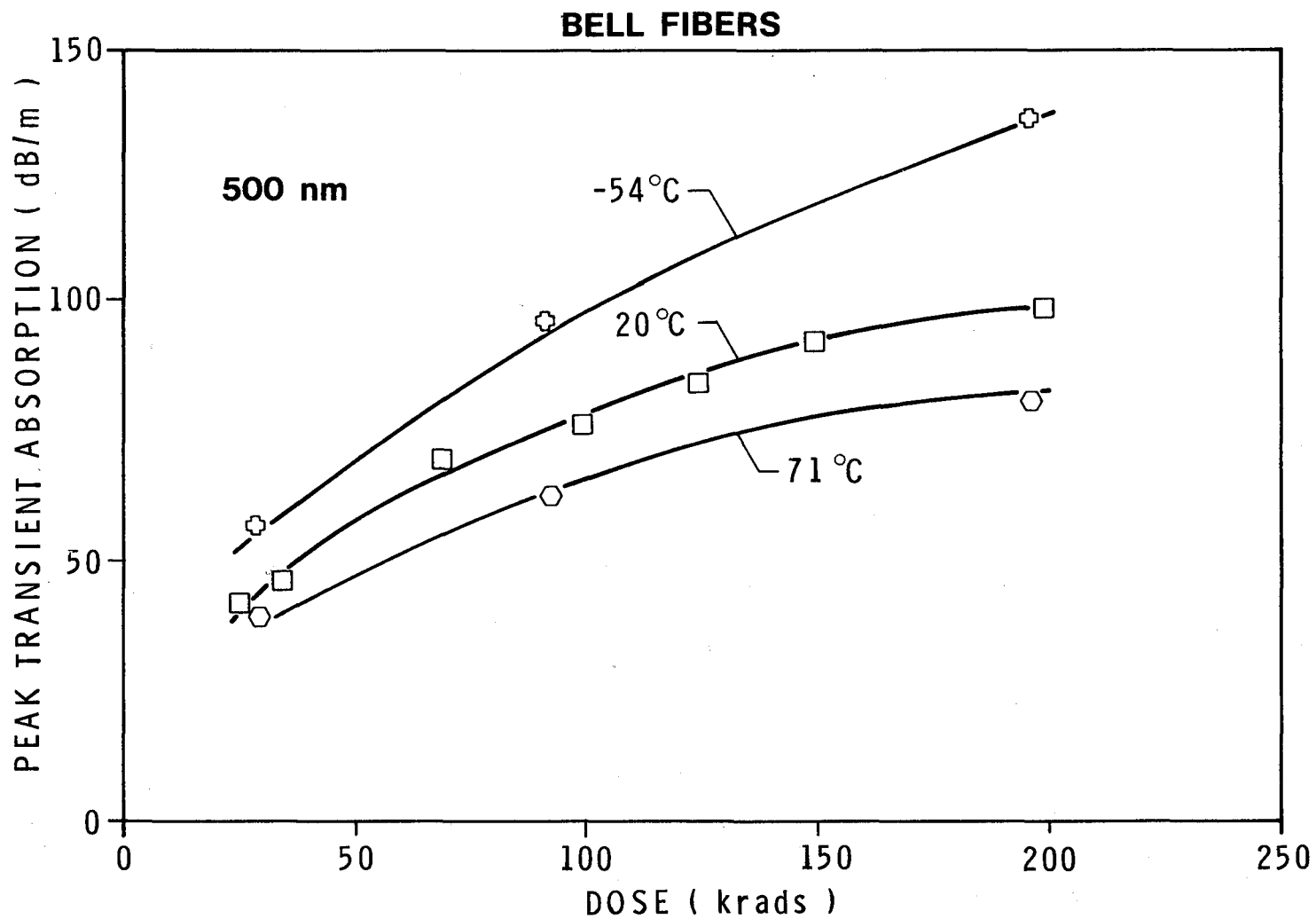


Figure 34. Peak Transient Absorption as a Function of Dose at 500 nm for Temperatures of -54, 20, and 71°C in Bell Telephone Laboratories Fibers. (Measurement error is less than 10 percent of values plotted.)

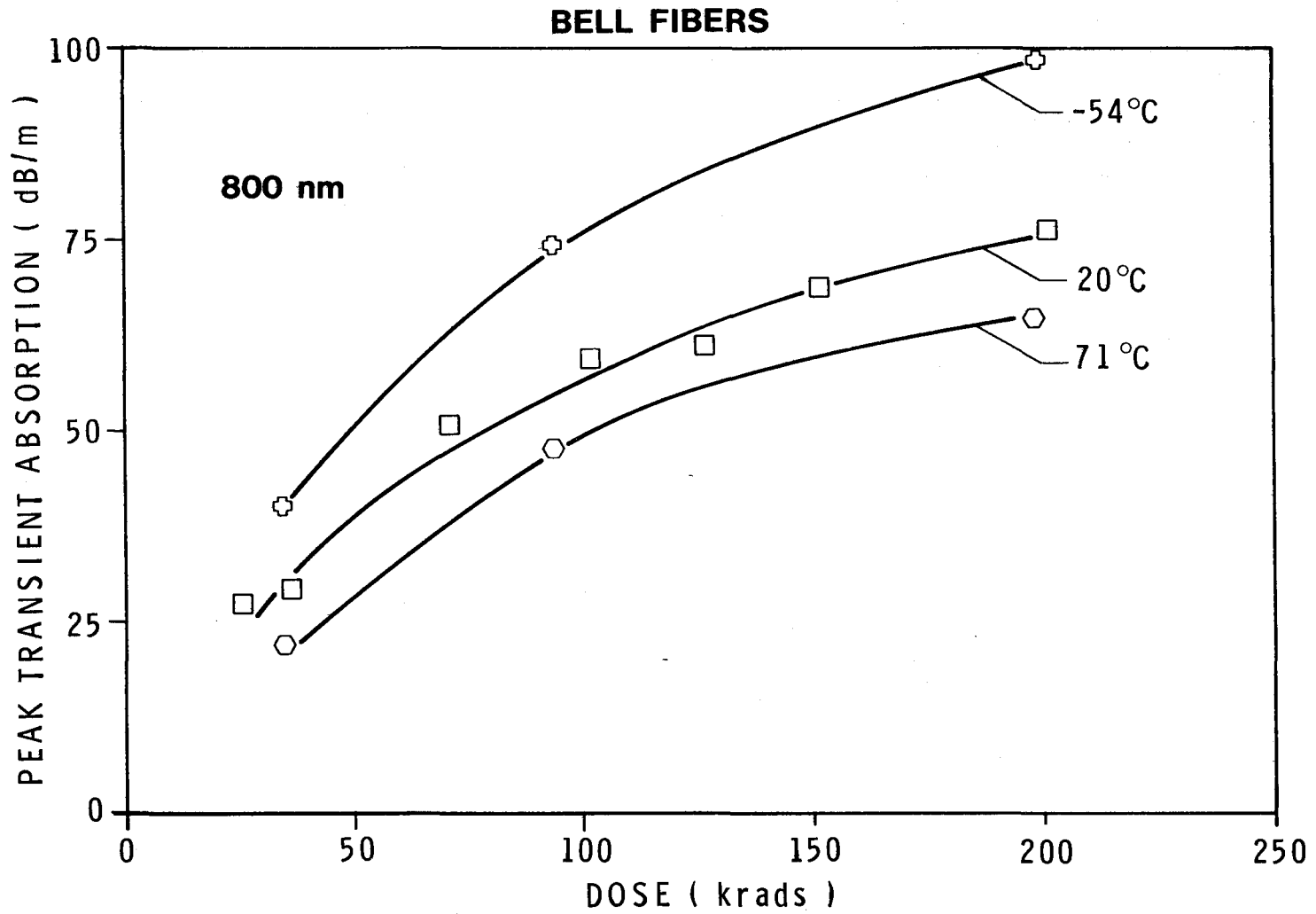


Figure 35. Peak Transient Absorption as a Function of Dose at 800 nm for Temperatures of -54, 20, and 71°C in Bell Telephone Laboratories Fibers. (Measurement error is less than 10 percent of values plotted.)

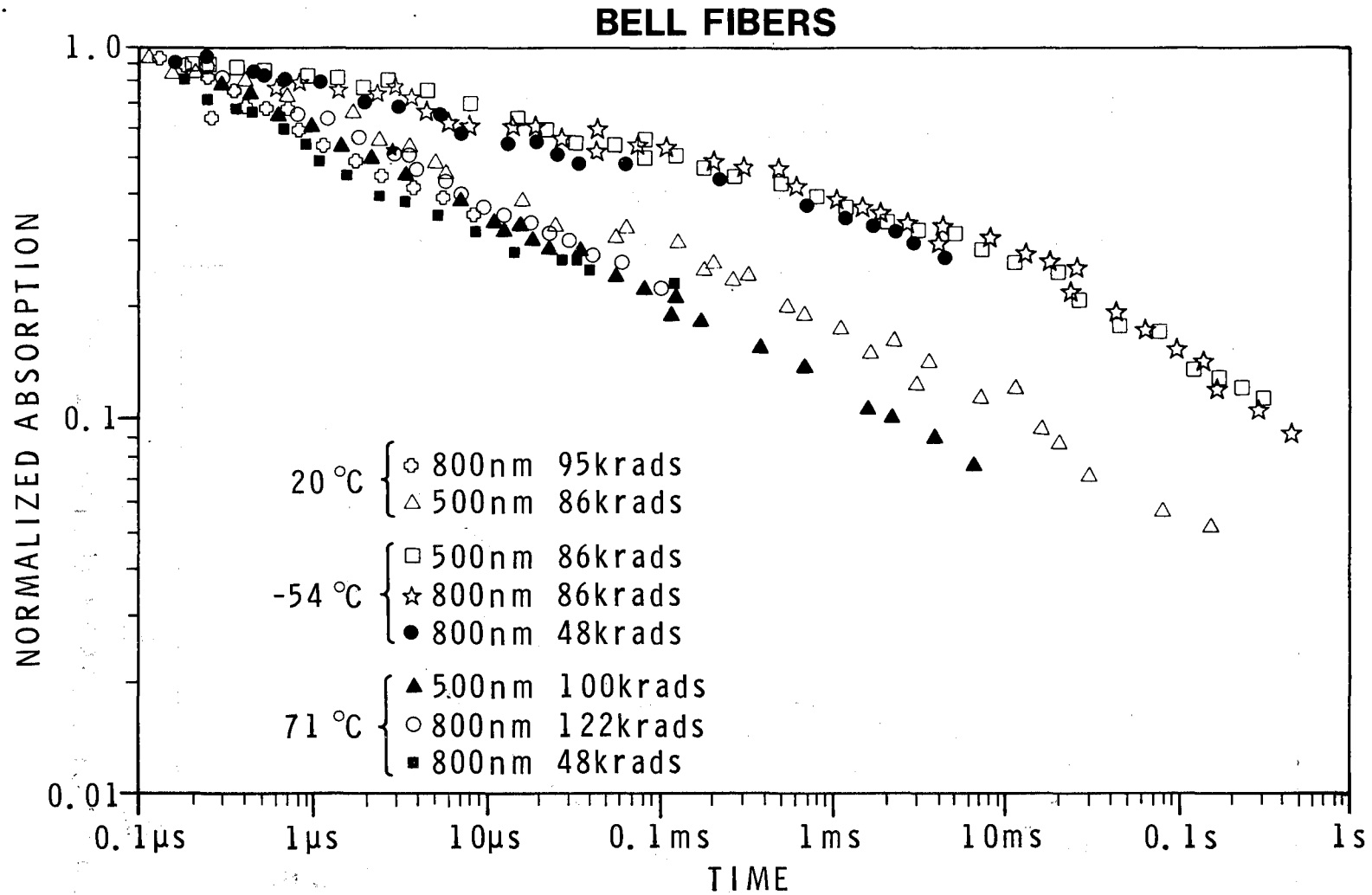


Figure 36. Transient Absorption Recovery in Pure Fused Silica Fibers From Bell Telephone Laboratories. A small temperature dependence is seen in the data with faster recovery at higher temperatures, while recovery is seen to be independent of dose and wavelength. (Measurement error is less than 10 percent of the values shown for times less than 0.1 ms, and less than 20 percent for longer times.)

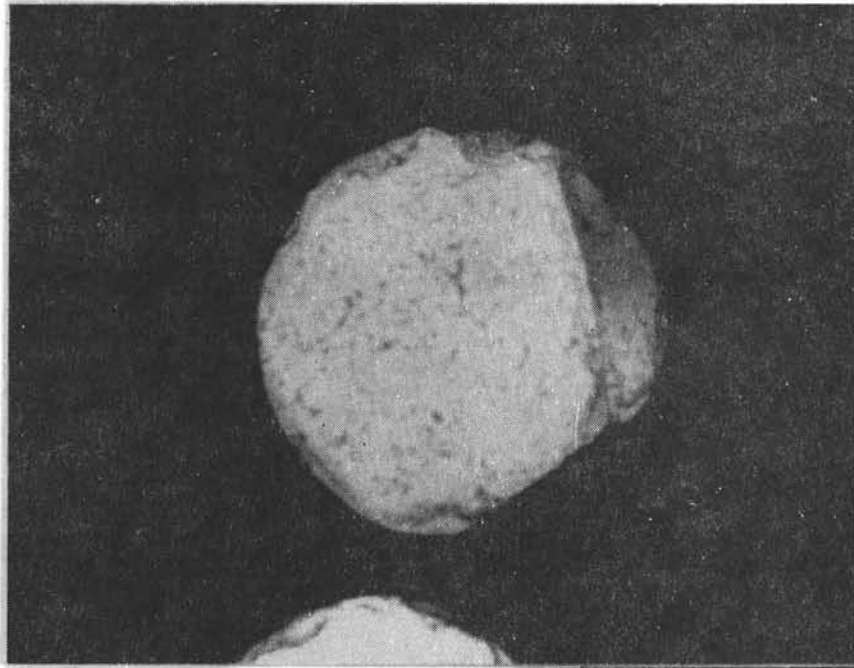
V. FIBEROPTIC CABLE CORPORATION PURE FUSED
SILICA FIBERS

Manufacturer: Fiberoptic Cable Corporation
P. O. Box 1492
Framingham, MA 01701

Core: Pure Fused Silica

Cladding: Optical quality plastic

Fiber Diameter: 0.25 mm



→ 0.1 mm ←

The plastic-clad, "pure" vitreous silica fibers produced by the Fiberoptic Cable Corporation are the commercially available forms of the Bell Telephone Laboratories research fiber described previously.

Peak transient absorptions as a function of wavelength are shown in Figures 37 and 38 for doses of 50 and 150 krads. The peak transient absorption obtained at 20°C is plotted as a function of dose and temperature in Figures 39 through 41 for wavelengths of 500 and 800 nm. In general, the results are similar to those for the other vitreous silica fibers studied; that is, the absorption increases with decreasing temperature, and the absorption at a dose of 250 krads is about three times larger at a temperature of -54 than at 71°C.

The recovery data for these fibers (Figure 42) show the normalized recovery to be independent of dose wavelength and temperature within the limits of measurement error. The recovery is similar to that for Valtec Fiberoptics fibers and slightly slower than that for Schott fibers.

FIBEROPTIC CABLE CORP

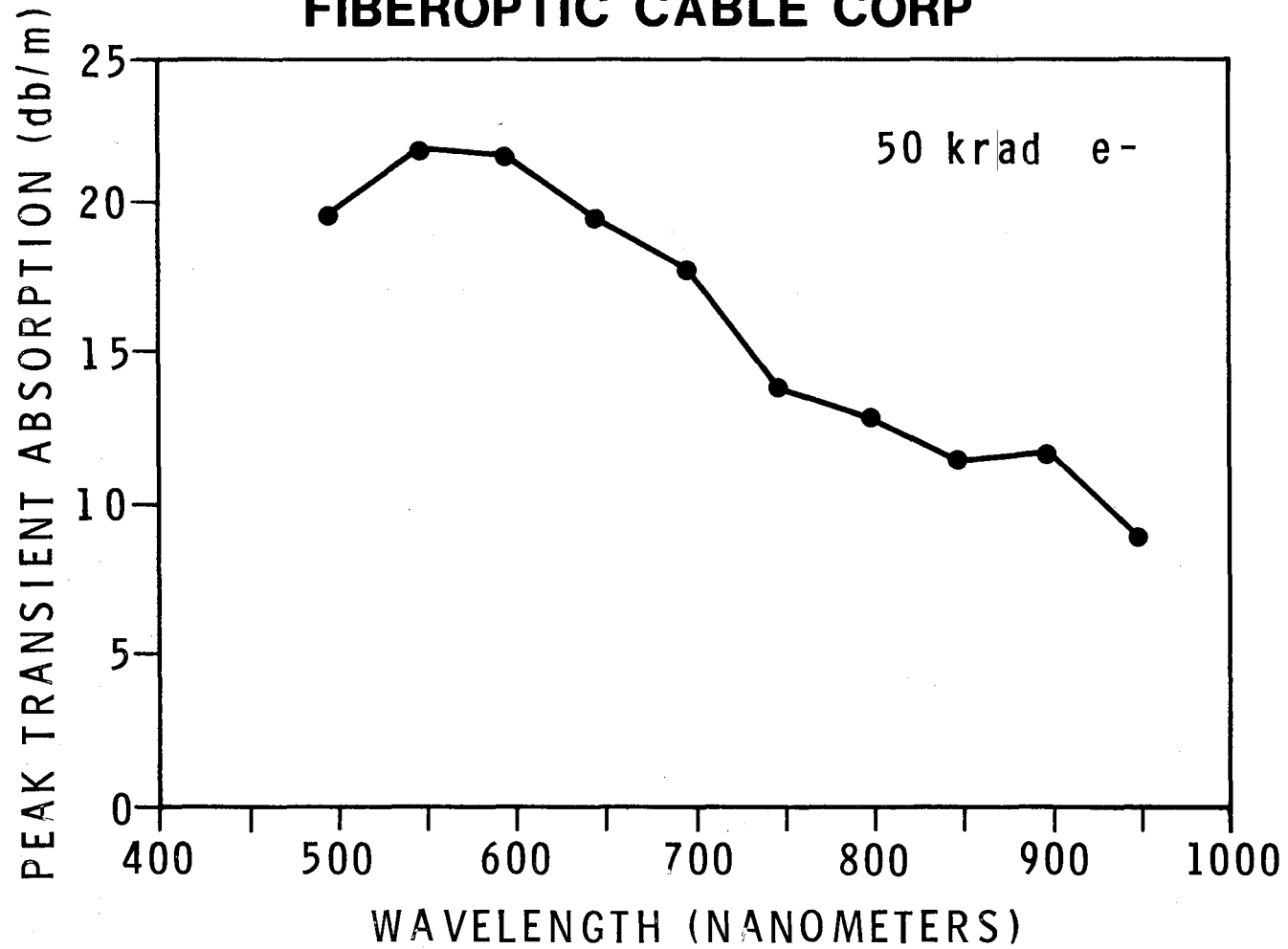


Figure 37. Peak Transient Absorption Spectrum for Fiberoptic Cable Corporation Pure Fused Silica Fibers Exposed to a 50 krad Electron Dose. (Measurement error is less than 10 percent of values plotted.)

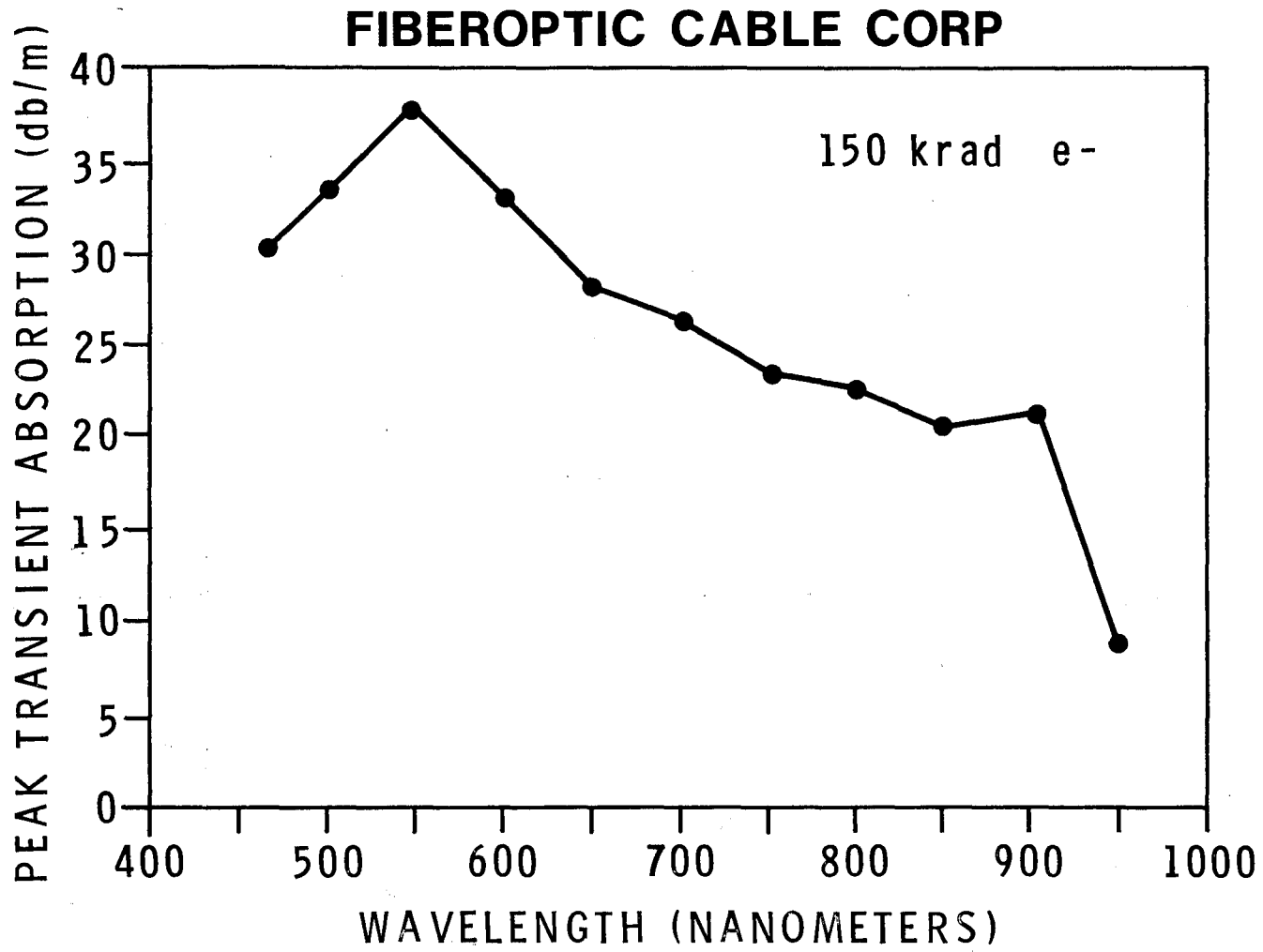


Figure 38. Peak Transient Absorption Spectrum for Fiberoptic Cable Corporation Pure Fused Silica Fibers Exposed to a 150 krad Electron Dose. (Measurement error is less than 10 percent of values plotted.)

FIBEROPTIC CABLE CORP

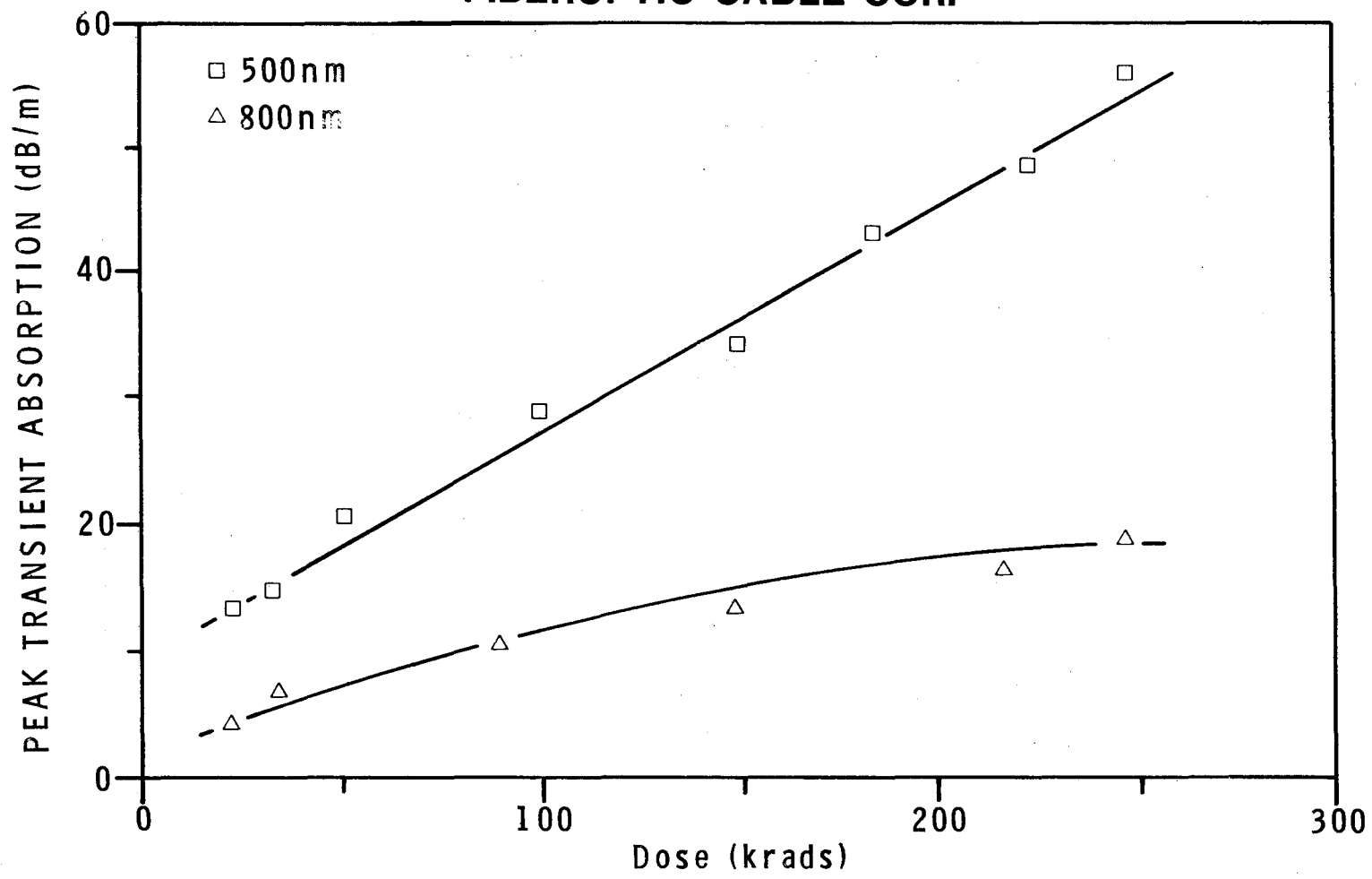


Figure 39. Peak Transient Absorption as a Function of Dose in the Fiberoptic Cable Corporation Fibers for Wavelengths of 500 and 800 nm. (Measurement error is less than 10 percent of values plotted.)

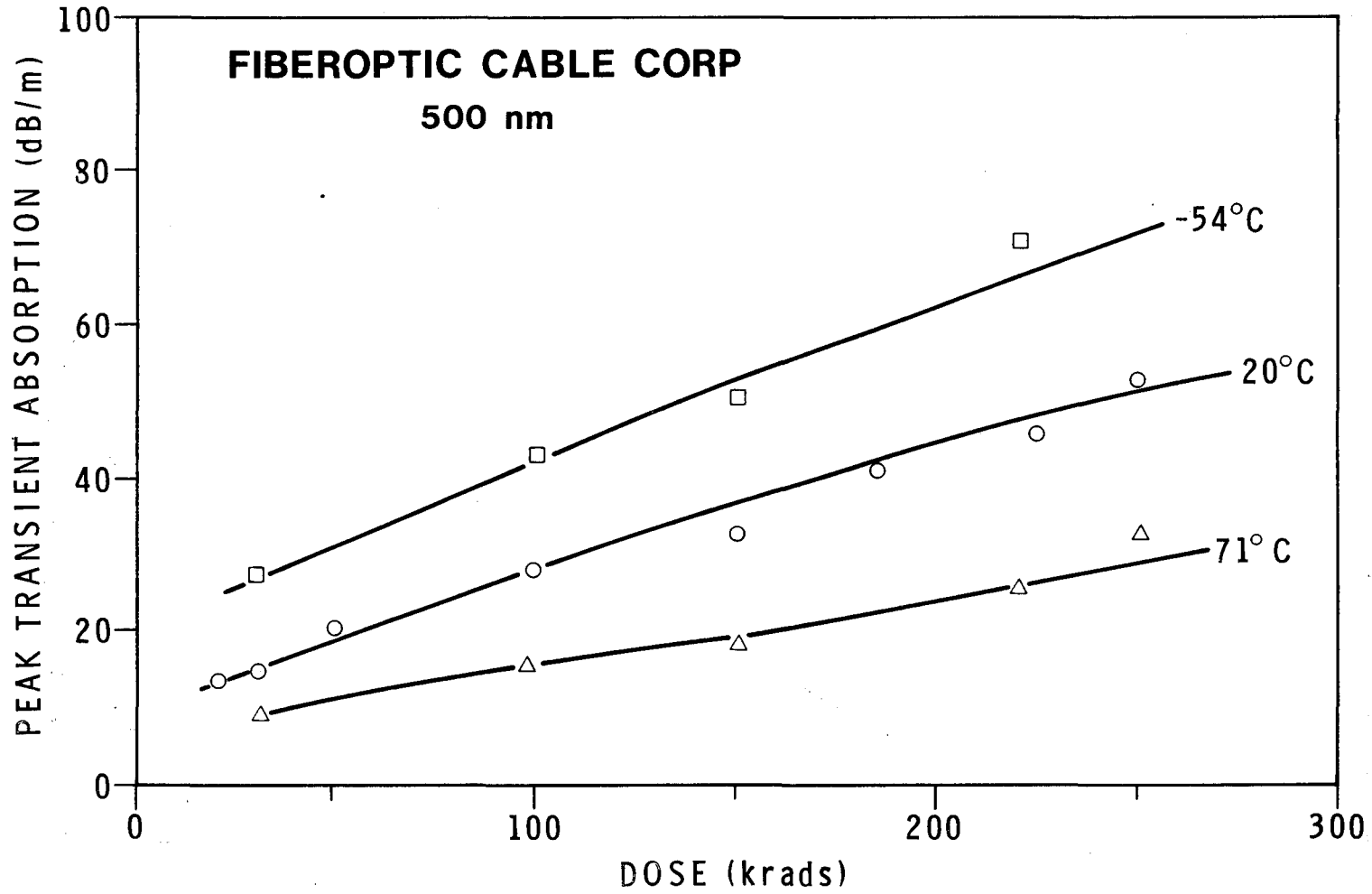


Figure 40. Peak Transient Absorption as a Function of Dose at 500 nm for Temperatures of -54, 20, and 71°C in Fiberoptic Cable Corporation Fibers. (Measurement error is less than 10 percent of values plotted.)

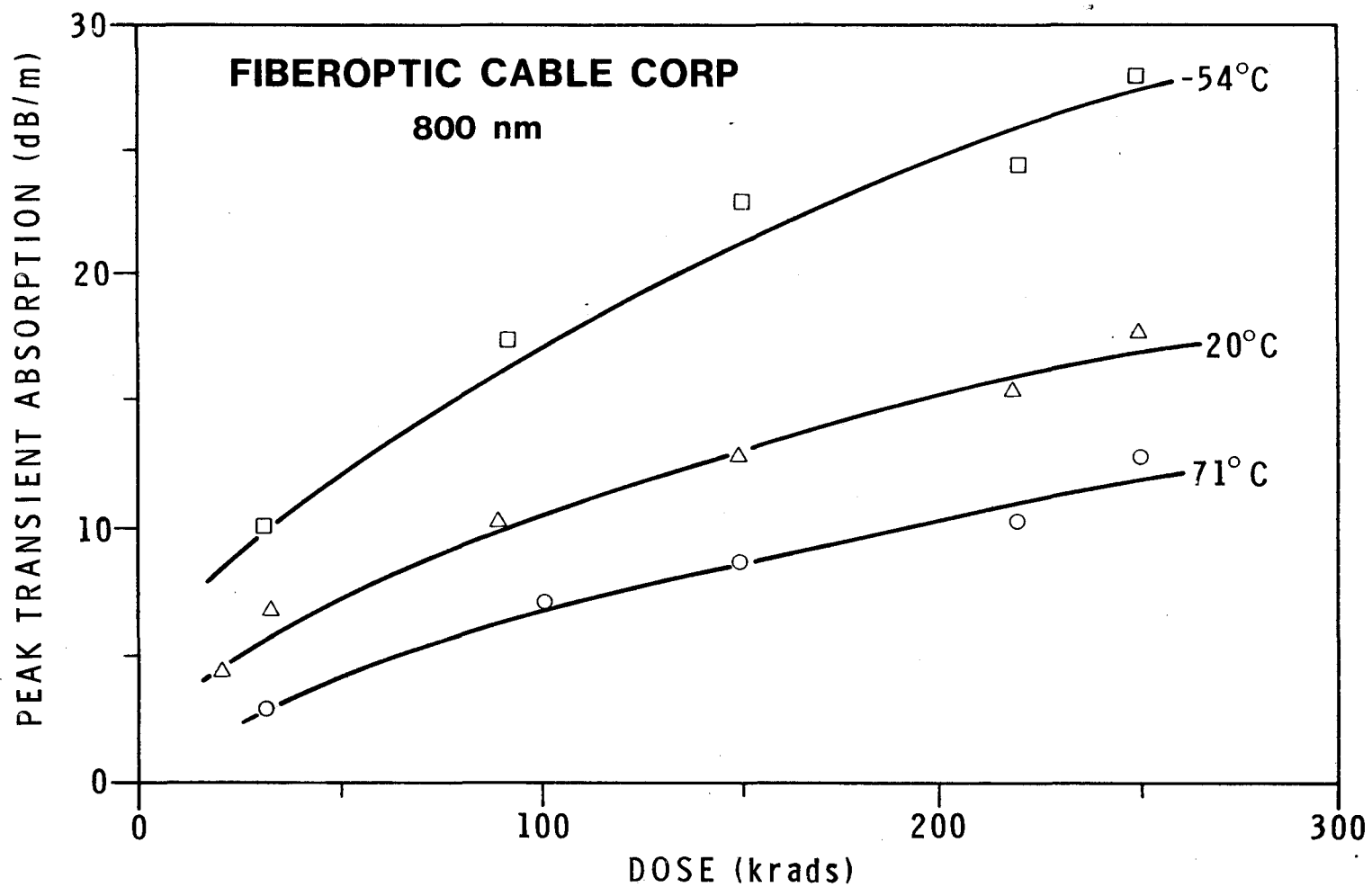


Figure 41. Peak Transient Absorption as a Function of Dose at 800 nm for Temperatures of -54, 20, and 71°C in Fiberoptic Cable Corporation Fibers. (Measurement error is less than 10 percent of values plotted.)

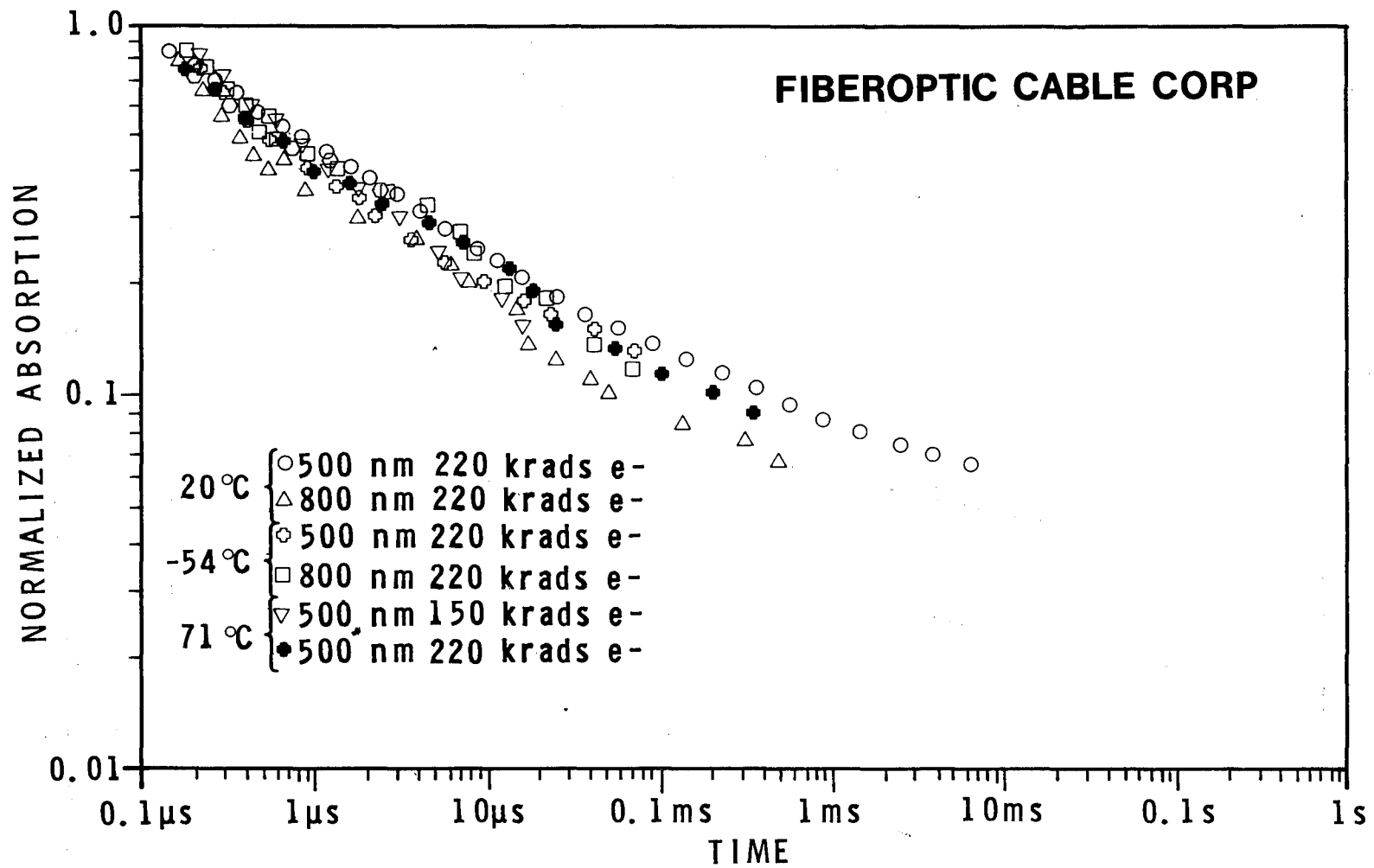


Figure 42. Transient Absorption Recovery in the Plastic-Clad Fused Silica Fibers From Fiberoptic Cable Corporation. The recovery is independent of dose, wavelength, and temperature.

FIBEROPTIC CABLE CORP

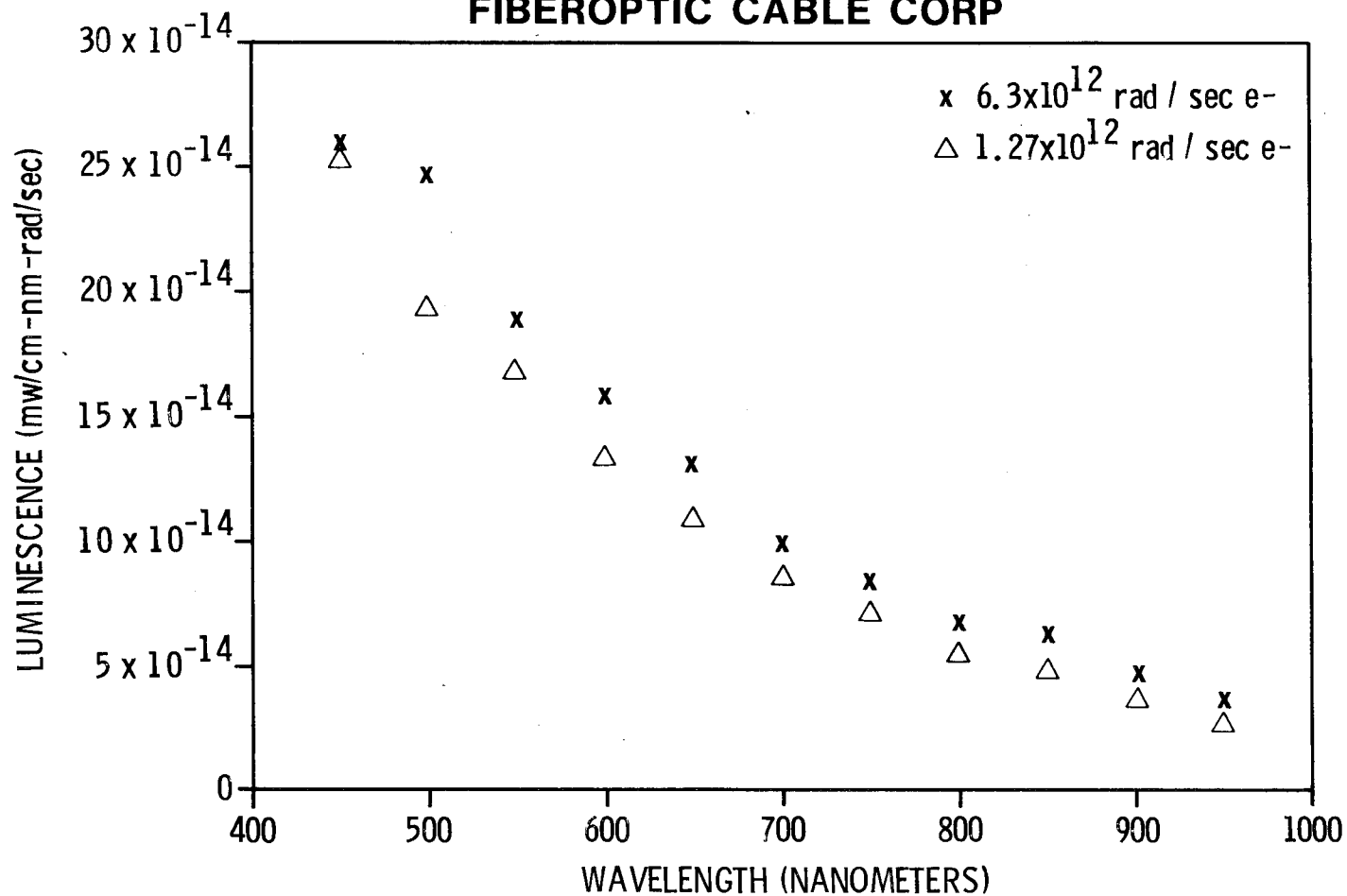


Figure 43. Transient Luminescences Spectra for Electron Irradiations in the Fused Silica Fibers From Fiberoptic Cable Corporation. The ordinate is proportional to the detected power in milliwatts per exposed centimeter of fiber, per nanometer of the effective detector bandwidth, per unit dose rate. Data were corrected for detector response, unirradiated fiber attenuation, and filter bandwidth. Data shown are for six Fiberoptic Cable Corporation fibers with a diameter of 0.25 mm.

VI. POLYSTYRENE CORE FIBERS

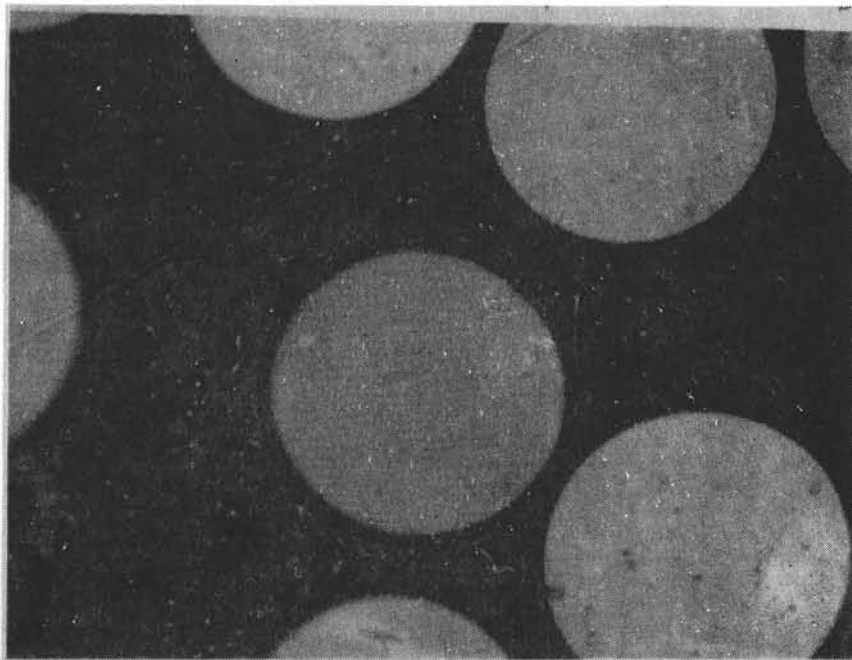
Manufacturers: International Fiberoptics
2644 Buckaroo Avenue
Oxnard, CA 93030

Poly-Optics, Incorporated
1815 East Carnegie
Santa Ana, CA 92705

Core: Polystyrene

Cladding: Polymethylmethacrylate (PMMA)

Fiber Diameter: 0.13 - 0.25 mm



→ 0.1 mm ←

The transient response of polystyrene core fibers to radiation is significantly different from that of the glass fibers studied. One striking difference is the shape of the curves for peak absorption versus wavelength (Figures 44 through 47) for a 1 krad X-ray dose, and for electron doses of 6, 30, and 300 krads. In all cases, a minimum in the peak value of induced absorption is observed in the wavelength region from 600 to 700 nm. The other fibers studied show an absorption peak at short wavelengths, with monotonically decreasing absorption values toward the longer wavelengths.

The peak absorption is shown as a function of dose in Figure 48 for wavelengths of 500, 650, and 800 nm. The insert shows data obtained using low doses of X rays. In general, the peak transient absorption values are larger than those observed in the "pure" vitreous silica core fibers. Although the peak, as well as the unirradiated, absorption values are larger than those for vitreous silica fibers, the plastic fibers are less expensive and have applications in short fiber lengths.

The effect of temperature on the peak transient absorption is much less pronounced in the plastic fibers than in the glass fibers studied. The peak transient absorptions are shown as a function of dose at temperatures of -54, 20, and 71°C in Figures 49 through 51 for wavelengths of 500, 650, and 800 nm.

The recovery behavior of the polystyrene core fibers is rather strongly affected by temperature (Figure 52), although independent of wavelength and dose within the limits of experimental error. For times greater than approximately 10 ms the recovery curves for all temperatures are approximately described by $\tau^{-1/4}$. This dependence also describes the temperature-independent portions of the recovery curves for vitreous silica fibers and for the other plastic fibers; however, it appears that a temperature-dependent mechanism is operating at short times ($<0.1 \mu\text{s}$) and is causing an increase in recovery rate with increasing temperature.

A noteworthy characteristic of the response of plastic fibers is the effect of environment on recovery behavior. As Figure 53 shows, recovery is slowed substantially when the fibers are irradiated and held in vacuum (~ 10 microns); and similar results are obtained when the irradiation occurs in a dry nitrogen atmosphere created by evacuating the exposure chamber and back-filling with nitrogen. Moreover, subsequent exposure to oxygen will speed up the recovery of fiber irradiated in an oxygen-free environment. The magnitude of the environmental effect, the fact of occurrence in a nitrogen environment, and a correlation of its onset with known diffusion rates,¹³ indicate that molecular oxygen scavenges the absorption centers, thereby increasing the recovery rate. The data in Figure 53 show that the recovery curves for vacuum-irradiated fibers are independent of temperature, a finding which implies the applicability of a tunneling model, as was observed for Schott, PFX, and Crofon fibers.

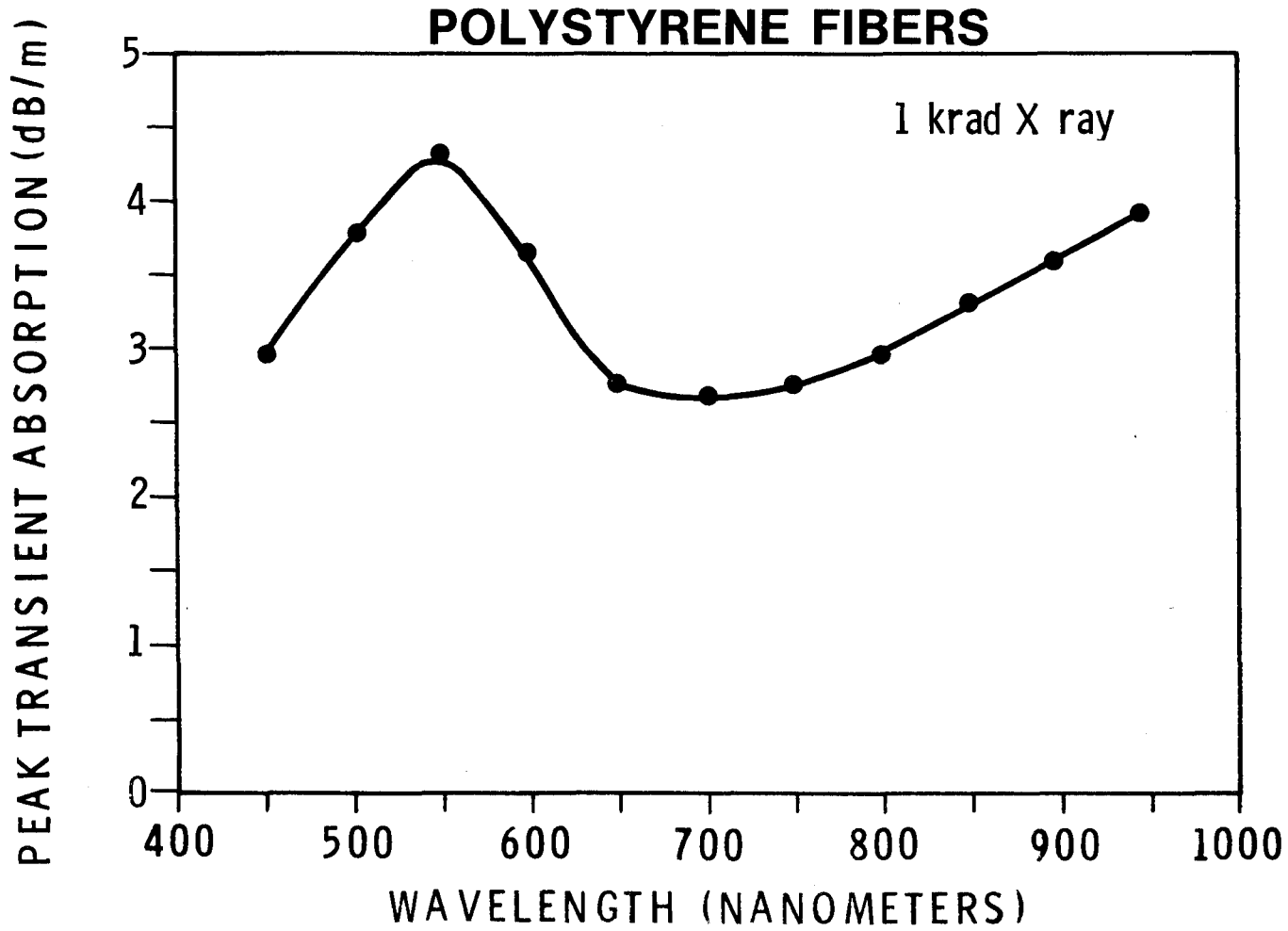


Figure 44. Peak Transient Absorption Spectrum in Polystyrene Fibers for an X-ray Dose of 1 krad. (Measurement error is less than 10 percent of values plotted.)

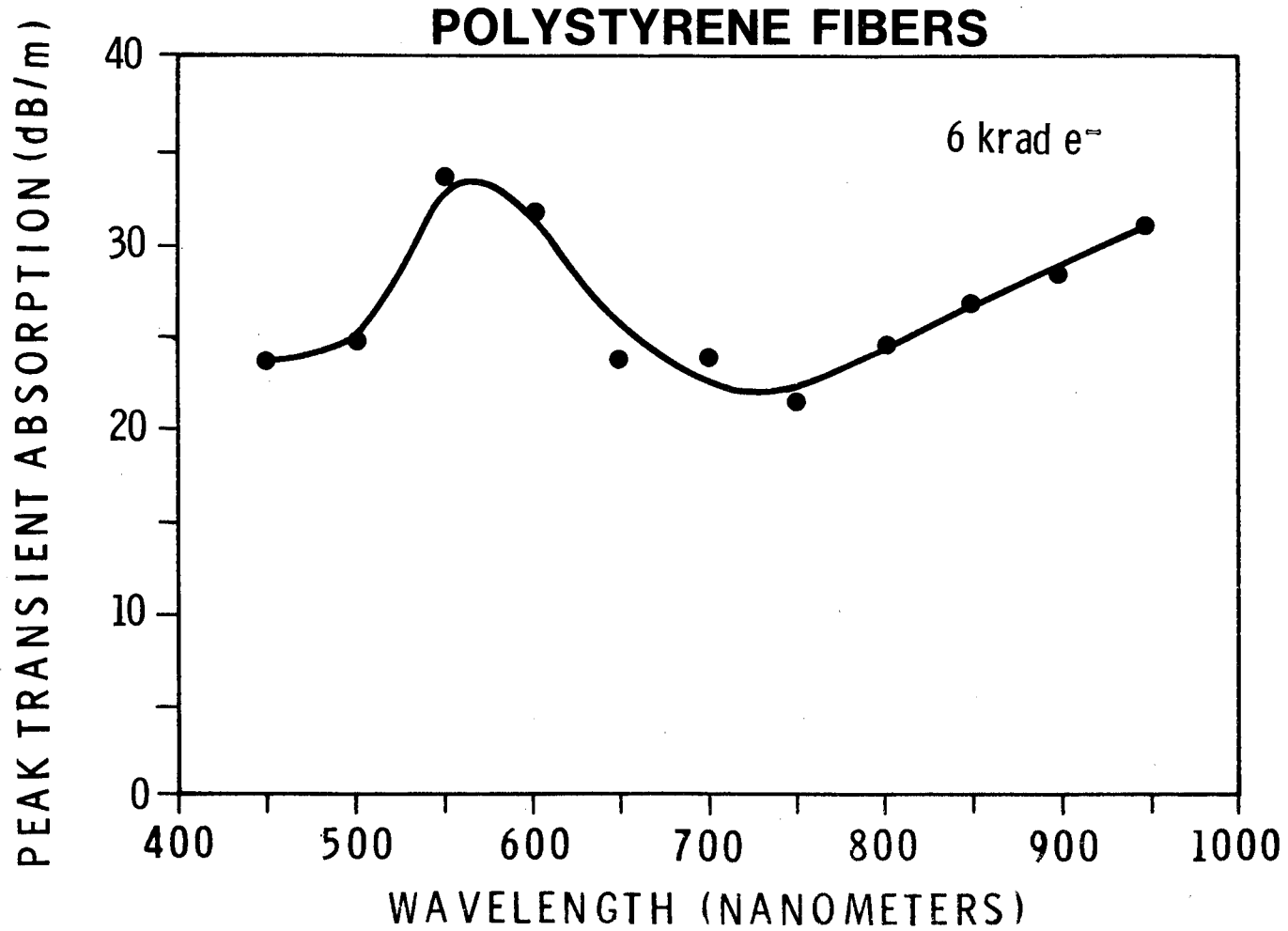


Figure 45. Peak Transient Absorption Spectrum in Polystyrene Fibers for an Electron Dose of 6 krad. (Measurement error is less than 10 percent of values plotted.)

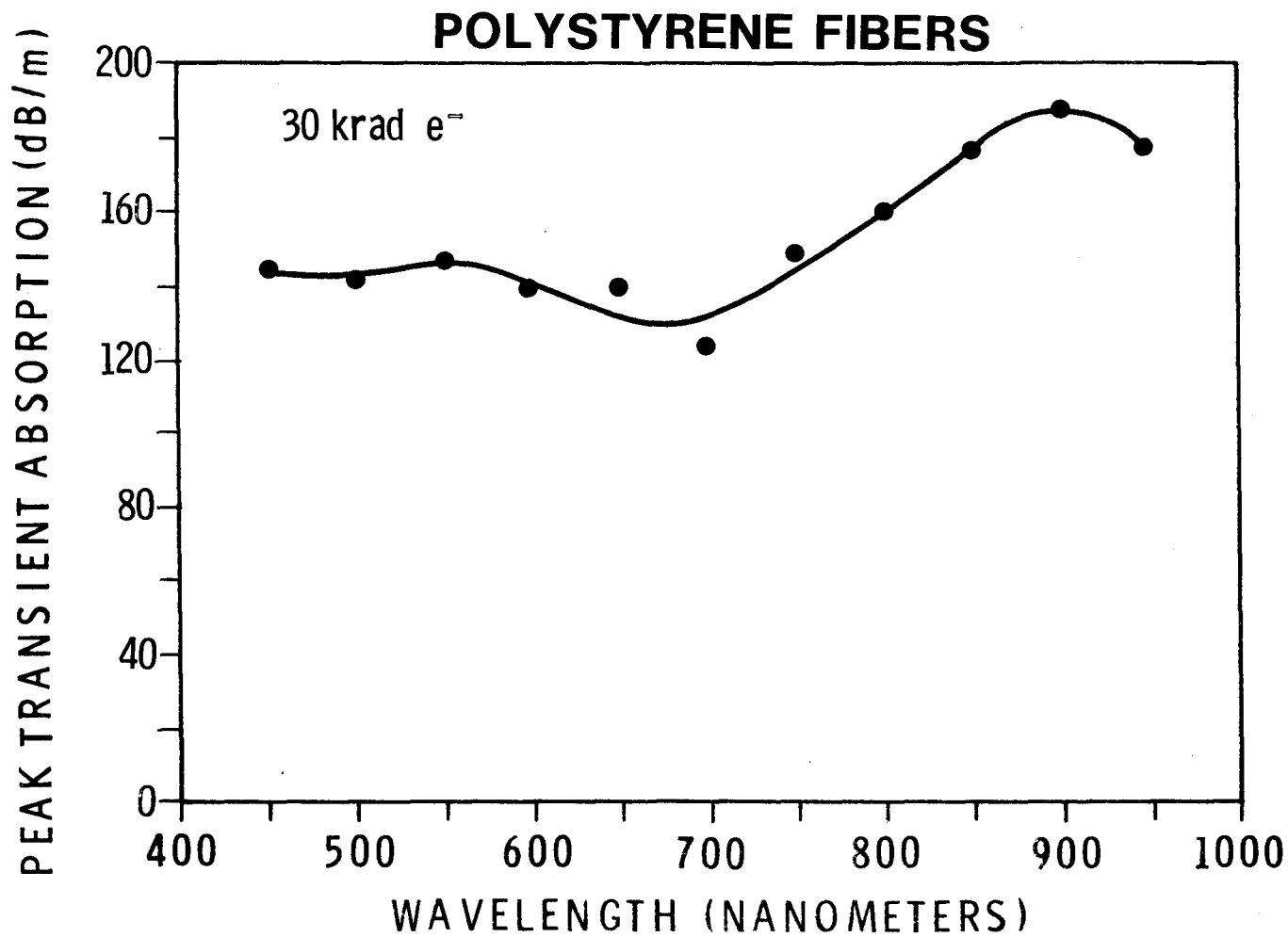


Figure 46. Peak Transient Absorption Spectrum in Polystyrene Fibers for an Electron Dose of 30 krad. (Measurement error is less than 10 percent of values plotted.)

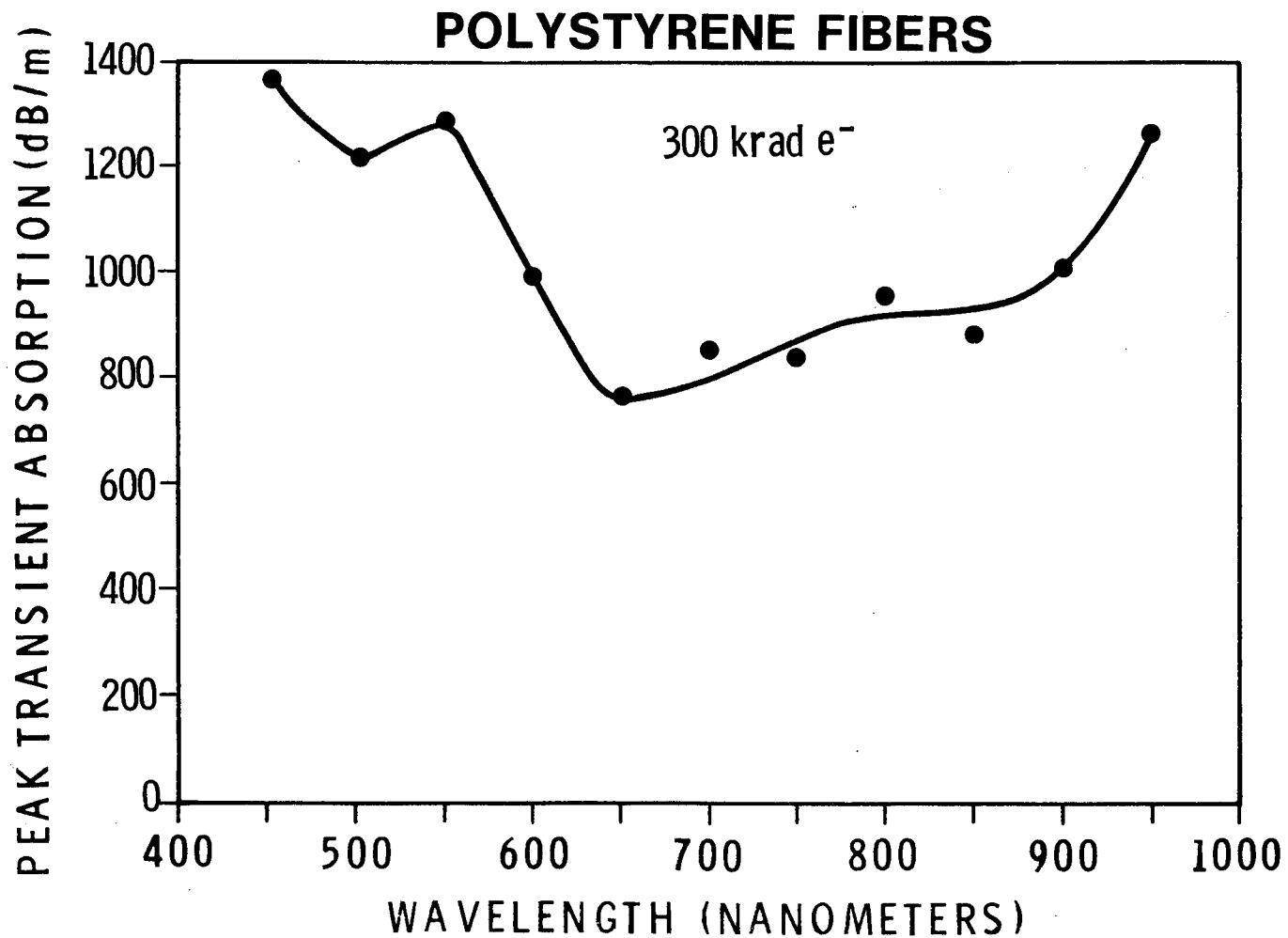


Figure 47. Peak Transient Absorption Spectrum in Polystyrene Fibers for an Electron Dose of 300 krad. (Measurement error is less than 10 percent of values plotted.)

POLYSTYRENE FIBERS

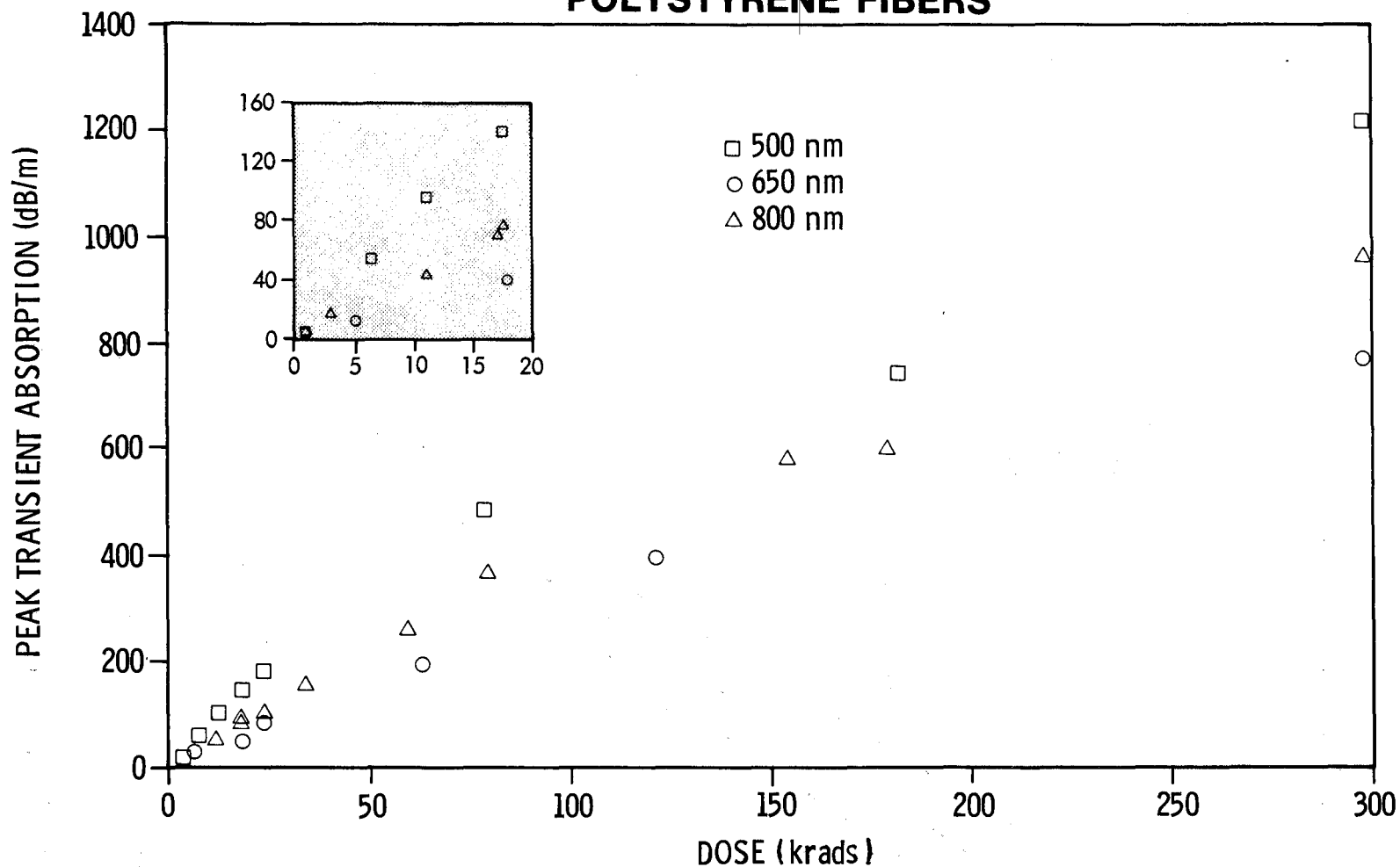


Figure 48. Peak Induced Absorption as a Function of Dose in Polystyrene Core Fibers for Wavelengths of 500, 650, and 800 nm. The insert provides an expanded scale for low doses. (Measurement error is less than 10 percent of values plotted.)

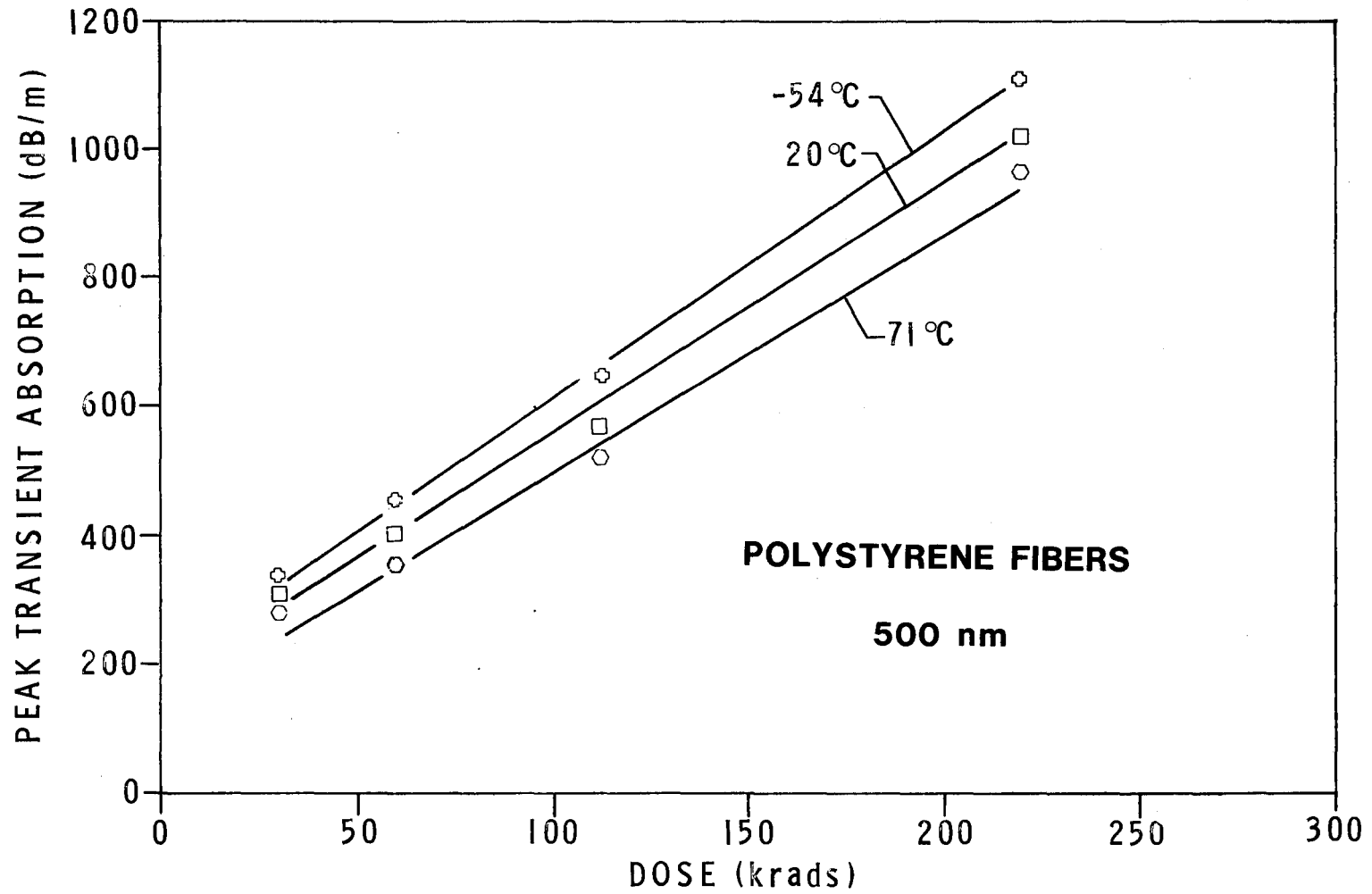


Figure 49. Peak Transient Absorption as a Function of Dose at 500 nm for Temperatures of -54, 20, and 71°C in Polystyrene Core Fibers. (Measurement error is less than 10 percent of values plotted.)

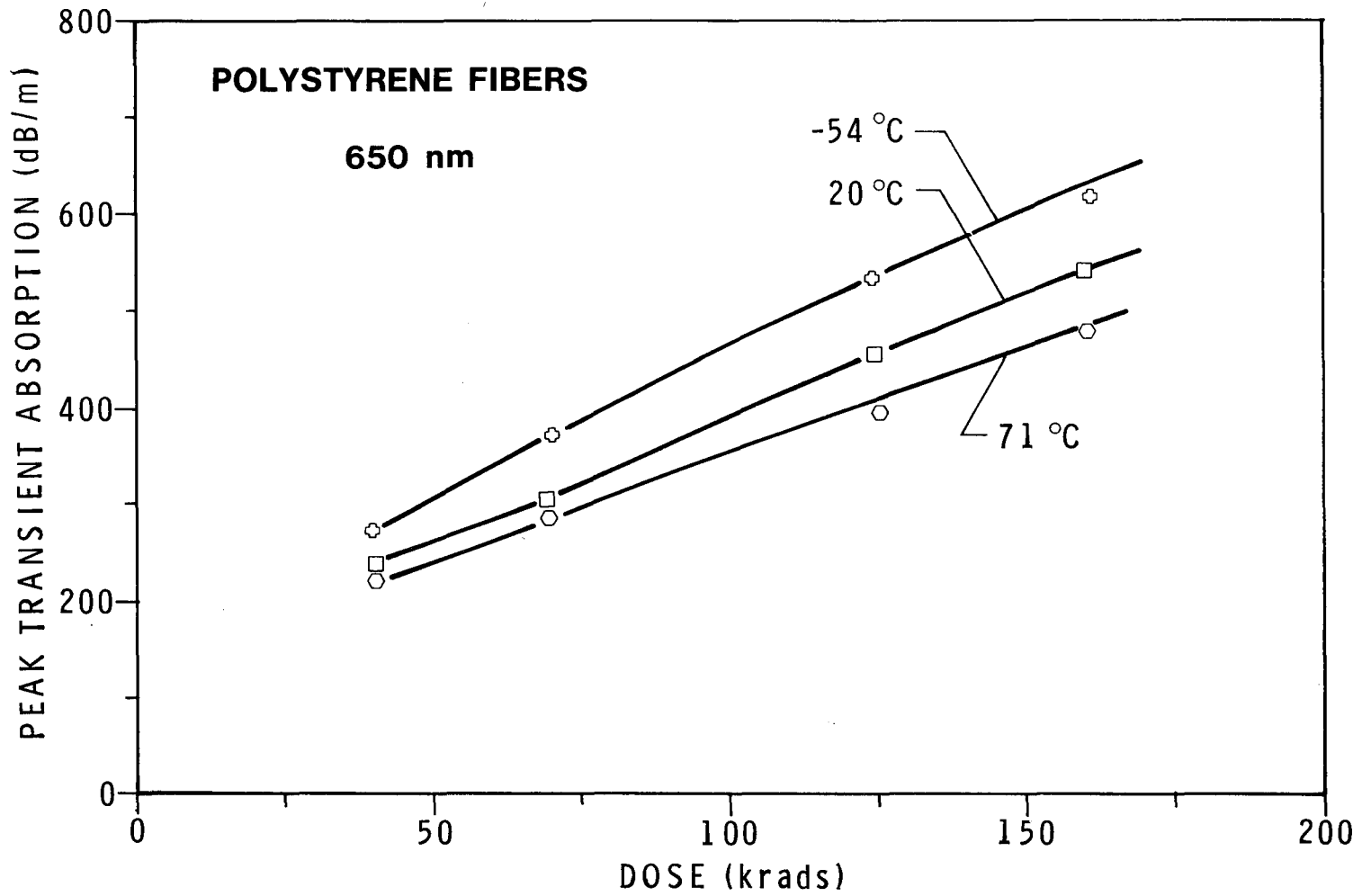


Figure 50. Peak Transient Absorption as a Function of Dose at 650 nm for Temperatures of -54, 20, and 71°C in Polystyrene Core Fibers. (Measurement error is less than 10 percent of values plotted.)

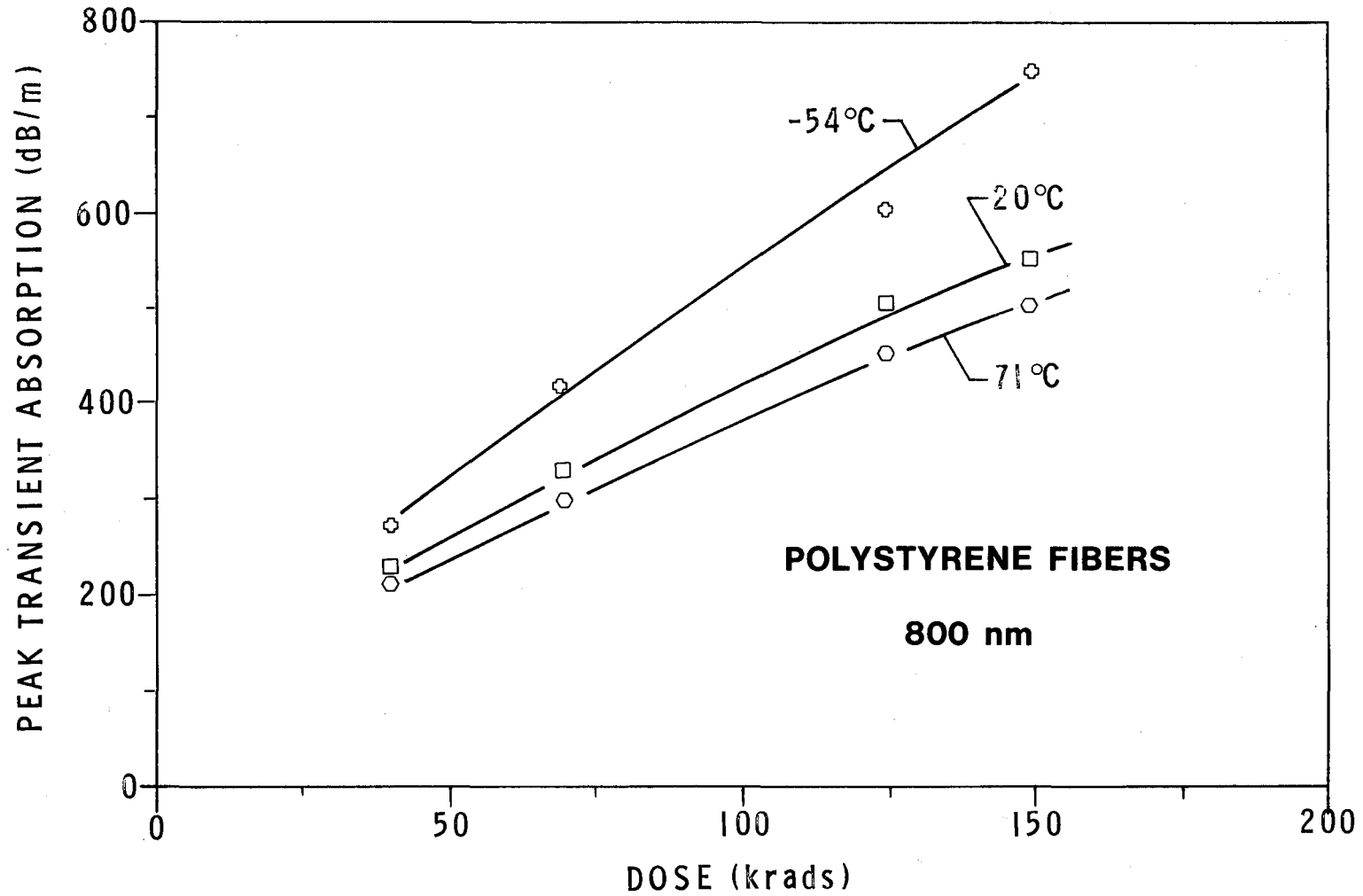


Figure 51. Peak Transient Absorption as a Function of Dose at 800 nm for Temperatures of -54, 20, and 71°C in Polystyrene Core Fibers. (Measurement error is less than 10 percent of values plotted.)

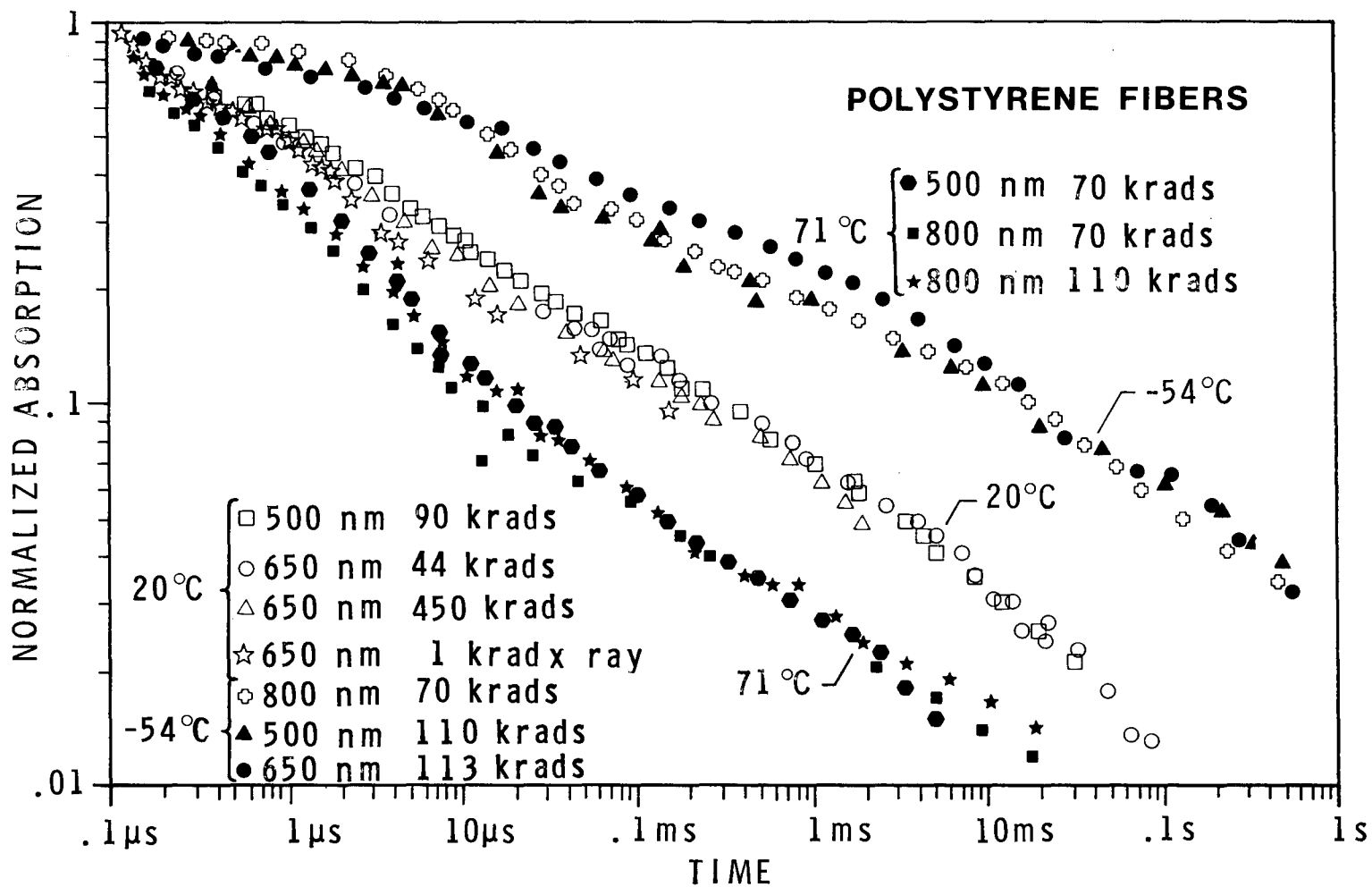


Figure 52. Transient Absorption Recovery in Polystyrene Core Fibers. The slopes of all curves approach $t^{-1/4}$ at long times. The same is true for the temperature-independent recovery in vitreous silica and Du Pont PFX fibers. However, there appears to be a temperature-dependent mechanism operating at short times, increasing the recovery rate with increasing temperature.

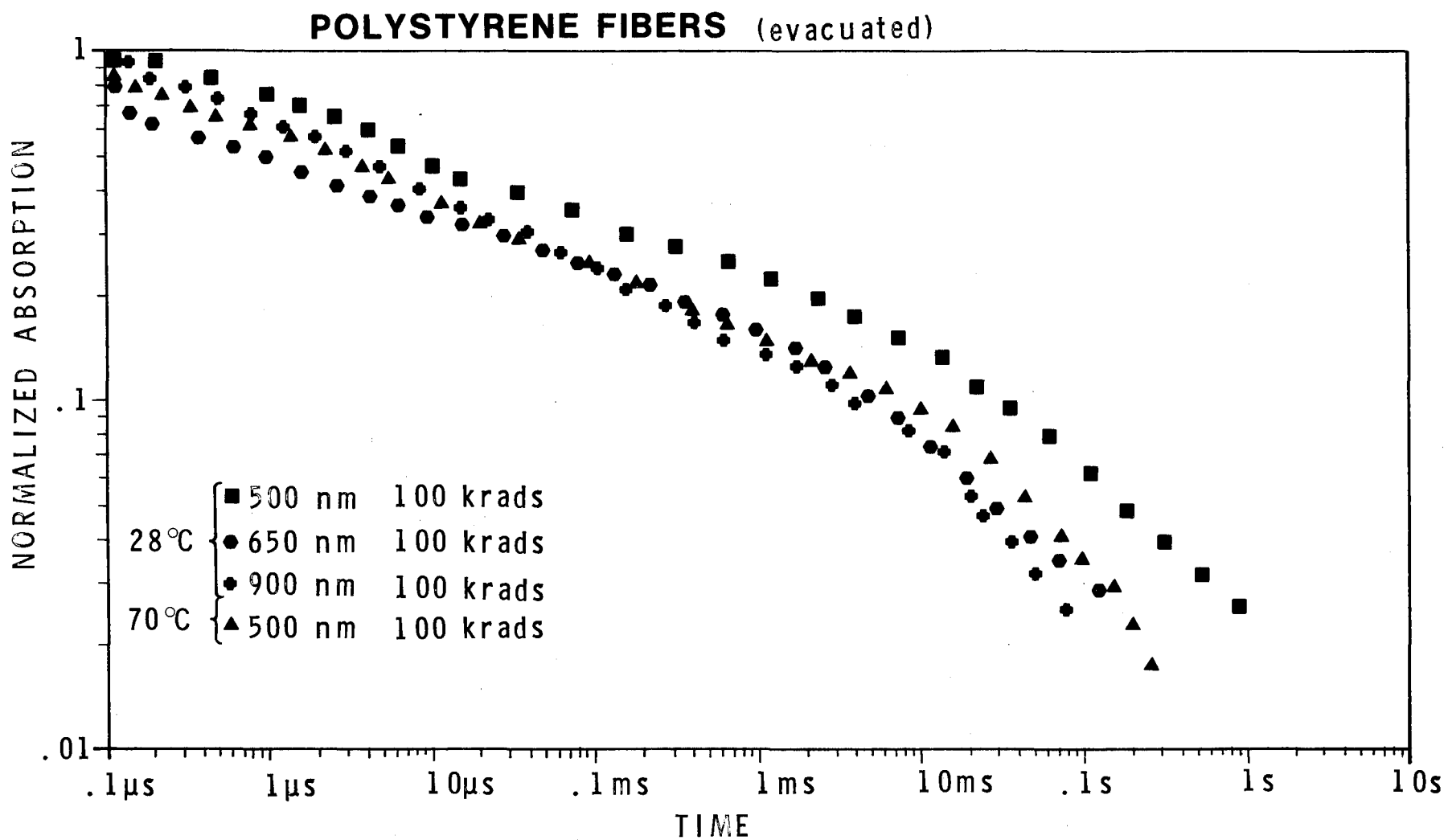


Figure 53. Transient Absorption Recovery in Polystyrene Core Fibers Irradiated in Vacuum or Dry Nitrogen Environments. The recovery is slower than when irradiated in air because of the absence of the molecular oxygen which acts as a scavenger. (Measurement error is less than 10 percent of the values shown for times less than 0.1 ms, and less than 20 percent at longer times.)

POLYSTYRENE FIBERS

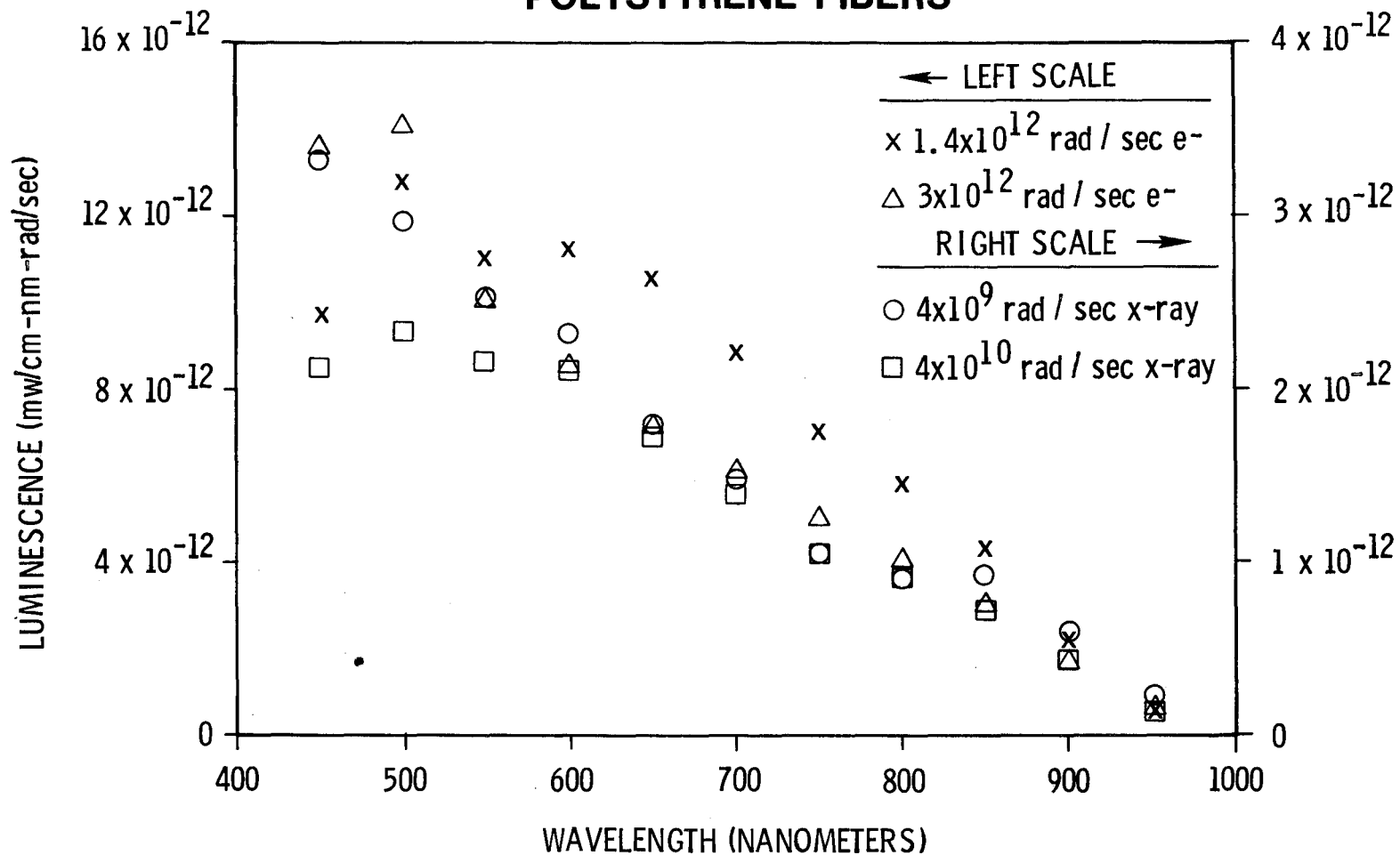


Figure 54. Transient Luminescence Spectra Induced in Polystyrene Core Fibers During Electron and X-ray Irradiation. The ordinate is proportional to the detected power in milliwatts per exposed cm of fiber, per nanometer of effective detector bandwidth, per unit dose rate. Data were corrected for detector response, unirradiated fiber attenuation, and fiber bandwidth. The left-hand scale is for electron data and the right-hand scale for X-ray irradiations. The data shown are for 55 polystyrene core fibers with a diameter of 0.25 mm.

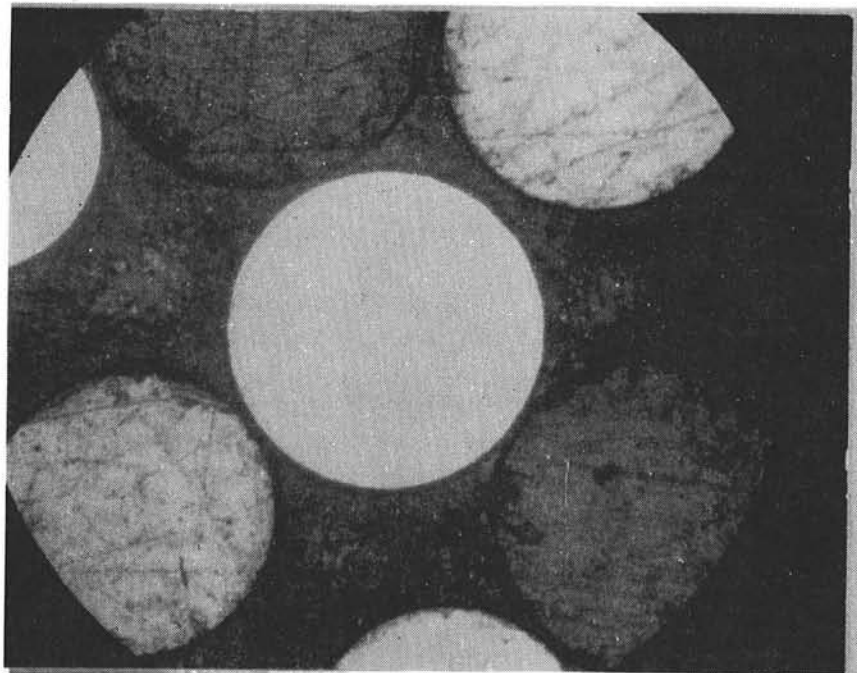
VII. DU PONT PFX FIBERS

Manufacturer: Plastics Department
E. I. Du Pont de Nemours & Company
Wilmington, DE 19898

Core: Polymethylmethacrylate (PMMA)

Cladding: Proprietary Plastic

Fiber Diameter: 0.38 mm



→ 0.1 mm ←

The polymethylmethacrylate (PMMA) core fibers from Du Pont (designated PFX fibers) are similar to Du Pont Crofon fibers,¹¹ but contain a lower impurity concentration, and thus display better unirradiated transmission characteristics at some wavelengths. In general, this fiber has the lowest unirradiated transmission (~550 db/km at 650 nm) of the plastic

fibers, and is probably the most satisfactory plastic fiber for many applications in radiation environments.

The spectral dependence of the transient absorption is plotted in Figures 55 and 56 for doses of 46 and 100 krads. The shapes of these curves are similar to those for the Crofon fibers, showing a peak at the short wavelengths and decreasing absorption with increasing wavelength. The peak transient absorption is shown as a function of dose in Figure 57 for wavelengths of 500, 650, and 800 nm. The peak transient absorption is slightly larger in these PFX fibers than in the Crofon, a condition which suggests that impurities in the Crofon act as scavengers during the radiation pulse.

The effect of temperature on the induced transient absorption is shown in Figures 58, 59, and 60 for wavelengths of 500, 650, and 800 nm, respectively. As observed in other plastic fibers, the absorption decreases with increasing temperature, although the effect is much smaller than in glass fibers studied. Although the peak absorption values as well as the unirradiated absorption values are larger than for silica core fibers, PFX fibers are less expensive and have applications in short fiber lengths.

The transient absorption recovery in PFX fibers (Figure 61) is similar to that for Crofon. The recovery curves are independent wavelengths within the limits of experimental error. However, they increase in slope with higher temperatures for times greater than 0.1 ms, whereas for times less than 0.1 ms, the recovery appears to be independent of temperature (-54 to 71°C) as well as of wavelength and dose.

The overall behavior might be interpreted as a combination of a tunneling process (temperature independent) and a thermally activated process. The tunneling model used to describe the recovery behavior in the Schott fibers, when applied here in modified form to include scavenging,^{2,12} shows that the tunneling curves are multiplied by an exponential of the form e^{-kct} , where k is the reaction rate constant between ions and scavenger and c is the scavenger concentration. With scavenging included, the theoretical recovery increases faster than $t^{-1/4}$ (tunneling model) after some characteristic time $\tau \approx 1/kc$ (0.1 ms in Figure 61). It is also likely that k increases the temperature, causing the change in recovery behavior to occur at shorter times and with steeper slopes for higher-temperature irradiations. The data shown in Figure 61 exhibit the behavior described above, which suggests that scavenging of some form may be occurring in irradiated PFX fibers.

Other experiments¹³ show that molecular oxygen may be the source of scavenging in these plastic fibers. The recovery rate for fibers irradiated and held in vacuum and in dry nitrogen environments (Figure 62) is slower than for fibers treated similarly in an air environment. The recovery is also independent of temperature, and data can be fitted to a tunneling model¹² with good agreement over several orders of magnitude in time.

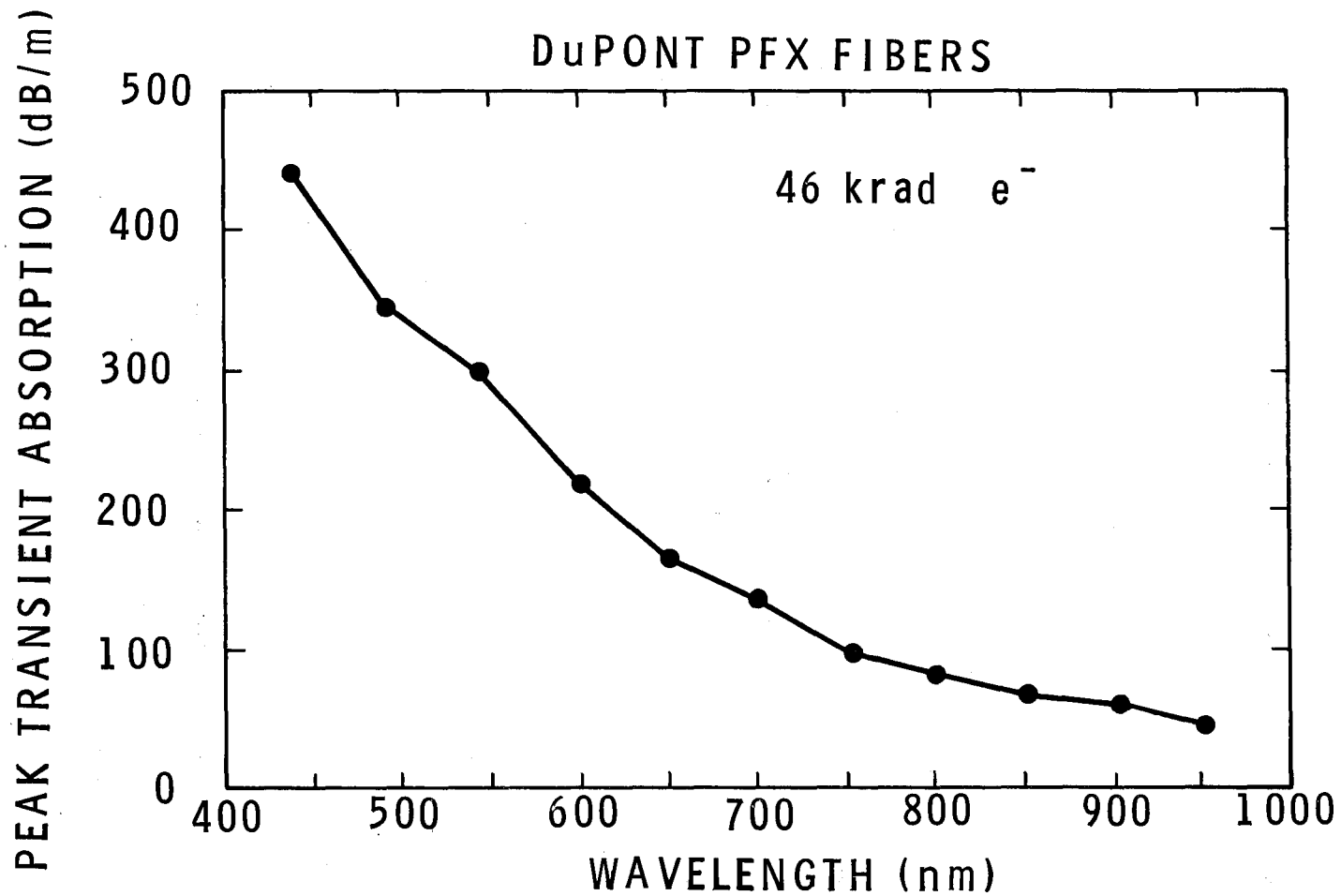


Figure 55. Peak Transient Absorption Spectrum in Du Pont PFX Fibers for an Electron Dose of 46 krad. (Measurement error is less than 10 percent of values plotted.)

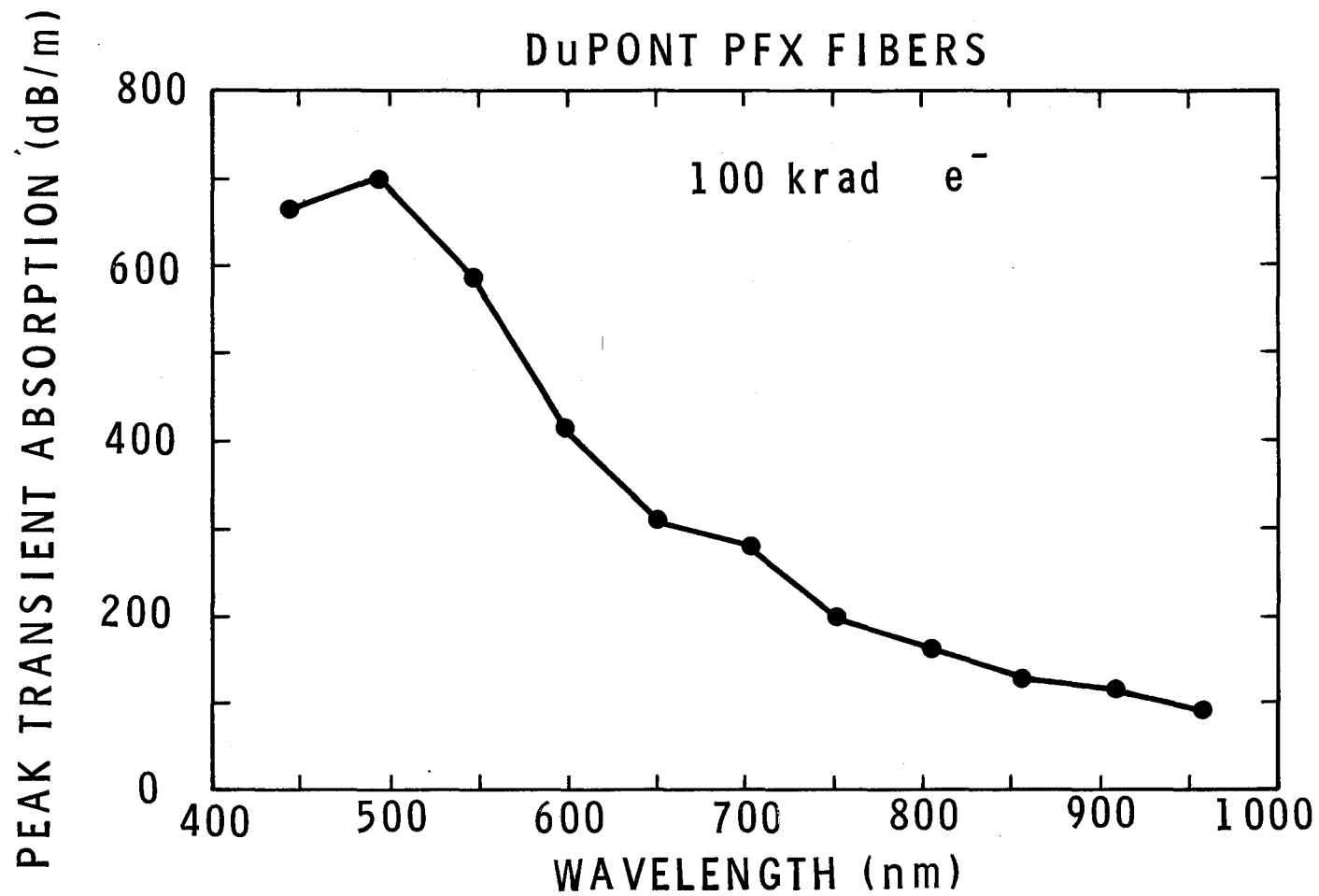


Figure 56. Peak Transient Absorption Spectrum in Du Pont PFX Fibers for an Electron Dose of 46 krad. (Measurement error is less than 10 percent of values plotted.)

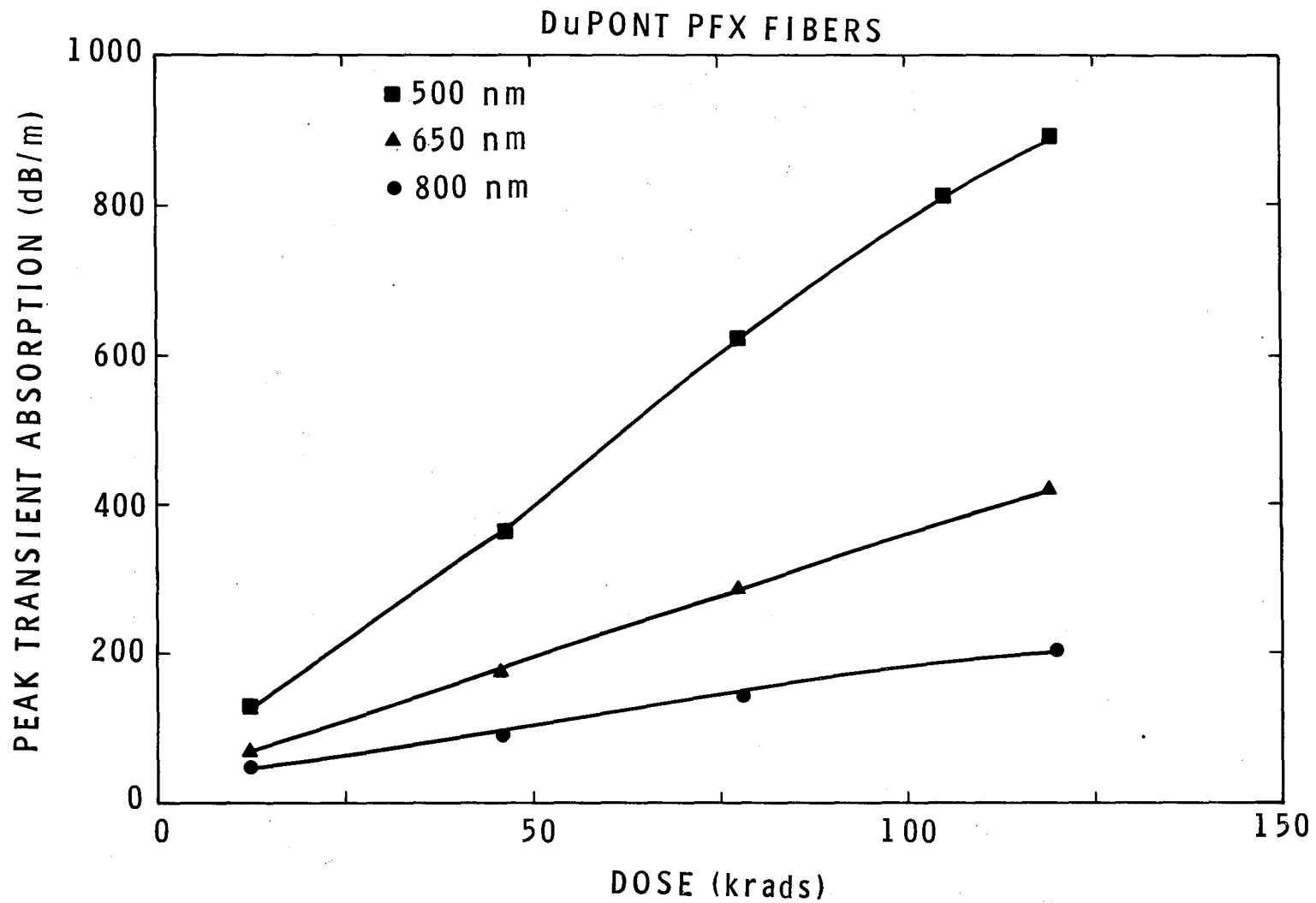


Figure 57. Peak Transient Absorption Versus Dose in Du Pont PFX Fibers for Wavelengths of 500, 650, and 800 nm at 10°C. (Measurement error is less than 10 percent of values plotted.)

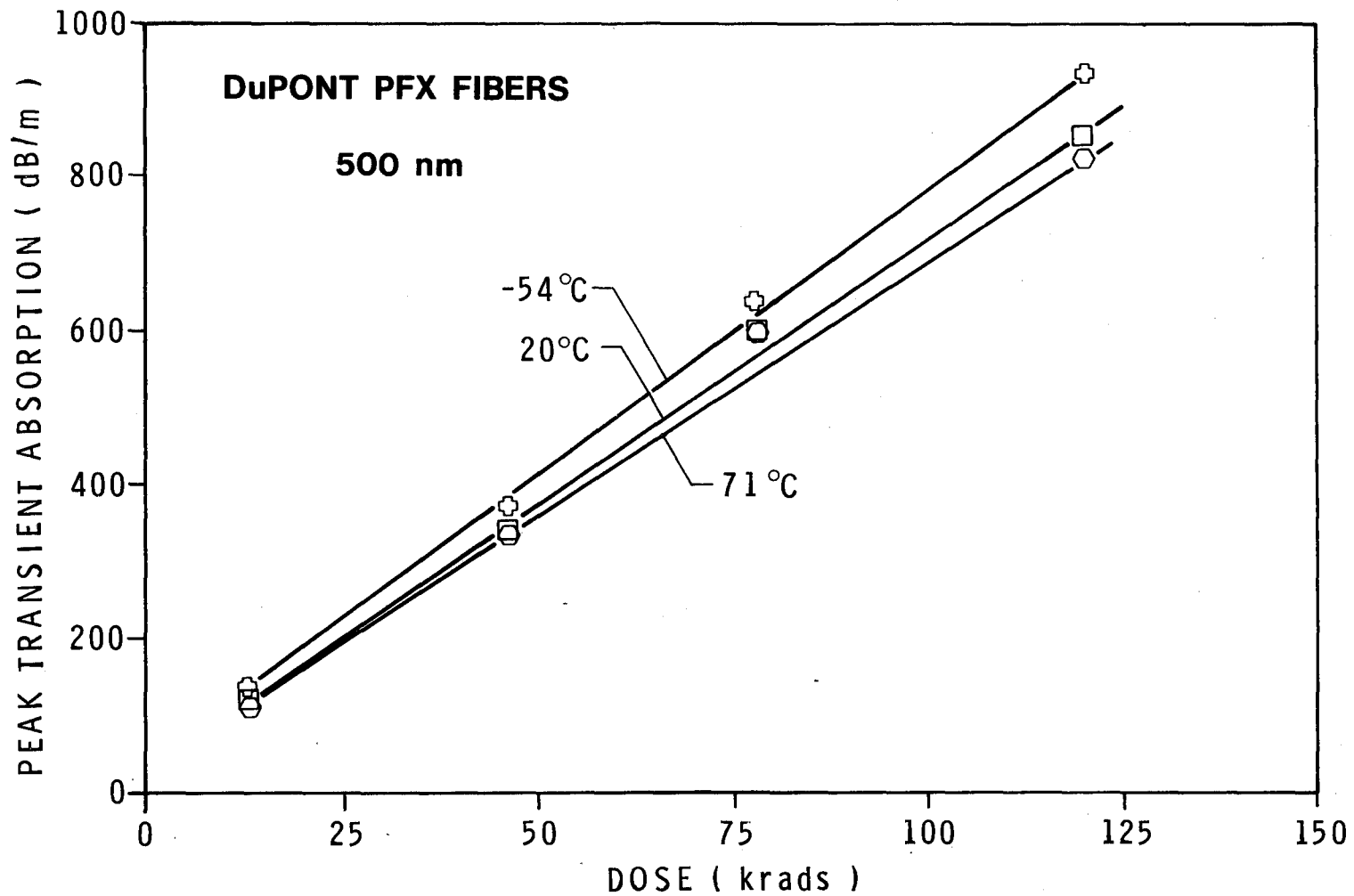


Figure 58. Peak Transient Absorption as a Function of Dose at 500 nm for Temperatures of -54, 10, and 71°C in Du Pont PFX Fibers. (Measurement error is less than 10 percent of values plotted.)

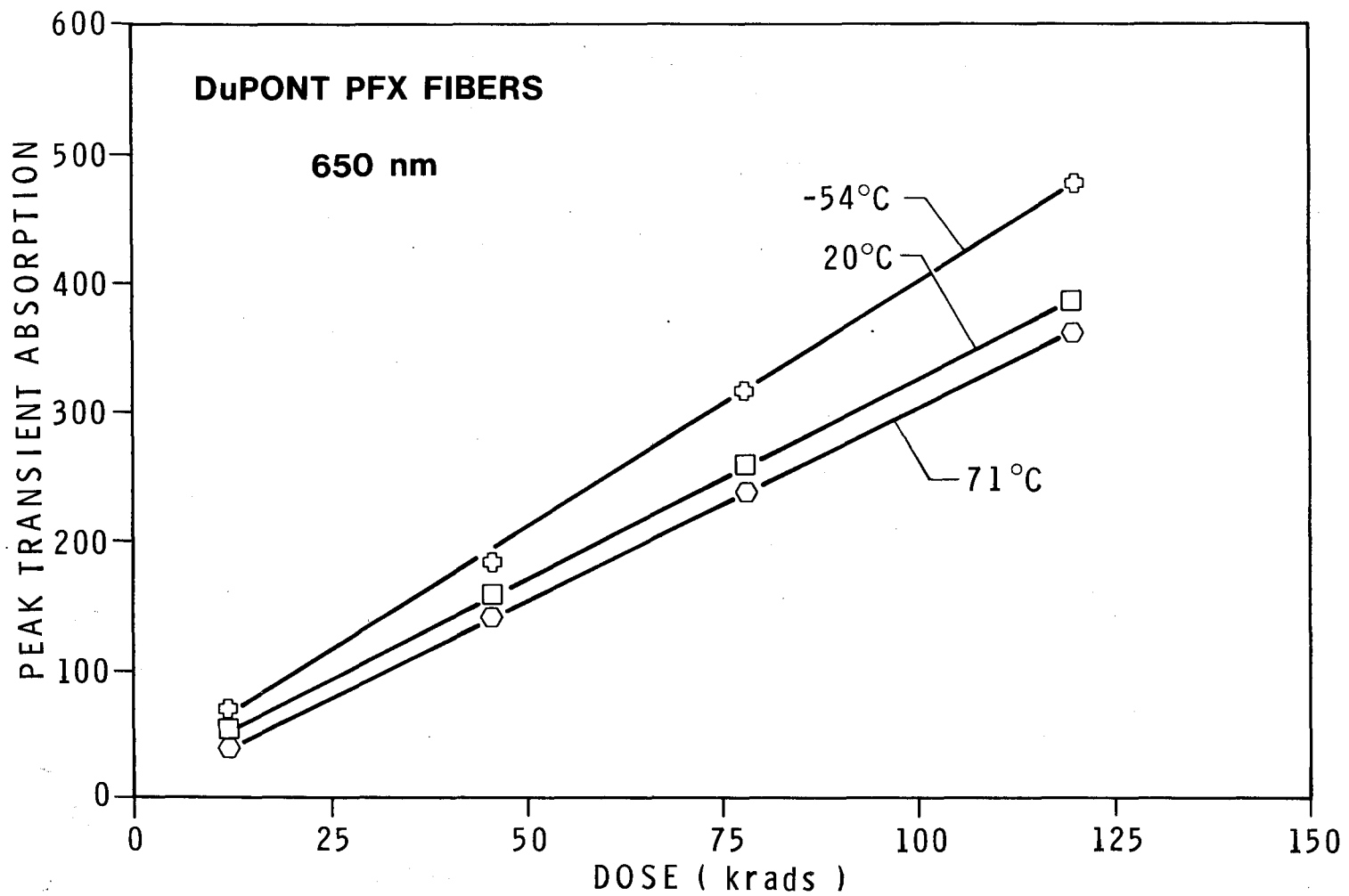


Figure 59. Peak Transient Absorption as a Function of Dose at 650 nm for Temperatures of -54, 20, and 71°C in Du Pont PFX Fibers. (Measurement error is less than 10 percent of values plotted.)

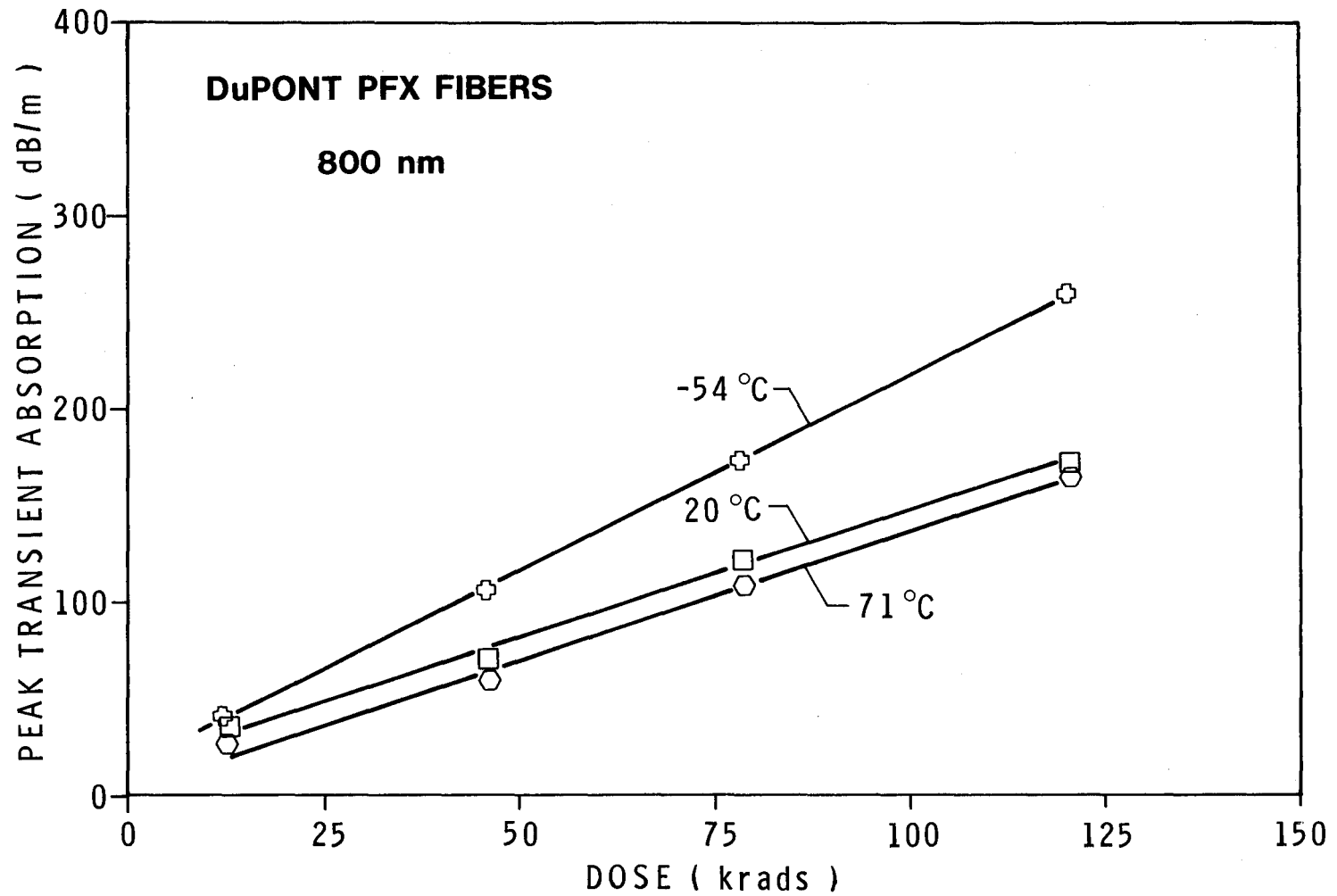


Figure 60. Peak Transient Absorption as a Function of Dose at 800 nm for Temperatures of -54, 20, and 71°C in Du Pont PFX Fibers. (Measurement error is less than 10 percent of values plotted.)

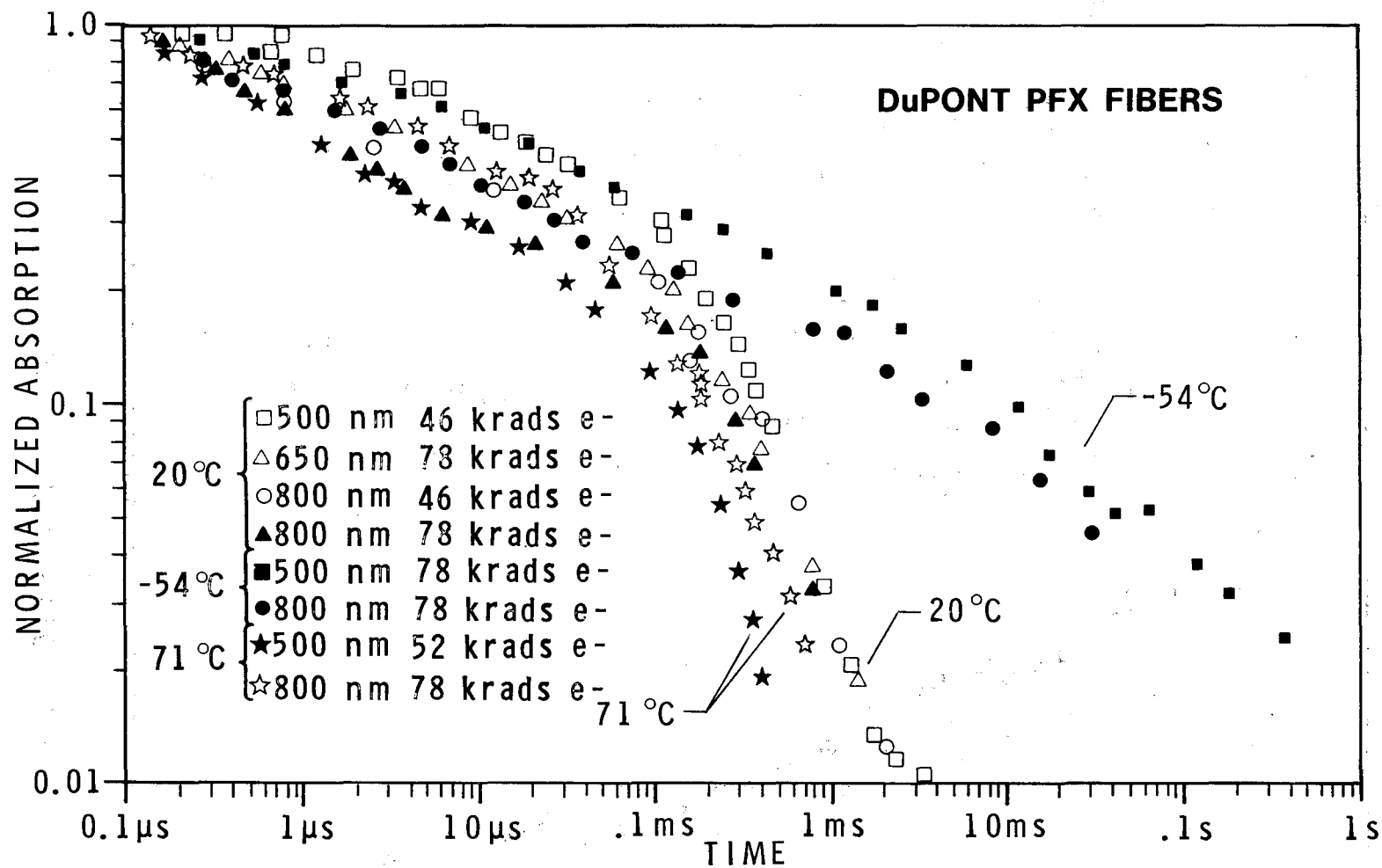


Figure 61. Transient Absorption Recovery in Du Pont PFX Fibers. The data are independent of dose and wavelength. The data are independent of temperature for times less than 0.1 ms, suggesting a tunneling process; at longer times, the data suggest a scavenging process (see text). The measurement error is less than 10 percent of values shown for times less than 0.1 ms, and less than 20 percent for longer times.

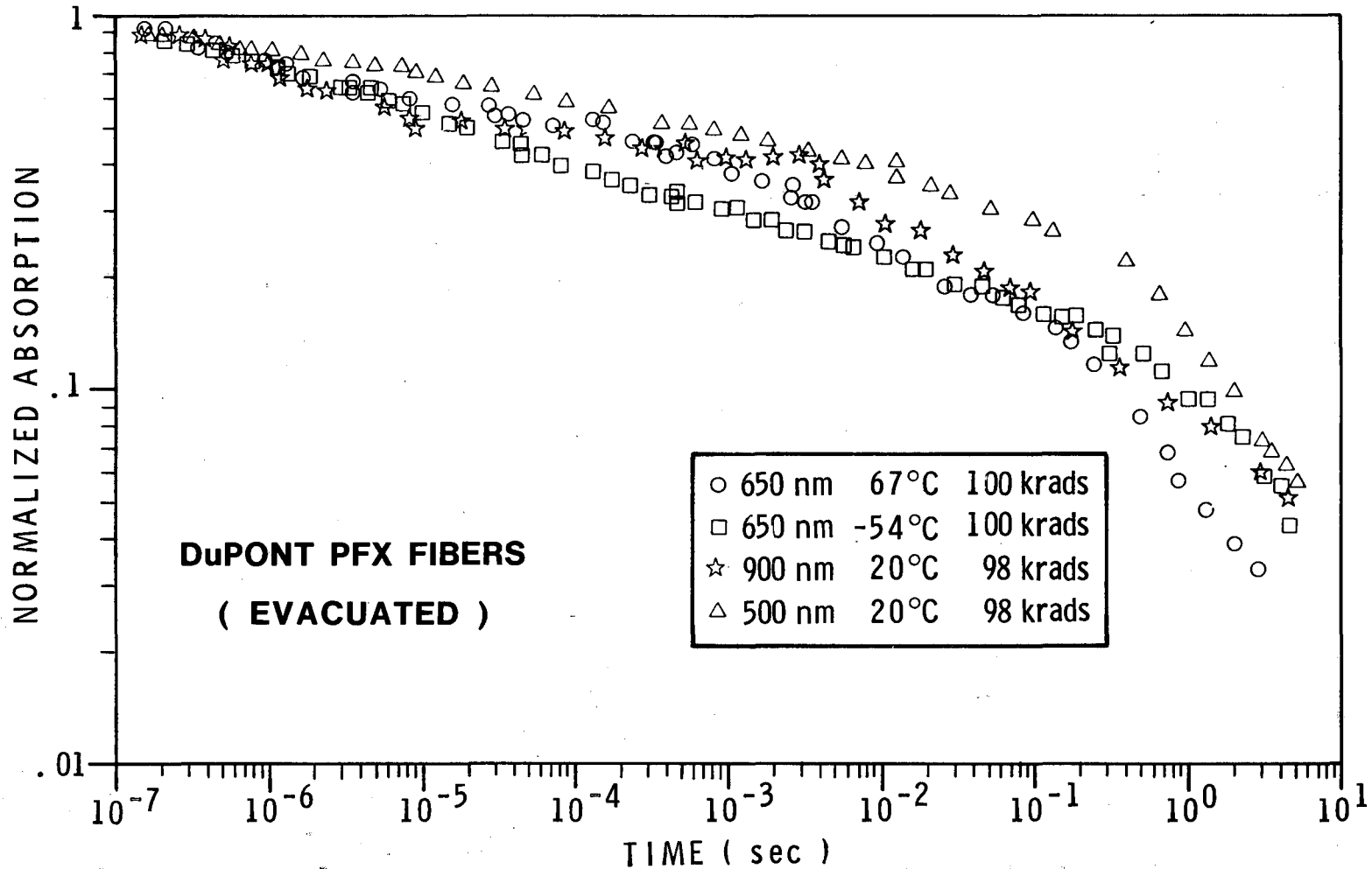


Figure 62. Transient Absorption Recovery for Du Pont PFX Fibers Irradiated in Vacuum or Dry Nitrogen Environment. Molecular oxygen has been removed from the fiber, eliminating the scavenging effect seen in the data of Figure 61 for times greater than 0.1 ms. The measurement error is less than 10 percent of the values shown for times less than 0.1 ms, and less than 20 percent for longer times.

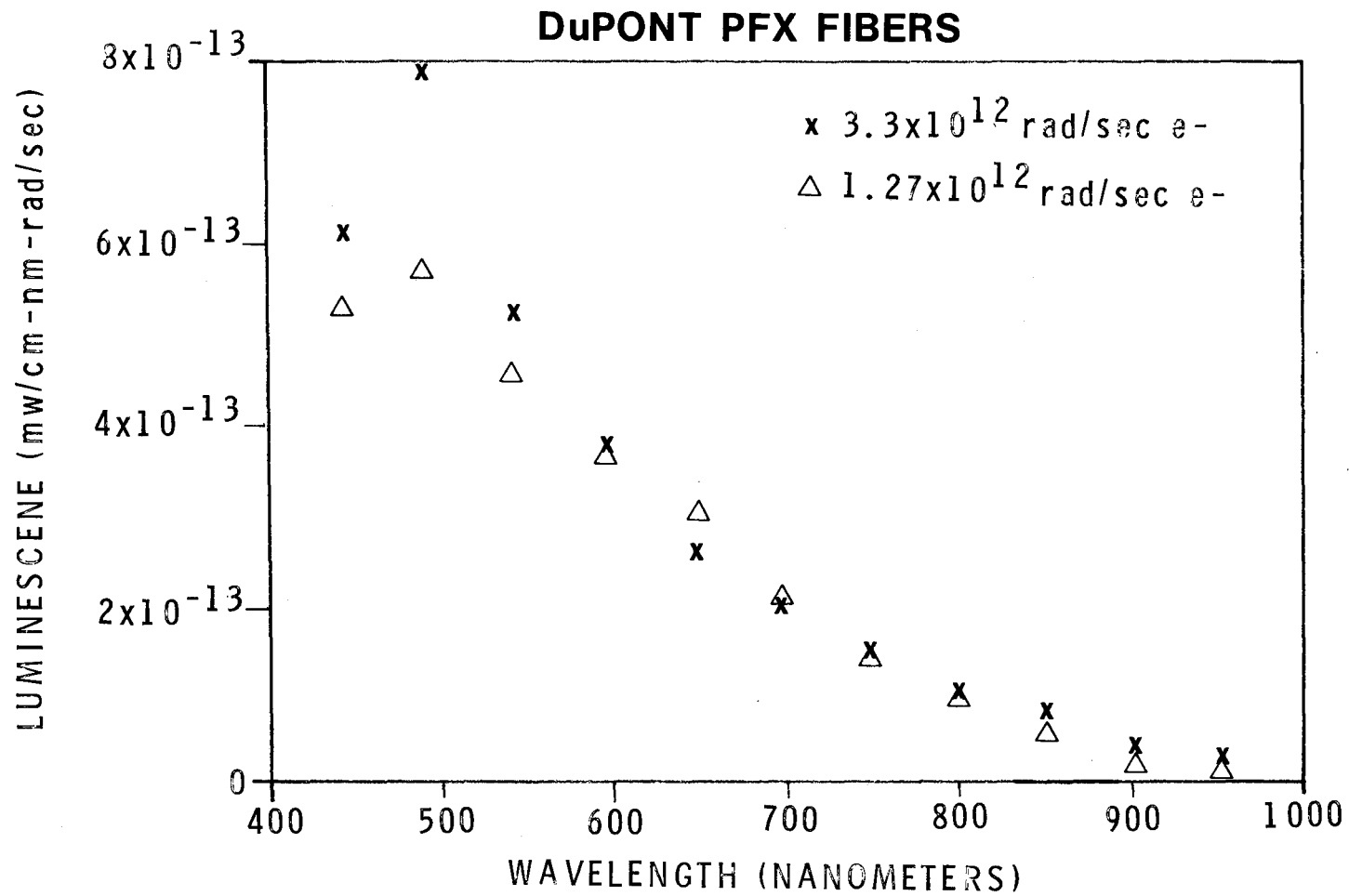


Figure 63. Transient Luminescences Spectra For Electron Irradiations in Du Pont PFX Fibers From Fiberoptic Cable Corporation. The ordinate is proportional to the detected power in milliwatts per exposed centimeter of fiber, per nanometer of the effective detector bandwidth, per unit dose rate. Data were corrected for detector response, unirradiated fiber attenuation and filter bandwidth. The data shown are for seven Du Pont PFX fibers with a diameter of 0.38 mm.

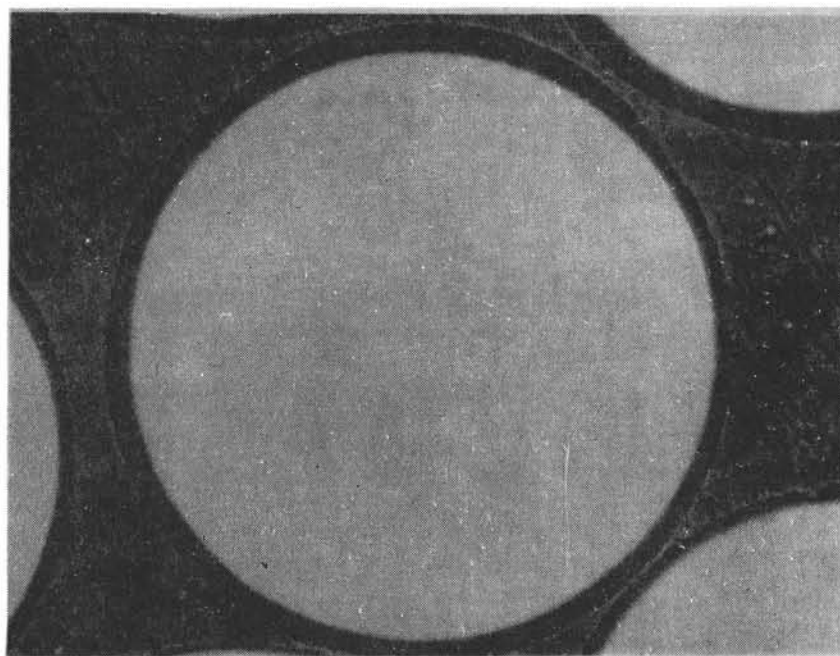
VIII. DU PONT CROFON FIBERS

Manufacturer: Plastics Department
E. I. du Pont de Nemours & Company
Wilmington, DE 19898

Core: Polymethylmethacrylate (PMMA)

Cladding: Proprietary Plastic

Fiber Diameter: 0.25 mm



→ 0.1 mm ←

These polymethylmethacrylate (PMMA) core fibers from Du Pont (designated Crofon) exhibit radiation responses similar to those of other PMMA core fibers (PFX) and of polystyrene core fibers. The spectral response of the peak transient absorption is shown in Figures 64 through 67 for an X-ray dose of 930 rads, and for electron doses of 6.9, 70, and

250 krads. The transient absorption shows a peak at short wavelengths, and it decreases toward the longer wavelengths in a fashion similar to that of the glass fibers studied.

The peak transient absorption is plotted as a function of dose in Figure 68 for wavelengths of 500, 650, and 800 nm. Although the magnitudes of the induced absorption and the absorption are greater in unirradiated materials than in the "pure" vitreous silica fibers, the fibers, nevertheless, have applications in systems employing short fiber lengths as do the other plastic fibers.

In the PMMA core fibers, as well as polystyrene fibers, the effect of temperature is not as pronounced as it is in the glass fibers studied. The peak transient absorption versus dose is plotted for temperatures of -54, 20, and 71°C at wavelengths of 500, 650, and 800 nm in Figures 69 through 71.

The absorption recovery of the Crofon fibers is plotted in Figure 72. The recovery is more complex than in the glass and the other plastic fibers studied, and exhibits several different mechanisms.² A pronounced change in the shape of the recovery curves is evident for times greater than 0.1 ms. For less than 0.1 ms, the recovery is relatively independent of temperature. This behavior suggests the operation of a tunneling process which is dominant over short times and a thermally activated process dominant over longer times.²

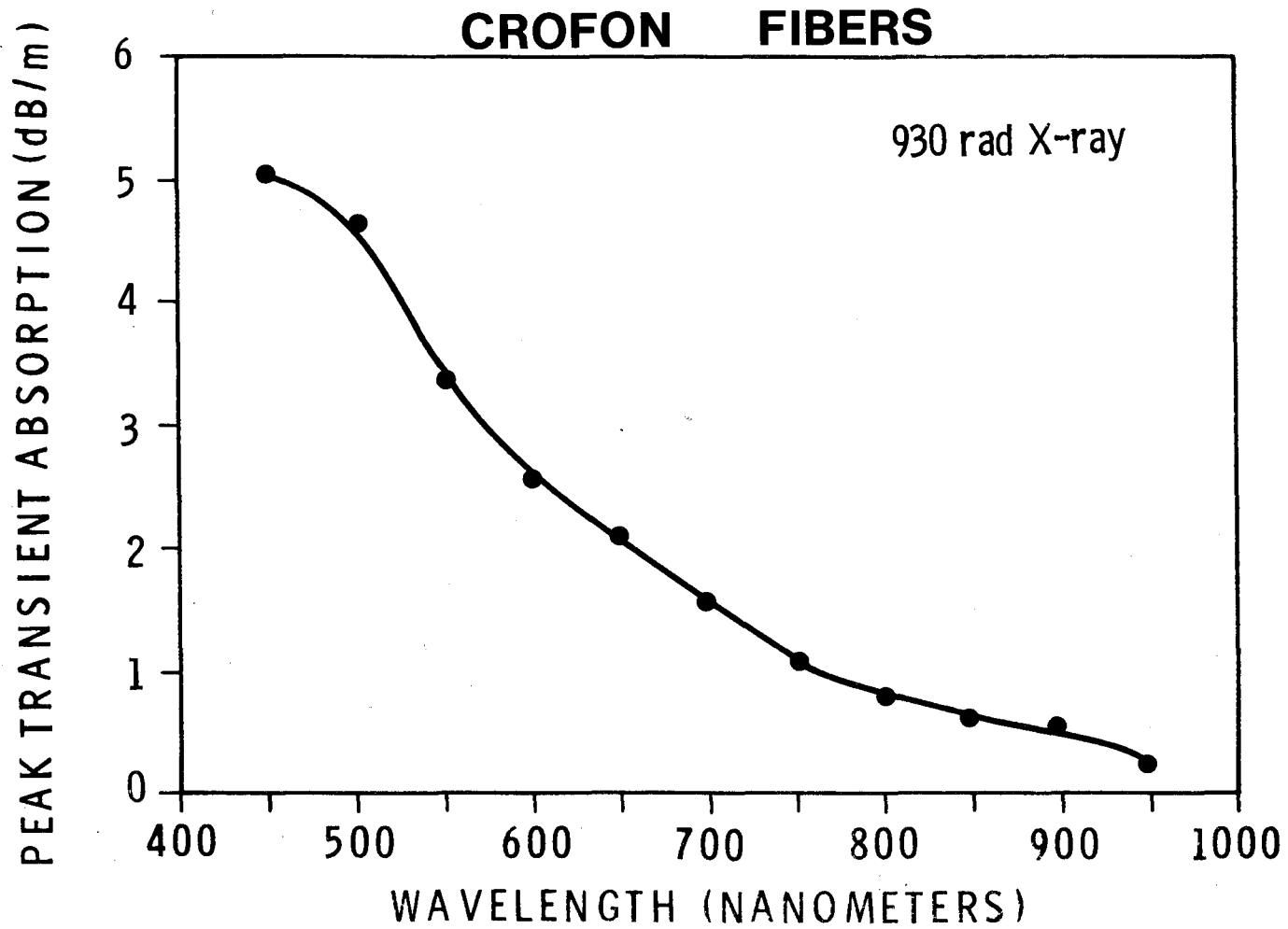


Figure 64. Peak Transient Absorption Spectrum in Du Pont Crofon Fibers for an X-ray Dose of 930 rads. (Measurement error is less than 10 percent of values plotted.)

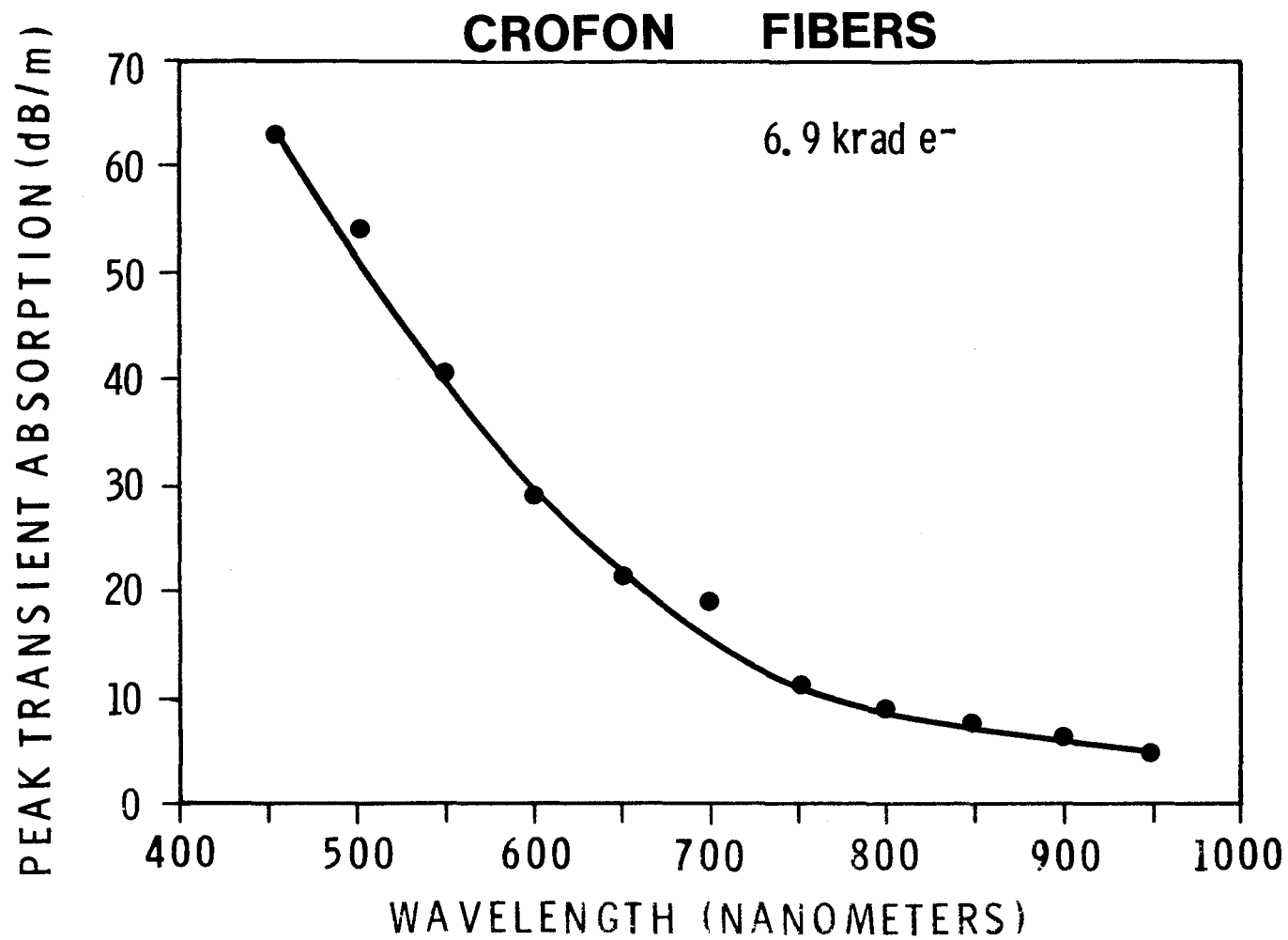


Figure 65. Peak Transient Absorption Spectrum in Du Pont Crofon Fibers for an Electron Dose of 6.9 krad. (Measurement error is less than 10 percent of values plotted.)

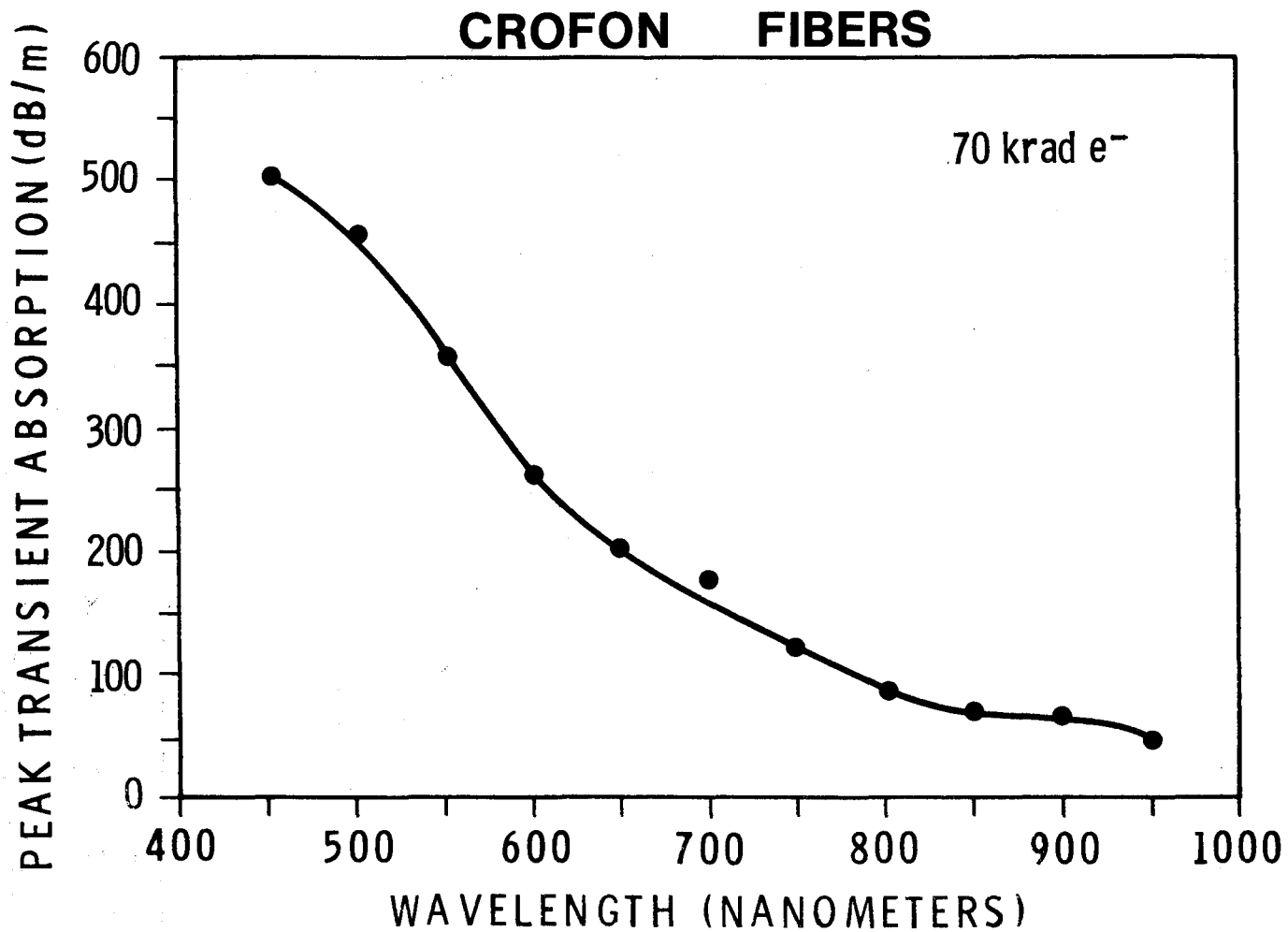


Figure 66. Peak Transient Absorption Spectrum in Du Pont Crofon Fibers for an Electron Dose of 70 krad. (Measurement error is less than 10 percent of values plotted.)

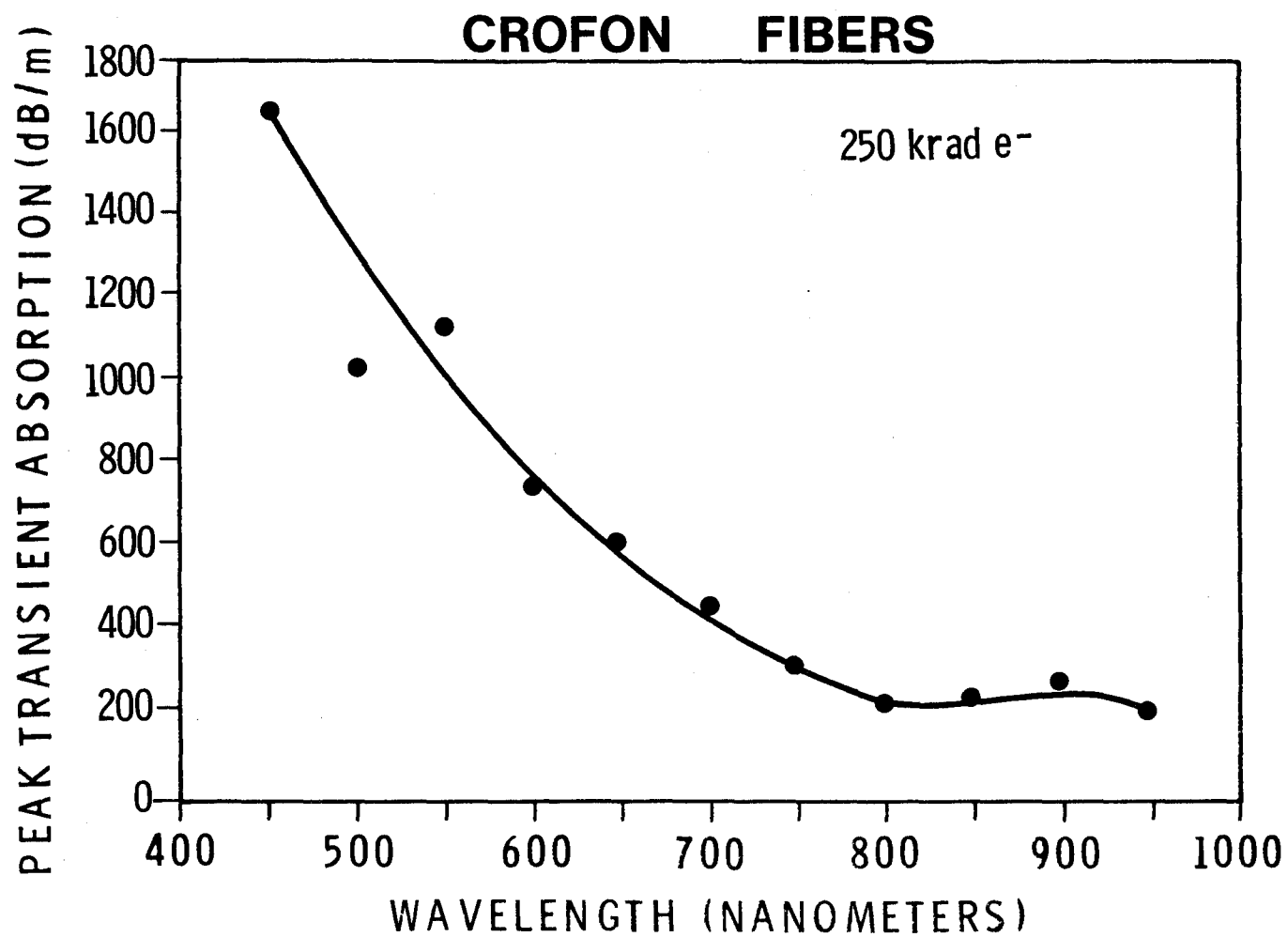


Figure 67. Peak Transient Absorption Spectrum in Du Pont Crofon Fibers for an Electron Dose of 250 krads. (Measurement error is less than 10 percent of values plotted.)

CROFON FIBERS

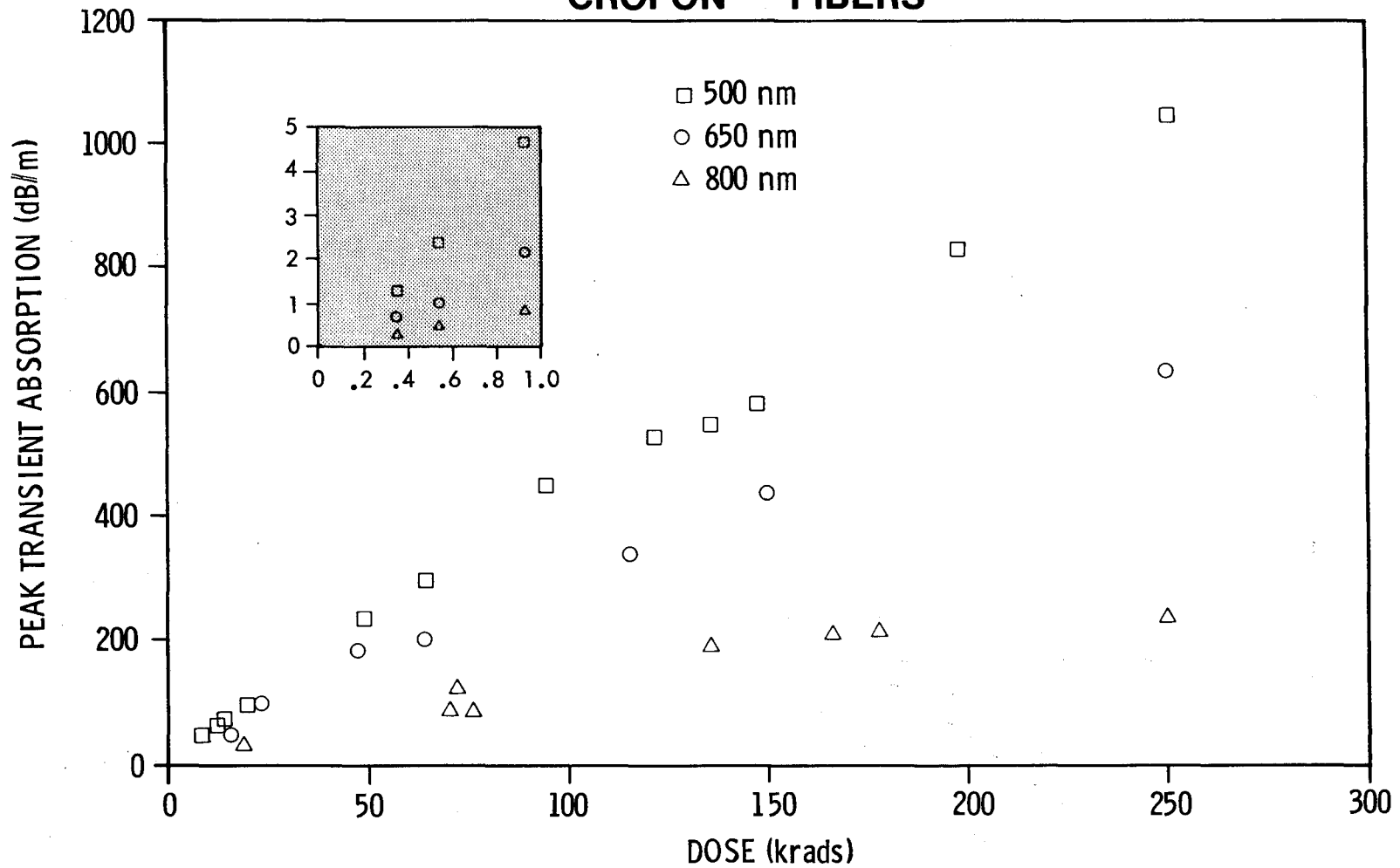


Figure 68. Peak Transient Absorption as a Function of Dose in Du Pont Crofon Fibers for Wavelengths of 500, 650, and 800 nm at 20°C. (Measurement error is less than 10 percent of values plotted.)

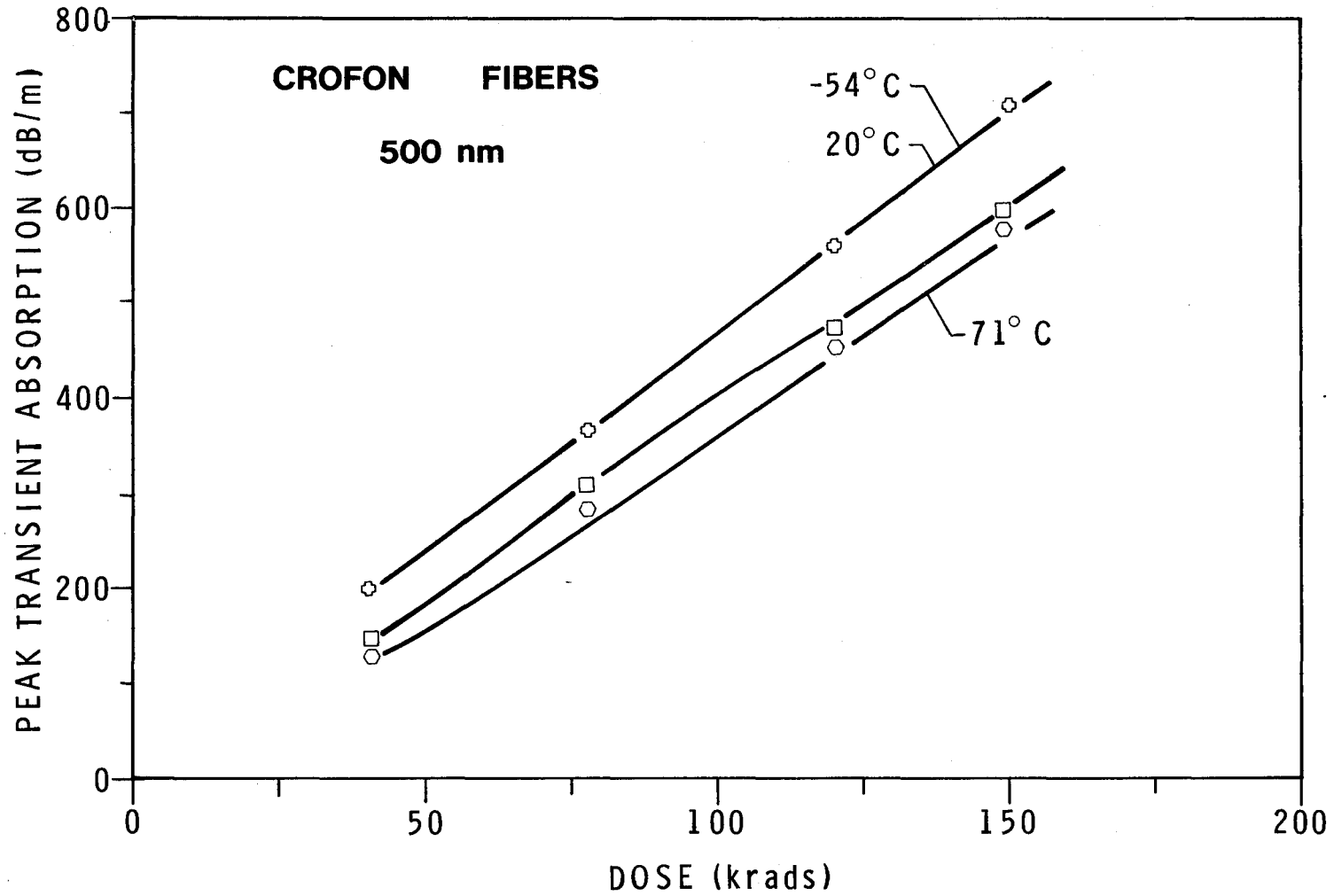


Figure 69. Peak Transient Absorption as a Function of Dose at 500 nm for Temperatures of -54, 20, and 71°C in Du Pont Crofon Fibers. (Measurement error is less than 10 percent of values plotted.)

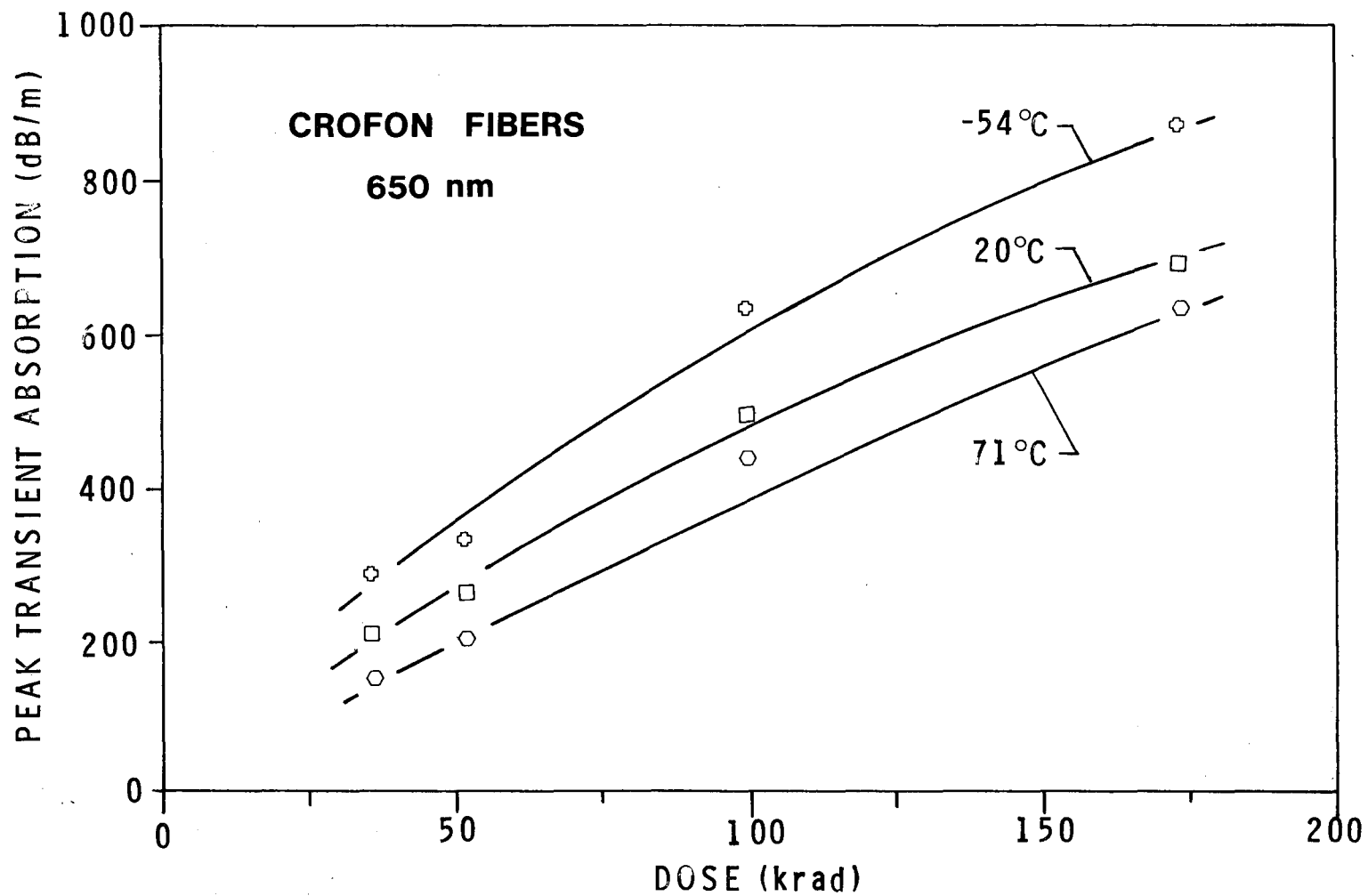


Figure 70. Peak Transient Absorption as a Function of Dose at 650 nm for Temperatures of -54, 20, and 71°C in Du Pont Crofon Fibers. (Measurement error is less than 10 percent of values plotted.)

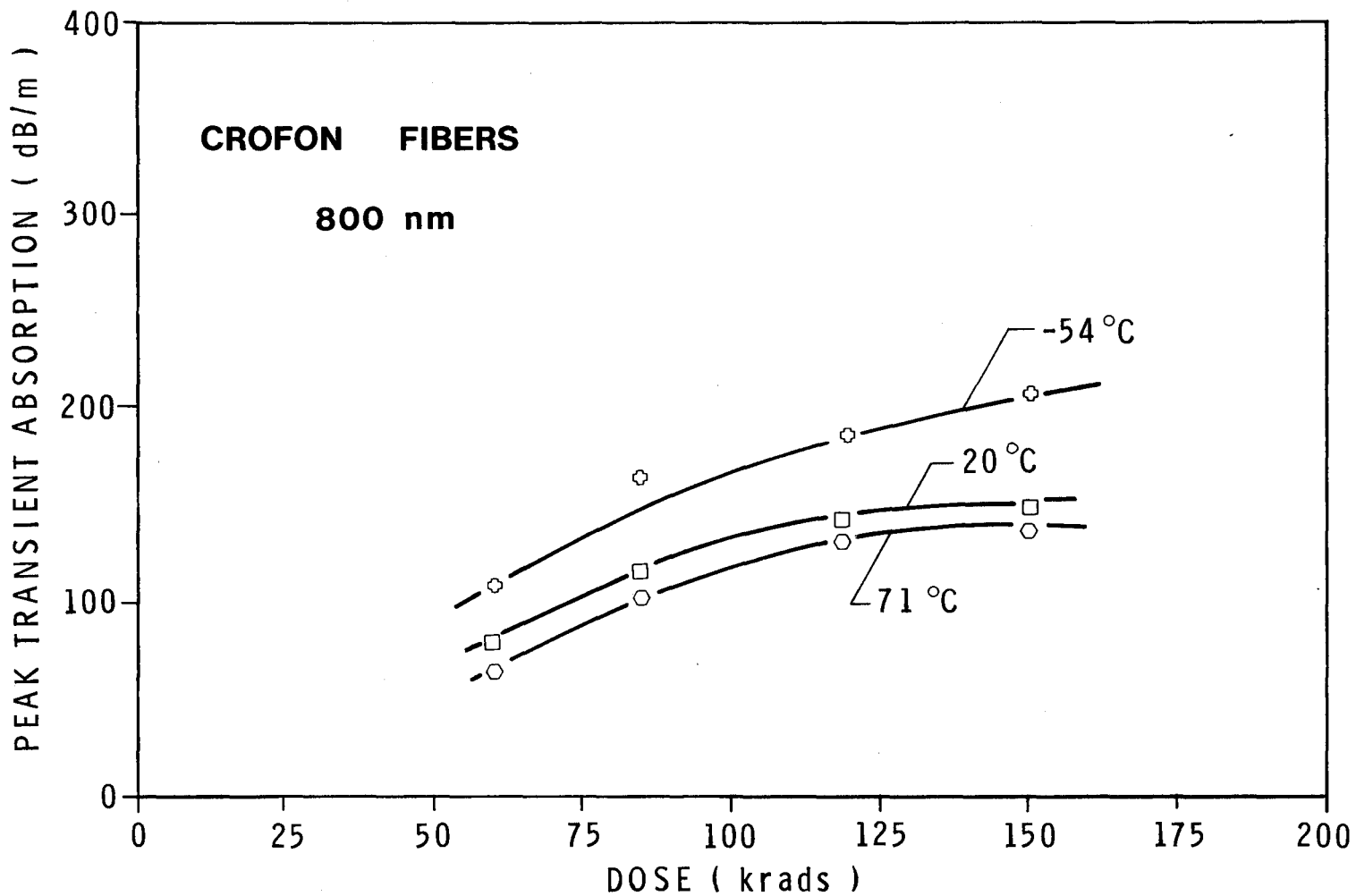


Figure 71. Peak Transient Absorption Versus Dose at 800 nm for Temperatures of -54, 20, and 71°C in Du Pont Crofon Fibers. (Measurement error is less than 10 percent of values plotted.)

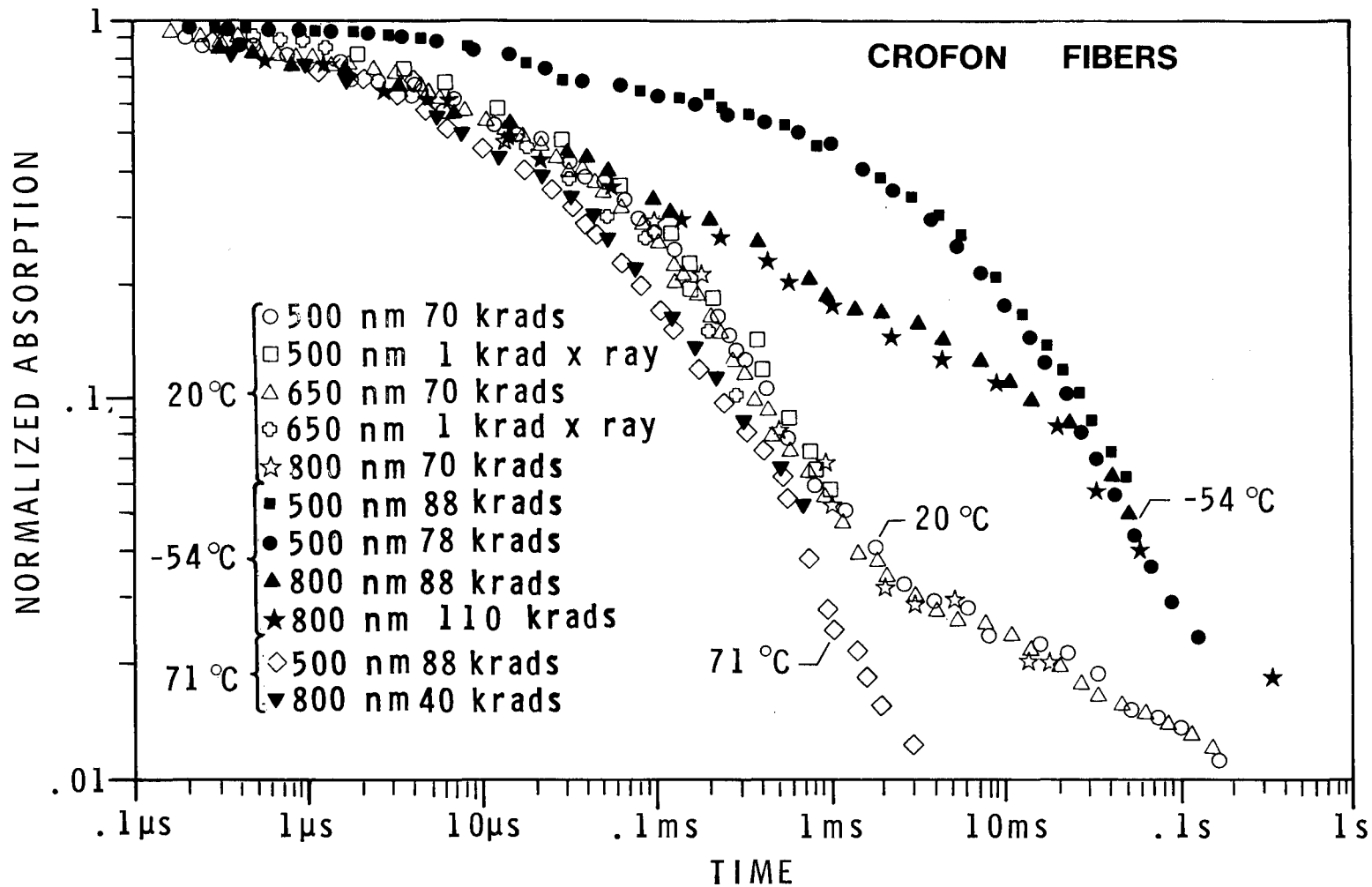


Figure 72. Transient Absorption Recovery in Du Pont Crofon Fibers for Several Doses, Wavelengths, and Temperatures. The recovery is more complex than in the PFX fibers and is attributed to the higher impurity concentration. The measurement error is less than 10 percent of the values shown for times less than 0.1 ms, and less than 20 percent for longer times.

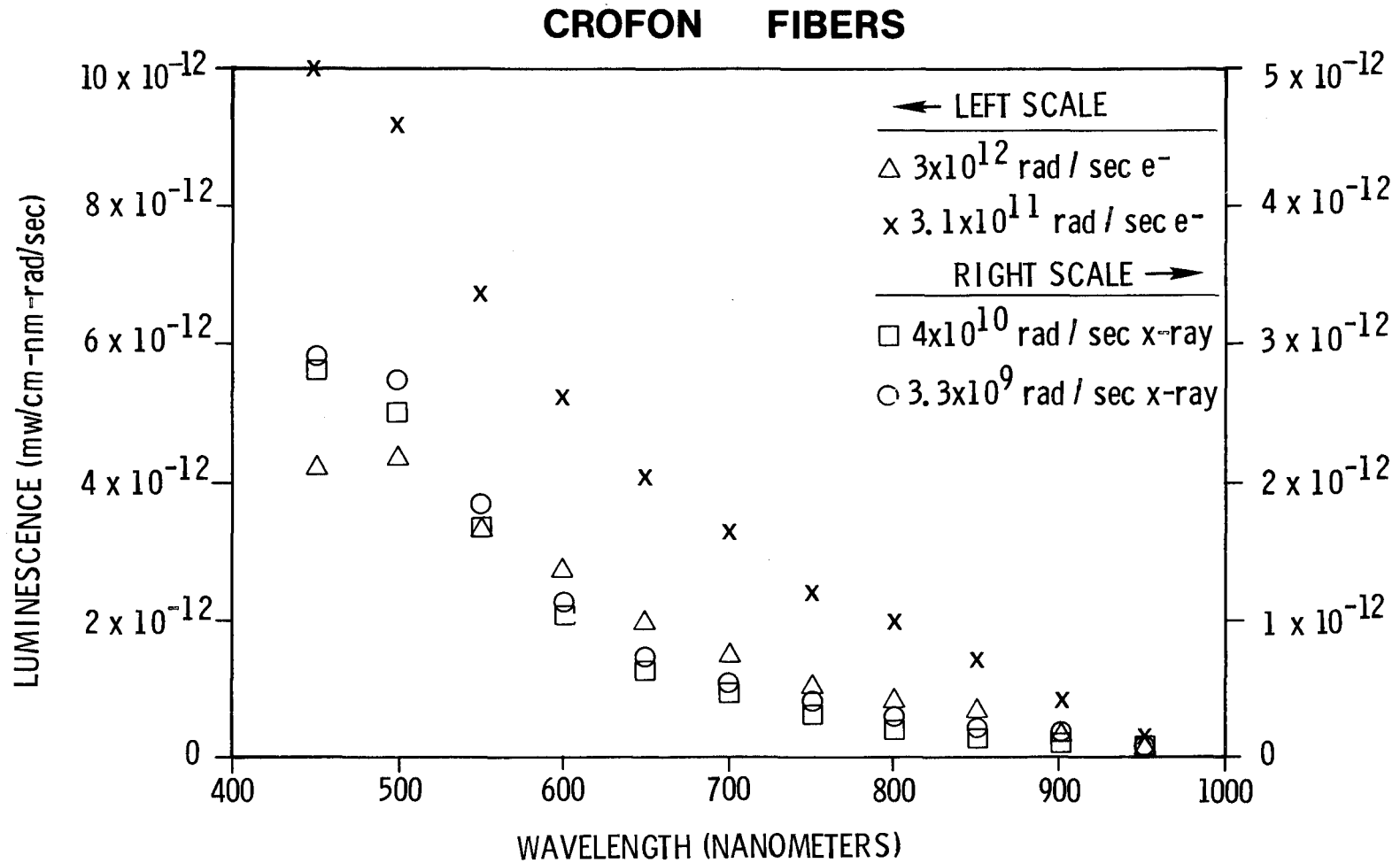


Figure 73. Transient Luminescence Spectra Induced in Du Pont Crofon Fibers During Electron and X-ray Irradiation. The ordinate is proportional to the detected power in milliwatts per exposed cm of fiber, per nanometer of effective detector bandwidth, per unit dose rate. Data were corrected for detector response, unirradiated fiber attenuation, and fiber bandwidth. The left-hand scale is for electron data and the right-hand scale for X-ray irradiations. The data shown are for seven Du Pont Crofon fibers with a diameter of 0.25 mm.

APPENDIX

Transmission spectra of the filters used for the transient absorption measurements are shown in Figures 74 through 84.

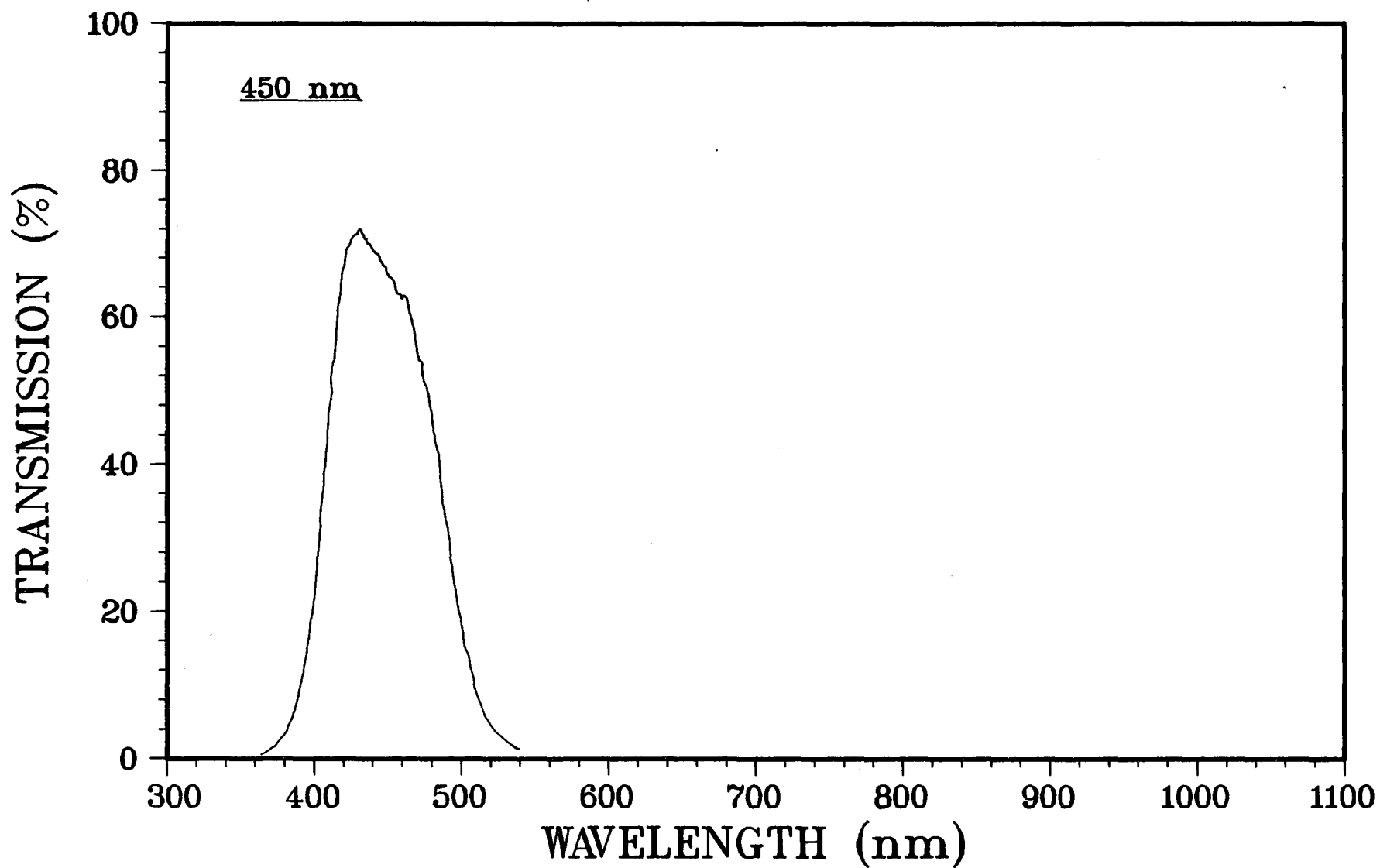


Figure 74. Cary 14 Spectrometer Trace Showing the Spectral Bandwidth of the 450 nm Filter

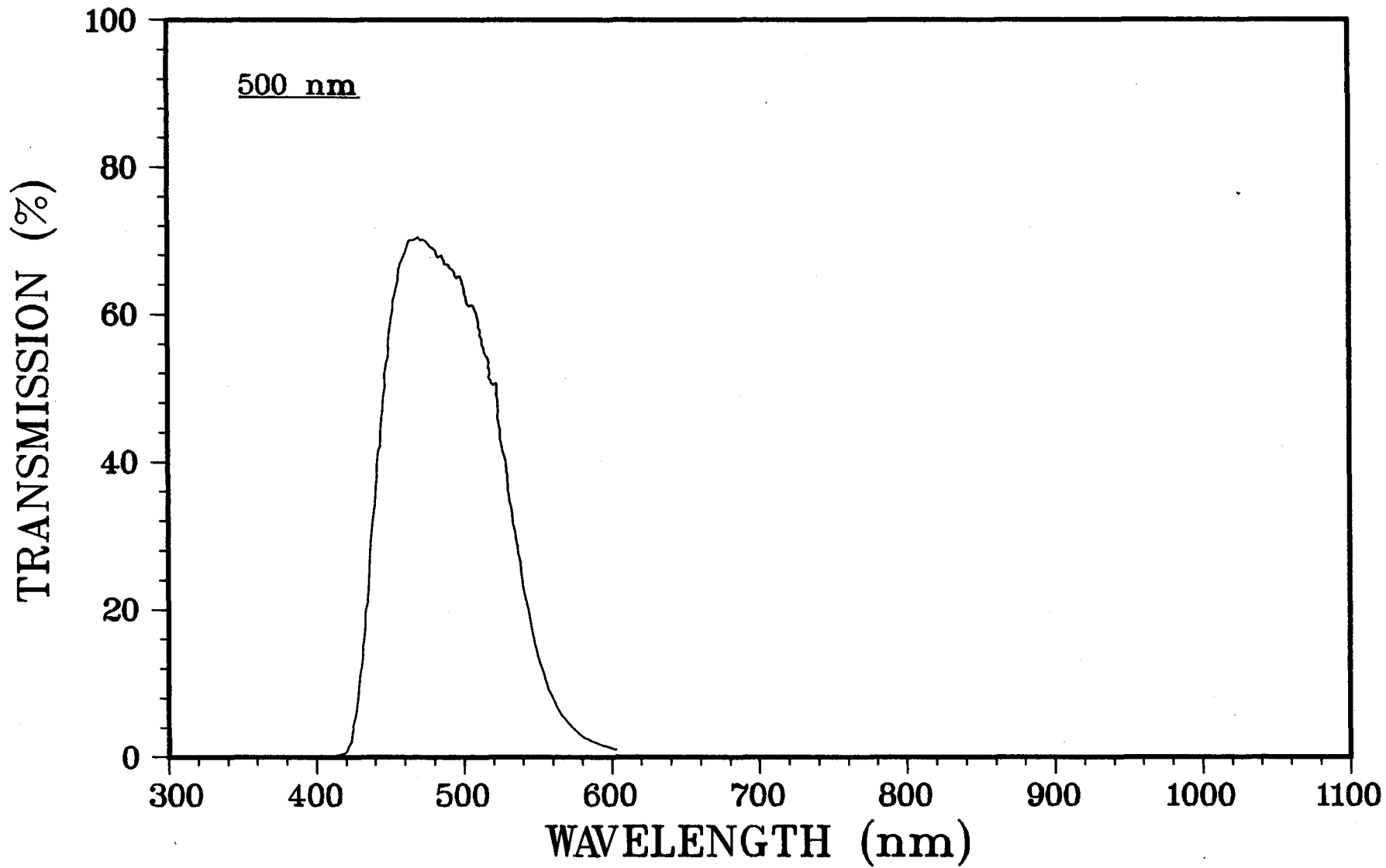


Figure 75. Cary 14 Spectrometer Trace Showing the Spectral Bandwidth of the 500 nm Filter

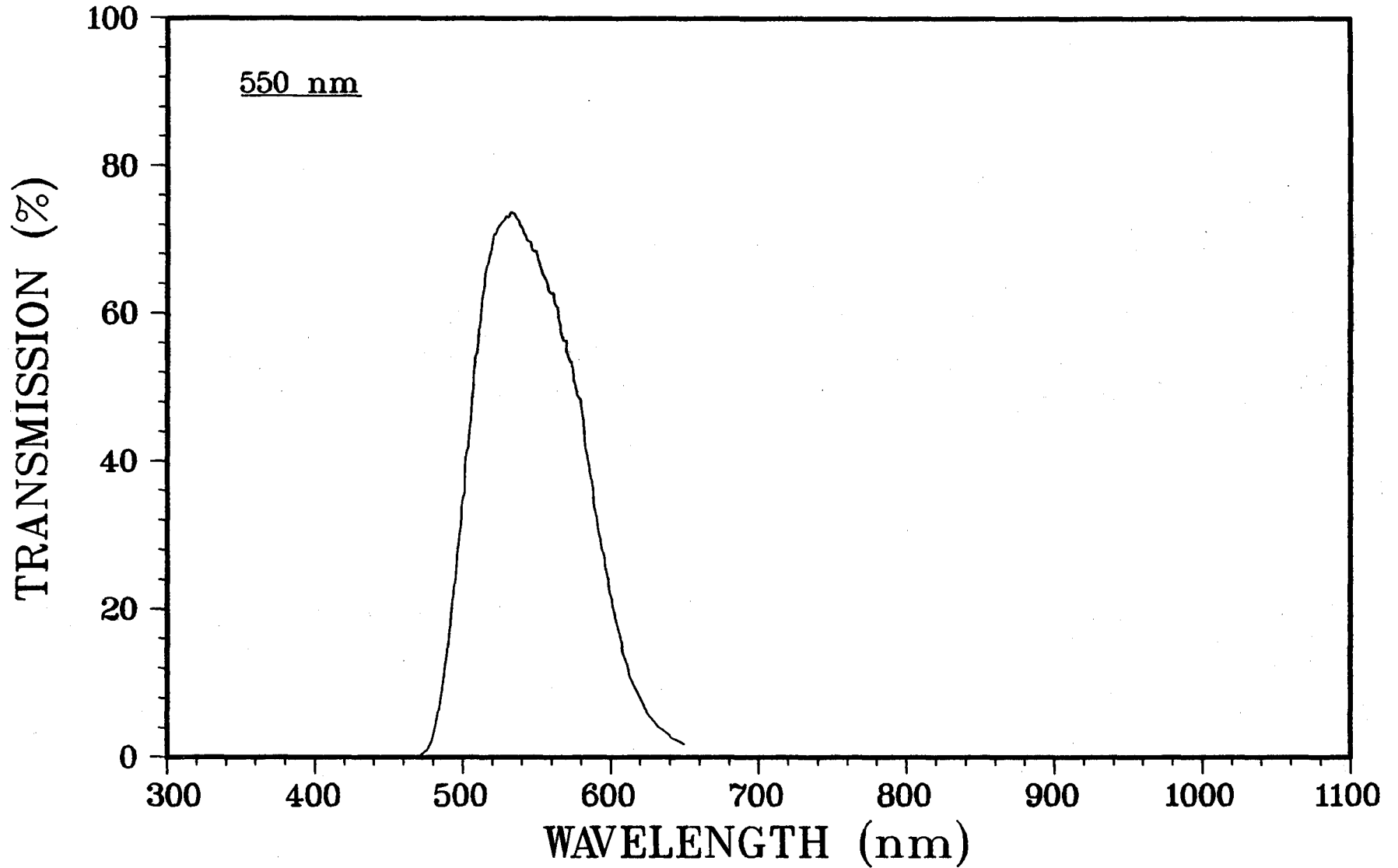


Figure 76. Cary 14 Spectrometer Trace Showing the Spectral Bandwidth of the 550 nm Filter

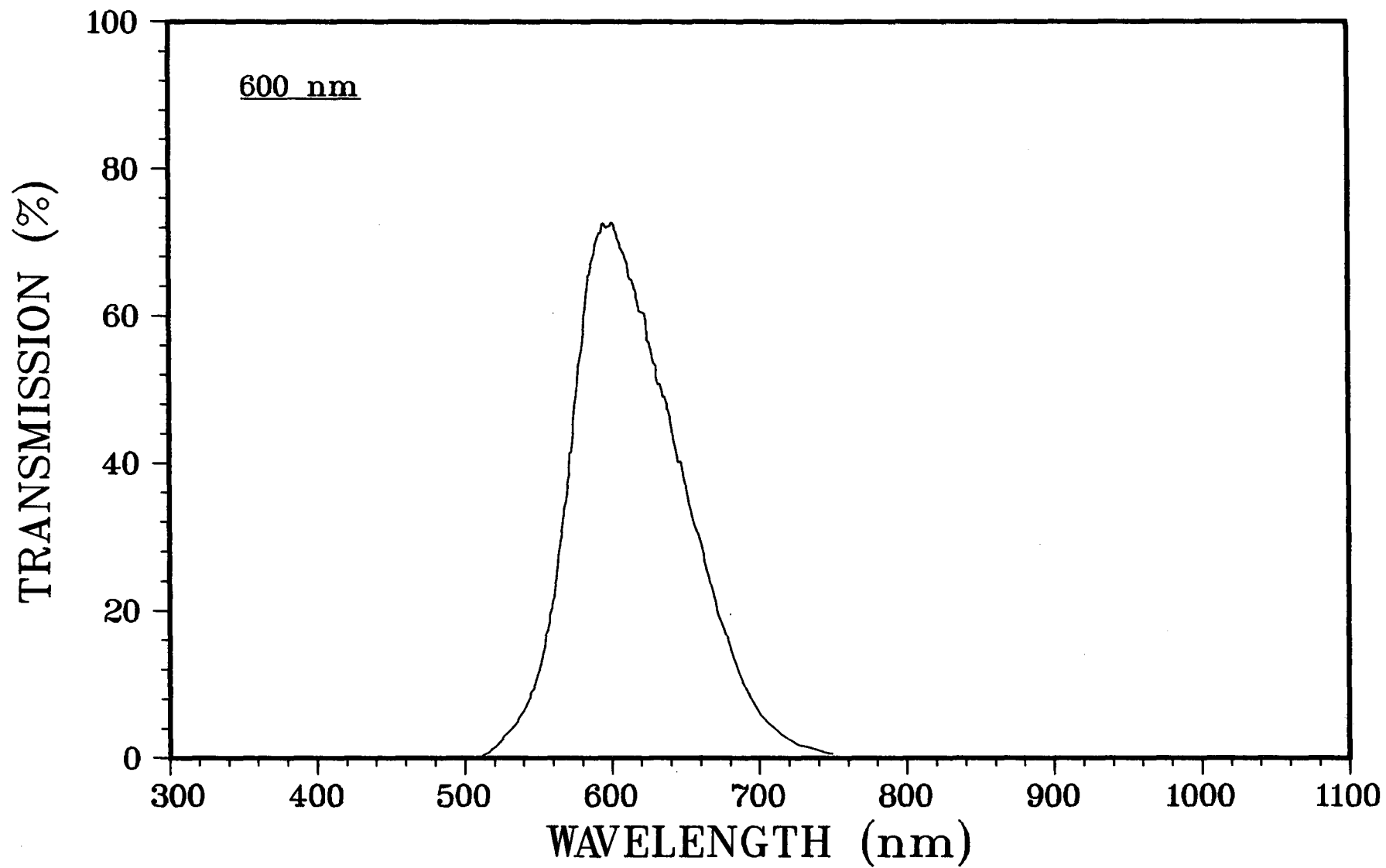


Figure 77. Cary 14 Spectrometer Trace Showing the Spectral Bandwidth of the 600 nm Filter

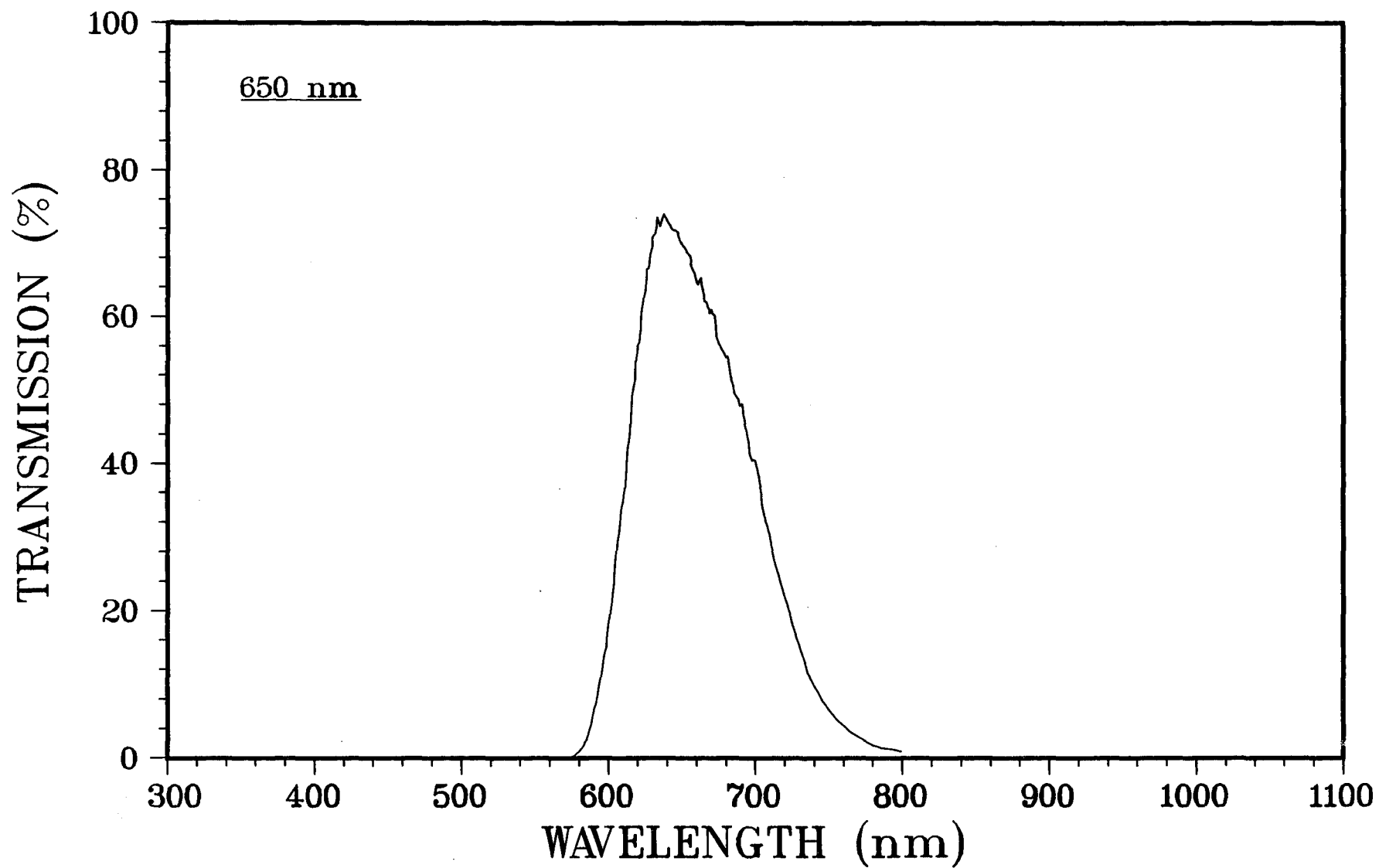


Figure 78. Cary 14 Spectrometer Trace Showing the Spectral Bandwidth of the 650 nm Filter

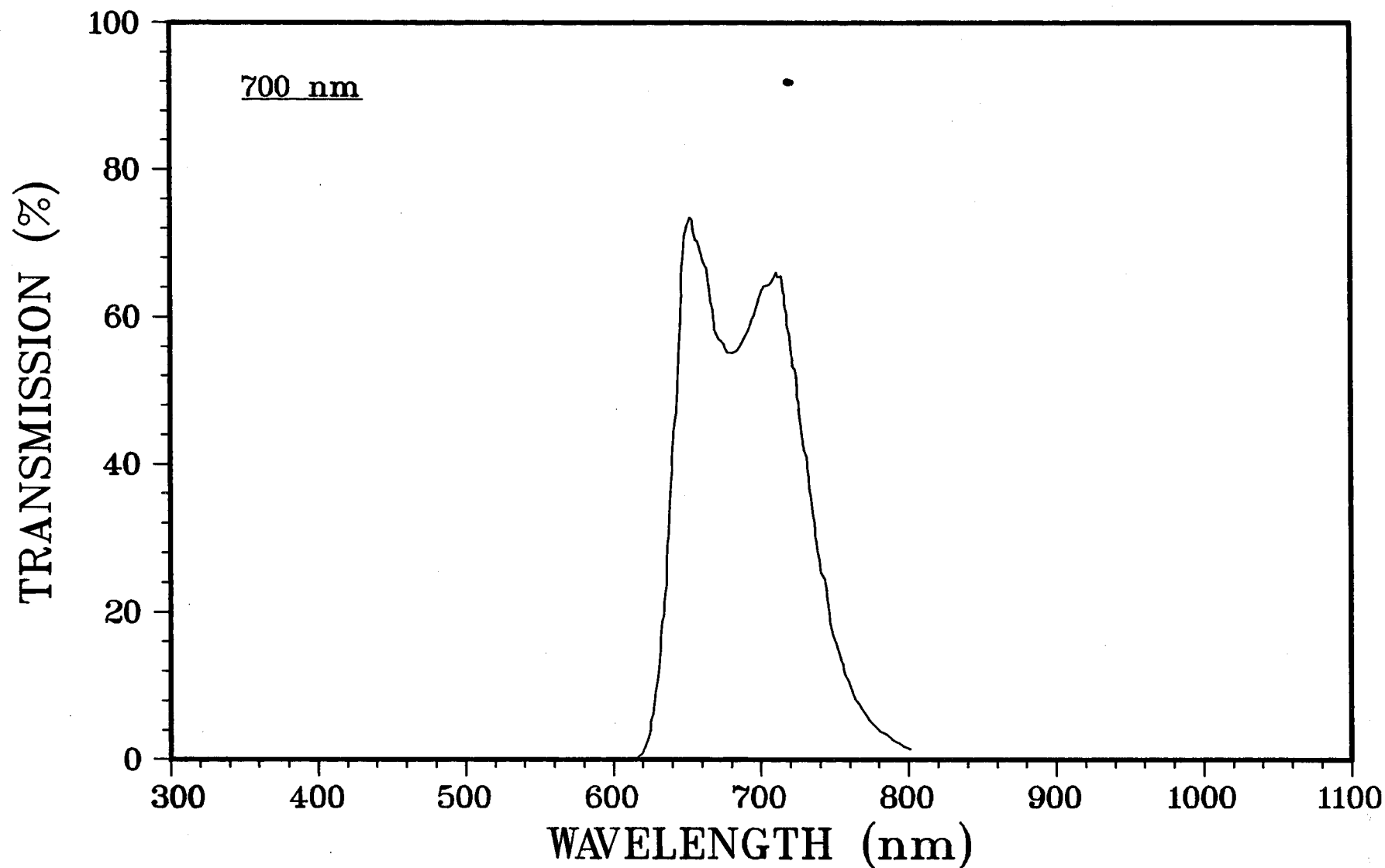


Figure 79. Cary 14 Spectrometer Trace Showing the Spectral Bandwidth of the 700 nm Filter.

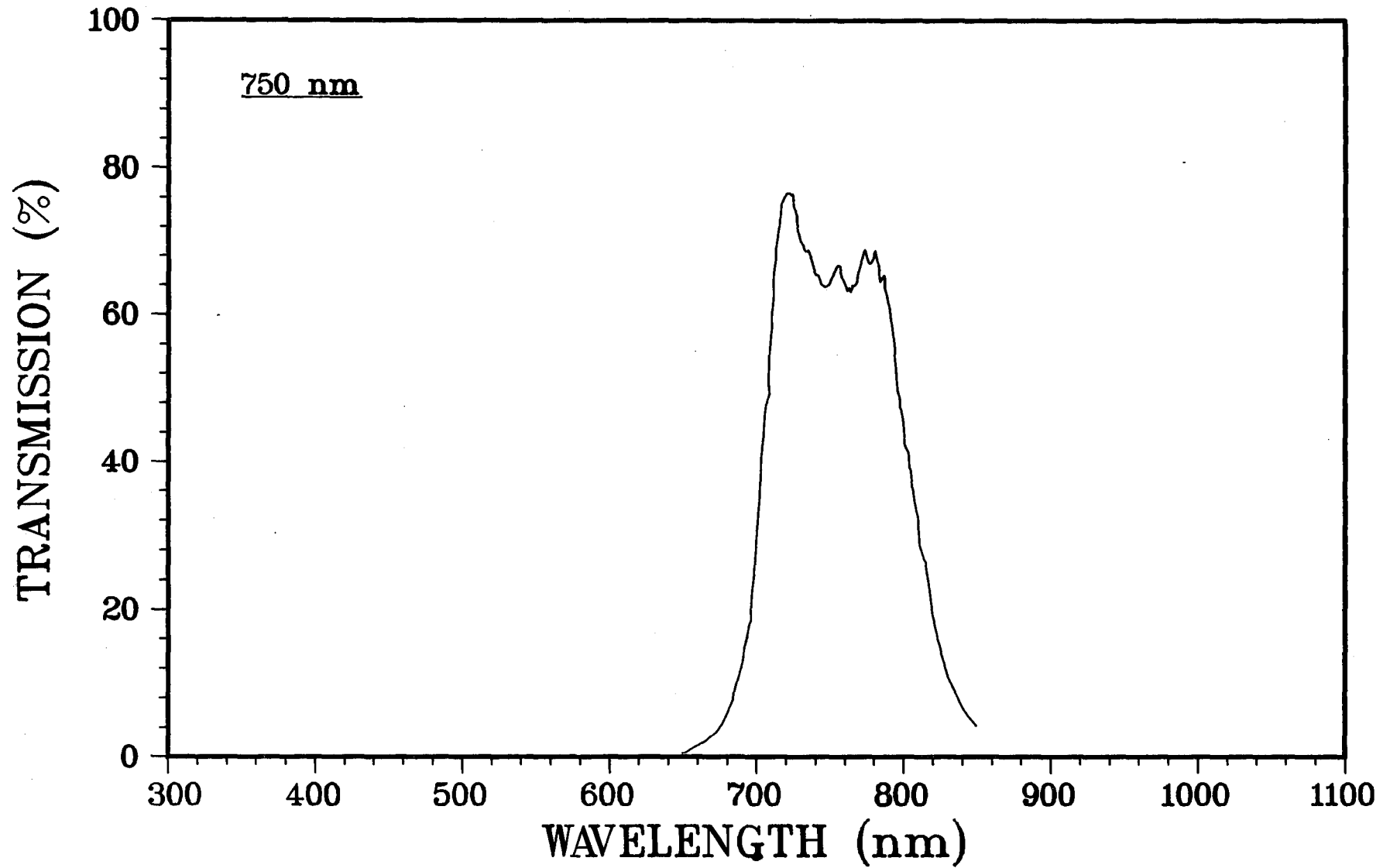


Figure 80. Cary 14 Spectrometer Trace Showing the Spectral Bandwidth of the 750 nm Filter

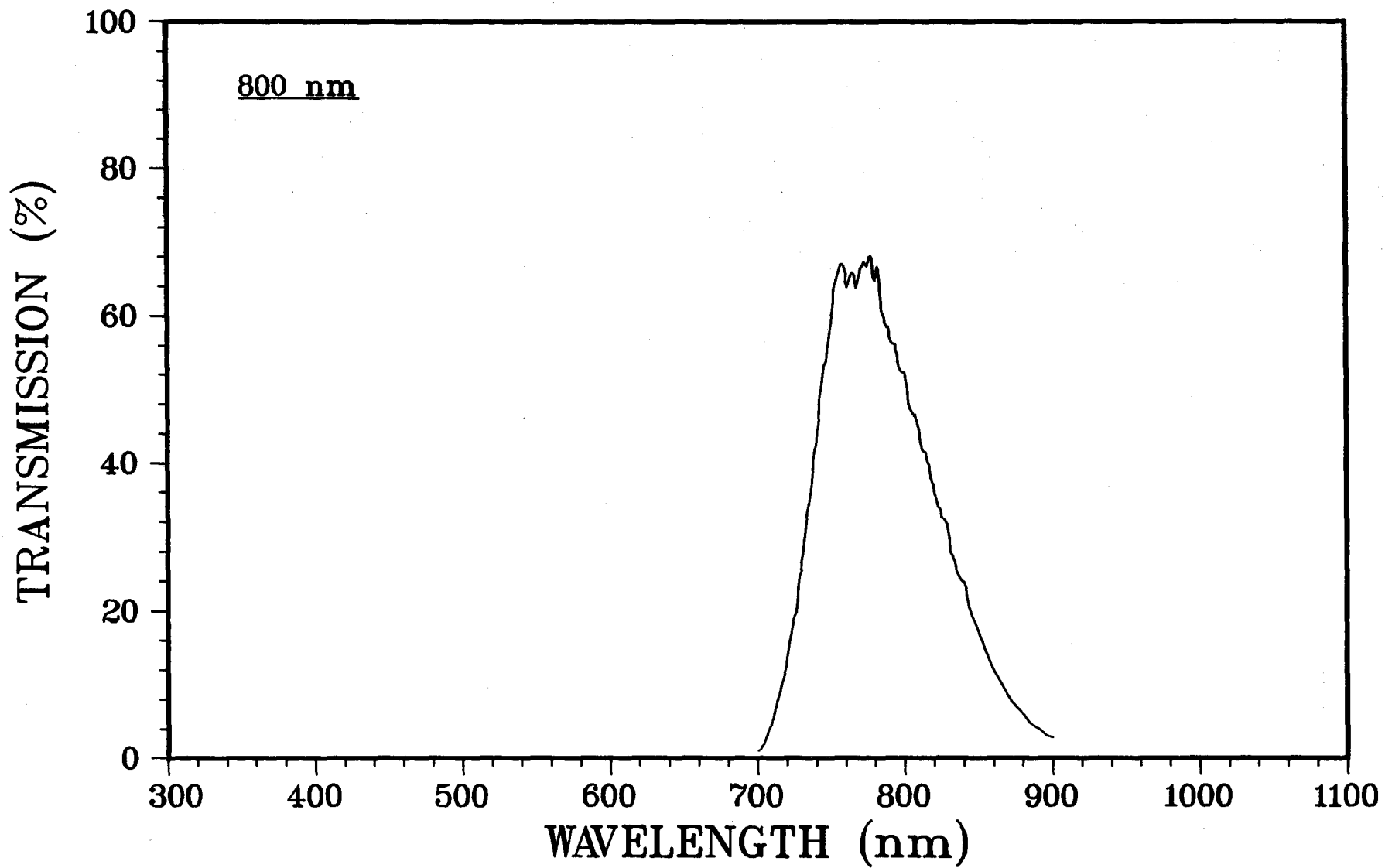


Figure 81. Cary 14 Spectrometer Trace Showing the Spectral Bandwidth of the 800 nm Filter

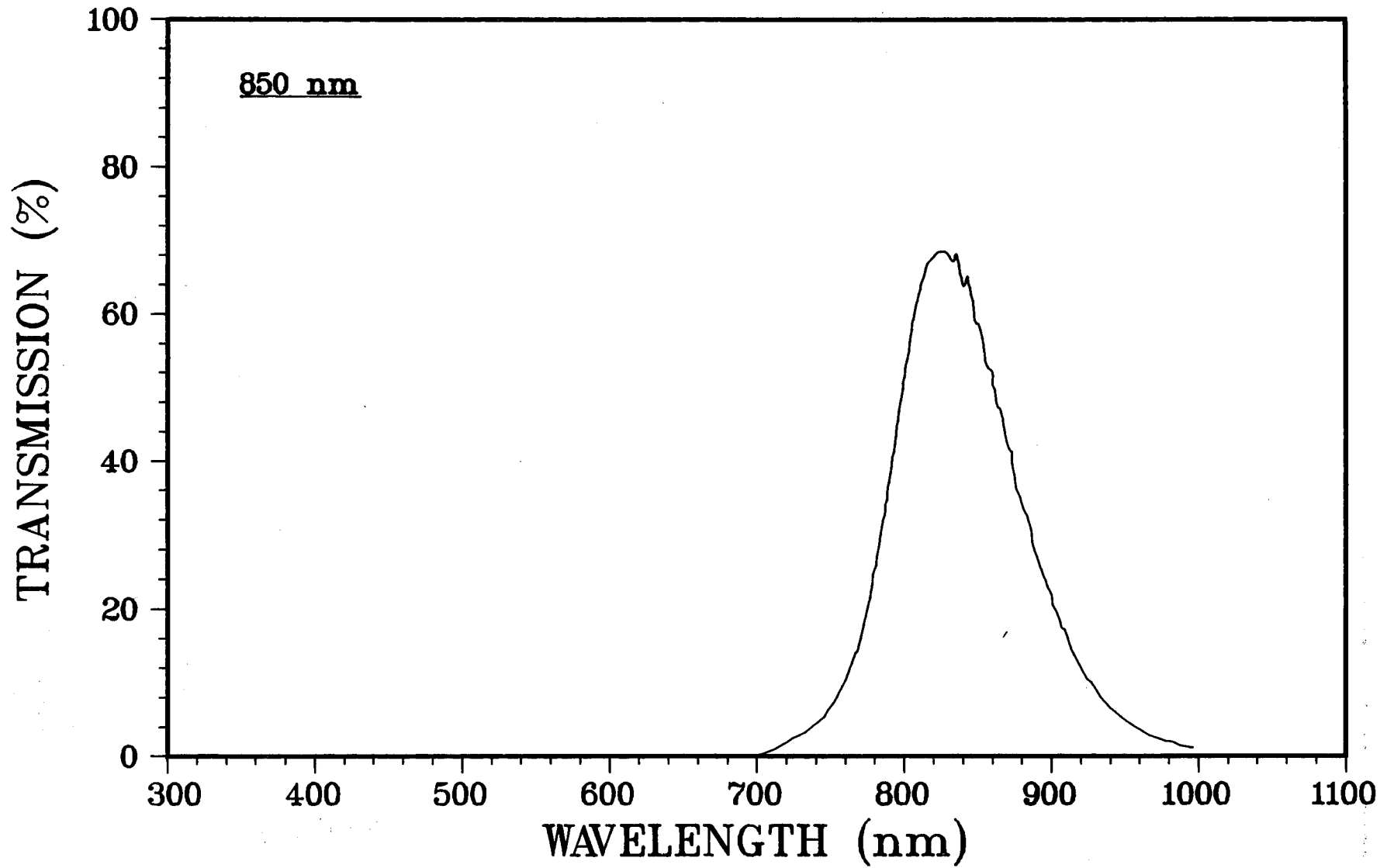


Figure 82. Cary 14 Spectrometer Trace Showing the Spectral Bandwidth of the 850 nm Filter

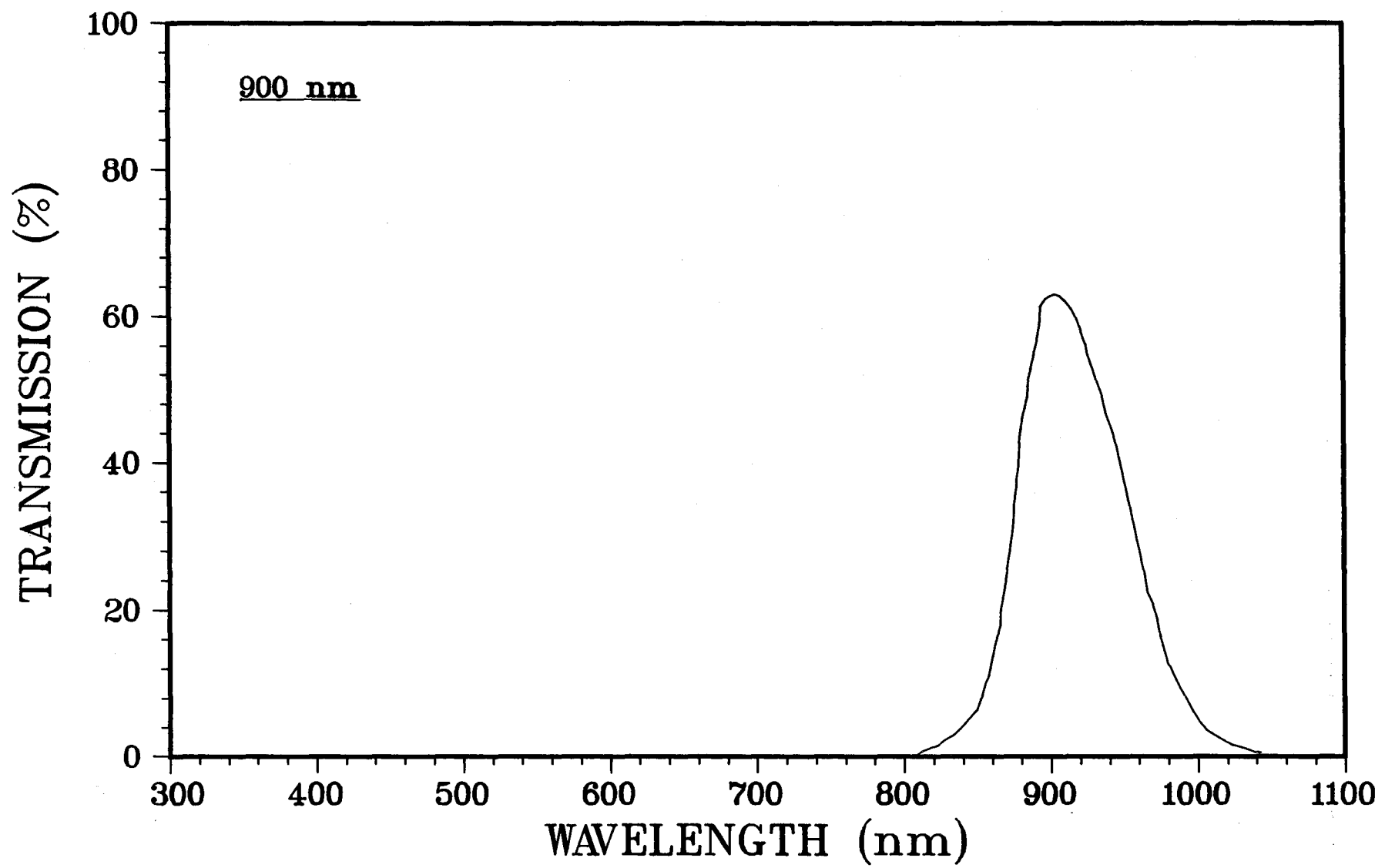


Figure 83. Cary 14 Spectrometer Trace Showing the Spectral Bandwidth of the 900 nm Filter

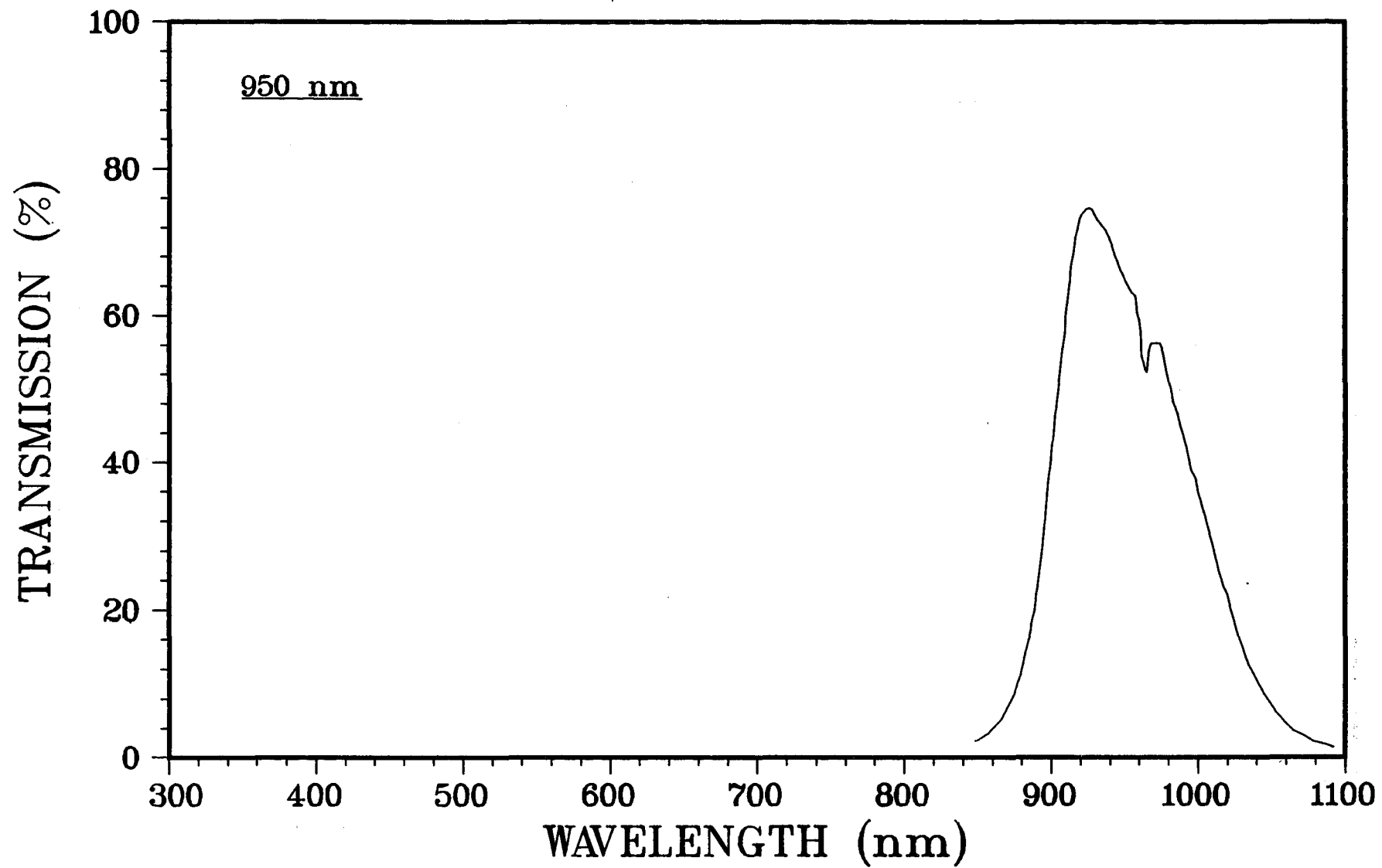


Figure 84. Cary 14 Spectrometer Trace Showing the Spectral Bandwidth of the 950 nm Filter

REFERENCES

1. P. L. Mattern, L. M. Watkins, C. D. Skoog, J. R. Brandon, and E. H. Barsis, IEEE Trans. on Nuclear Science NS-21, 81 (1974); P. L. Mattern, SLL-73-0207, Sandia Laboratories, Livermore, October 1974.
2. P. L. Mattern, L. M. Watkins, C. D. Skoog, and E. H. Barsis, IEEE Trans. on Nuclear Science NS-22, 6 (1975).
3. L. M. Watkins, Absorption Induced in Fiber Waveguides by Low Dose-Rate Electron and Gamma-Ray Radiation, SAND75-8222, Sandia Laboratories, Livermore, March 1975.
4. L. M. Watkins and E. H. Barsis, Absorption Induced in Glass and Plastic Fibers by 14 MeV Neutrons, SAND75-8714, Sandia Laboratories, June 1976.
5. B. D. Evans and G. H. Sigel, Jr., IEEE Trans. on Nuclear Science NS-21, 113 (1974).
6. Stefan J. Rzed, Pierre P. Infelta, John M. Warman, and Robert H. Schuler, J. Chem. Phys. 52, 3971 (1970), and references therein.
7. See, e.g., G. C. Abell, A. Mozumder, and J. L. Magee, J. Chem. Phys. 56, 5422 (1972), and references therein.
8. Aaron Barkatt, Michael Ottolenghi, and Joseph Rabani, J. Chem. Phys. 77, 2857 (1973), and Aaron Barkatt, Michael Ottolenghi, and Joseph Rabani, J. Phys. Chem. 76, 203 (1973).
9. I. A. Taub and H. A. Gillis, J. Am. Chem. Soc. 91, 6507 (1969), Chem. Phys. Lett. 22, 180 (1973).
10. John R. Miller, J. Chem. Phys. 56, 5173 (1972), and John R. Miller, Chem. Phys. Lett. 22, 180 (1973).
11. M. Shuttleworth, private communication.

12. P. L. Mattern, C. D. Skoog, and E. H. Barsis, "Recombination Processes in Pulse Irradiated Glass Waveguides, " to be published.
13. J. R. Brandon, C. D. Skoog, P. L. Mattern, and E. H. Barsis, "The Effects of Scavenging on the Recovery Kinetics of Pulse Irradiated Plastic Waveguides, " to be published.

UNLIMITED RELEASE

INITIAL DISTRIBUTION:

Aerospace Corporation
P. O. Box 92957
Los Angeles, CA 90009
Attn: I. Garfunkel
V. Josephson
A. W. Merrill
J. Pitre
P. Stadler
H. M. Stoll
W. Willis

Aerospatiage
78 Les France
Attn: J. Maneurier

Advanced Research Projects Agency
1400 Wilson Boulevard
Arlington, VA 22209
Attn: R. G. Cook
C. M. Stickley

Air Force Avionics Laboratory
Wright-Patterson Air Force Base
Dayton, OH 45433
Attn: M. C. Hamilton
K. R. Hutchinson
K. Trumble

Air Force Cambridge Research Lab
L. G. Hanscom Field
Bedford, MA 01730
Attn: E. A. Burke
J. Silverman
J. A. Wall

Air Logistics Corporation
3600 E. Foothills Boulevard
Pasadena, CA 91109
Attn: K. M. Stiles

Air Force Materials Laboratory
AFML/LPC
Wright-Patterson Air Force Base
Dayton, OH 45433
Attn: R. Rondeau

Air Force Materials Laboratory
AFML/LPL
Wright-Patterson Air Force Base
Dayton, OH 45433
Attn: J. R. Fenter

Air Force Systems Command
Andrews Air Force Base
Washington, D. C. 20331
Attn: Maj. D. C. Luke
Maj. R. Smith, DLCA
Col. Portasyk, DLCAW

Air Force Weapons Laboratory
Kirtland Air Force Base
New Mexico 87117
Attn: Lt. K. J. Soda/ELP (15)
Capt. W. L. Stein/ELC
D. C. Wunsch

American Optical Company
Southbridge, MA 01550
Attn: V. Canty
R. L. Shaw

American University of Cairo
Cairo, EGYPT
Attn: A. Bishay

Ames Research Center
Moffett Field, CA 94035
Attn: W. D. Gunter, Jr.

Argonne National Laboratory
9700 S. Cass Avenue
Argonne, IL 60439

Army Communications Command
Fort Hauchuca, AZ 85613
Attn: Capt. L. L. Chitester
M. E. Nick

Army Electronics Command
Technical & Industrial Liaison
Fort Monmouth, NJ 07703
Attn: J. F. X. Mannix
Chief/AMSEL-RD-S

Army Electronic Command
Fort Monmouth, NJ 07703
Attn: R. G. Buser
L. Dworkin
E. J. Schiel
S. Kronenberg, AMSEL-TL-EN

Army Research Office
Box CM, Duke Station
Durham, NC 27706
Attn: M. Cliftan

AWRE, MOD (PE)
Aldermaston, Reading
ENGLAND
Attn: A. J. Smith

Battelle Columbus Laboratories
505 King Avenue
Columbus, OH 43201
Attn: C. M. Verber

Battelle Memorial Institute
965 Harbor Scenic Way
Long Beach, CA 90802
Attn: F. G. White

Bausch & Lomb
820 Linden Avenue
Rochester, NY 14625
Attn: R. Hensler
W. Ribca

BDM Corporation
2600 Yale, SE
Albuquerque, NM 87106
Attn: C. R. Jenkins

Bell Telephone Laboratories
Murray Hill, NJ
Attn: L. Blyler
W. G. French
R. E. Jaeger
C. R. Kurkjian
J. B. MacChesney
S. E. Miller
A. D. Pearson
G. E. Peterson
M. Rigterink
J. C. Williams

Boeing Company
Electronics Systems Division
P. O. Box 3999, MS 79-68
Seattle, WA 98124
Attn: W. Fields

Boeing Company
Org. 2-5320
P. O. Box 3999, MS 2R-00
Seattle, WA 98124
Attn: A. R. Lowrey
R. S. Caldwell

Boeing Company
12618 S. E. 51st Place
Bellevue, WA 98006
Attn: R. Brown

Booz-Allen
106 Apple Street
New Shrewsbury, NJ 07724
Attn: W. Jarva

British Embassy
3100 Massachusetts Avenue, NW
Washington, D. C.
Attn: D. J. Garrad, c/o ACO(W)

Brookhaven National Laboratory
Upton, NY 11973
Attn: P. W. Levy
K. J. Swyler

California Institute of Technology
Electrical Engineering Department
645 Hill Street
Pasadena, CA 91106
Attn: A. Yariv

California Institute of Technology
Jet Propulsion Laboratory
4800 Oak Grove Drive
Pasadena, CA 91103
Attn: R. V. Powell

Carnegie-Mellon University
Forbes Avenue
Pittsburg, PA 15213
Attn: C. S. Tsai

Catholic University of America
Vitreous State Laboratory
Washington, D. C. 20017
Attn: P. B. Macedo

Central Intelligence Agency
11628 Vintage Hill Road
Reston, VA 22090
Attn: L. L. Campbell

Central Intelligence Agency
Washington, D. C. 20505
Attn: A. A. Padgett

Certification Department
Z Avenue E.,
Toulouse, FRANCE
Attn: J. Bourrieau

Collins Radio
1200 N. Alma
Richardson, TX 75081
Attn: R. Hass, MS 401-125

Collins Radio Company
Dallas, TX 75207
Attn: S. L. Quilici

Corning Glass Works
Corning, NY 14830
Attn: B. W. Bielawski
R. D. Maurer
R. A. Miller
P. C. Schultz
F. L. Thiel

Defense Nuclear Agency
Washington, D. C. 20305
Attn: R. Davis
R. Pohl

Director of Defense Research
and Engineering
The Pentagon - Room 3E144
Washington, D. C. 20301
Attn: Capt. G. H. Smith
Lt. Col. Whittaker

Charles Stark Draper Labs
68 Albany Street
Cambridge, MA 02139
Attn: E. Sich
A. Stecyk

E-A Industries Corporation
4500 N. Shallonford Road
Camblee, GA
Attn: R. J. Jelley

EG&G
134 Robin Hill Road
Goleta, CA 93017
Attn: M. Nelson

EG&G
P. O. Box 204
San Ramon, CA
Attn: R. Zielonka

Electronic Systems Division
L. G. Hanscom Field
Bedford, MA 01730
Attn: Maj. A. Willoughby/ESD/XR

Electro-Optics Telecommunications
Arthur D. Little, Incorporated
Acorn Park
Cambridge, MA 02140
Attn: H. A. Elion

Fairchild Space & Defense Systems
301 Robbins Lane
Syosset, NY 11791
Attn: J. Koehler

Fiberoptic Cable Corporation
P. O. Box 1492
Framingham, MA 01701
Attn: Sheldon Glazer
Don Levine

Fleet Missile Systems Analysis and
Evaluation Group (FMSAEG)
Corona, CA 91720
Attn: J. B. Shannon

ECOM-AMSEL-TL-1R
Fort Monmouth, NJ 07703
Attn: E. T. Hunter

Flight Dynamics Laboratory
FDL/FGL
Wright-Patterson Air Force Base
Dayton, OH 45433
Attn: Dr. A. deThomas

E. I. Du Pont de Nemours & Company
Plastics Department
Experimental Station Laboratory
Wilmington, DE
Attn: A. MacLeod
H. M. Schleinitz
F. C. Wilson
F. M. Mannis

Galileo Electro-Optics Corporation
Galileo Park
Sturbridge, MA 01518
Attn: M. A. Archarekar
J. St. Clair

GE-SSO
Room 8301 - CE
P. O. Box 8661
Philadelphia, PA 19101

General Dynamics
MZ2654
P. O. Box 748
Ft. Worth, TX 76101
Attn: R. E. Fields

General Dynamics/Convair Aerospace
P. O. Box 80847, MZ 624-30
San Diego, CA 92138
Attn: J. A. Hughes
R. V. Weas

General Electric Company
1 River Road, Building 5
Schenectady, NY 12301
Attn: P. C. Bogiages

General Electric Company
Research & Development Center
P. O. Box 8
Schenectady, NY 12301
Attn: J. D. Kingsley

General Electric Company
P. O. Box 8555
Philadelphia, PA 19101
Attn: J. L. Andrews

General Electric Company
Electronic Systems Division
Farrel Road Plant, Building 1
Syracuse, NY 13201
Attn: J. F. Lomber

General Electric Company
Ordnance Department
100 Plastics Avenue
Pittsfield, MA 01201
Attn: J. Reidl, Rm. 2455A

Grumman Aerospace Corporation
Bethpage, NY 17714
Attn: W. H. Howard

GTE Sylvania Inc.
189 "B" Street
Needham, MA 01294
Attn: R. Chin

GTE Laboratories
40 Sylvan Road
Waltham, MA 02154
Attn: M. L. Dakss

Harry Diamond Laboratories
AMXDO-RCE
Washington, D. C. 20439
Attn: H. Eisen
A. Epstein

Harry Diamond Laboratories
2800 Powder Hill Road
Adelphi, MD
Attn: R. M. Gilbert, B-330
R. M. McCoskey
F. B. McClean
J. E. Tompkins
L. P. Randolph
G. A. Ausman

Harry Diamond Laboratories
AMXDO-RB
Department of the Army
Washington, D. C. 20438
Attn: E. E. Conrad

Hewlett-Packard Company
640 Page Mill Road
Palo Alto, CA 94304
Attn: R. J. Archer
P. Green
D. Hammond
D. Hanson

Hollander Associates
P. O. Box 2276
Fullerton, CA 92633
Attn: G. L. Hollander

Hughes Aircraft Company
Centinela & Teale Streets
Culver City, CA 90230
Attn: J. W. Winslow, 6/D133
Ken Waler, 6/D133

Hughes Research Laboratories
3011 Malibu Canyon Road
Malibu, CA 90265
Attn: M. K. Barnoski
V. Evthov
R. G. Hunsperger

IBH
Sonnestrassse 33
8 Munich 60
GERMANY
Attn: H. D. Bruemmer

IRT Corporation
P. O. Box 80817
San Diego, CA 92138
Attn: E. Bloom
A. H. Kalma
J. A. Naber
B. Passenheim
C. Porter
R. Stahl
D. P. Snowdon
W. D. Swift
M. J. Treadaway

ITT - Cable-Hydrospace Division
National City Marine Terminal
National City, CA 92050
Attn: M. A. Williams

ITT - Components Group Europe
Edinburgh Way
Harlow, Essex
ENGLAND
Attn: P. B. Page

ITT Defense Space Group
500 Washington Avenue
Nutley, NJ 07110
Attn: E. DeFaymoreau
F. L. Koved

John F. Kennedy Space Center
Kennedy Space Center, FL 32899
Attn: P. K. Burdine

Joint Tactical Communications Officw
Air Force Liaison Office
Fort Monmouth, NJ 07703
Attn: Lt. Col. Charles Benton

Los Alamos Scientific Laboratory
P. O. Box 1663
Los Alamos, NM 87545
Attn: Peter Lyons, MS410

Lockheed Electronics
U. S. Route 22
Plainfield, NJ 07061
Attn: A. Tarasevich, MS141

Lockheed Missiles & Space Company
P. O. Box 504
Sunnyvale, CA
Attn: H. T. Schneemann
Org. 84-12, Bldg. 565

LTV Aerospace Corporation
9314 W. Jefferson
Dallas, TX 75222
Attn: J. A. Hegg

Martin-Marietta Company
P. O. Box 5837, MP 413
Orlando, FL 32805
Attn: H. Cotes
H. T. Gates
M. Kerr, MP 417
J. Mavrides

Massachusetts Institute of Technology
Applied Physics Group
Lincoln Laboratory
P. O. Box 73
Lexington, MA 02173
Attn: I. Melingailis
G. E. Stillman

Maxwell Laboratories
9244 Balboa Avenue
San Diego, CA 92123
Attn: R. G. Robertson

McDonnell Aircraft Company
St. Louis Airport
St. Louis, MO 63166
Attn: G. Weinstock

Meret, Incorporated
1815 24th Street
Santa Monica, CA 90404
Attn: D. B. Medved

MITRE Corporation
Bedford, MA 01730
Attn: V. Sakalys
E. Boose

Mucletudes
27 Ter Rue de Progres
Montreal, FRANCE
Attn: J. Pigneret

National Academy of Engineering
Committee on Telecommunications
2101 Constitution Avenue, NW
Washington, D. C. 20418
Attn: R. V. Mrozinski

National Bureau of Standards
Washington, D. C.
Attn: D. G. Lewis, Bldg. 225
Rm. 346

National Security Agency
9800 Savage Road
Fort George G. Mead, MD 20755
Attn: C. L. Reese
A. L. Russo

Naval Air Systems Command
AIR 310B
Washington, D. C. 20361
Attn: J. Willis

NAV Inshore Warfare
Naval Air Base
Coronado, CA
Attn: Lt. R. C. Smith

Naval Electronics Laboratory Center
San Diego, CA 92152
Attn: D. J. Albares
J. Bryant
D. H. Marcus
D. J. Williams

Naval Electronic Systems Command
Code 3204
Washington, D. C. 20306
Attn: W. S. Kaminga

Deputy Chief of Naval Material
Washington, D. C. 20360
Attn: RADM F. C. Jones

Naval Research Laboratories
Washington, D. C. 20375
Attn: C. Klick
A. Schindler
G. Sigel
E. Zonker

Naval Surface Weapons Center
132-209
White Oak, MD 20910
Attn: R. J. Sanford

Naval Undersea Center
P. O. Box -97
Kailua, Hawaii 96734
Attn: R. L. Remick

Naval Underwater Systems Center
New London, CT 06320
Attn: F. Allard

Naval Weapons Center
Code 6015
China Lake, CA 93555
Attn: L. D. Hutcheson

NBS
Tech. Building B356
Washington, D. C.
Attn: K. F. Galloway

Nissho-Iwai American Corporation
120 Montgomery Street
San Francisco, CA
Attn: M. Ohtake

HQ NORAD DCS/Intelligence
Ent Air Force Base
Colorado Springs, CO 80912
Attn: G. W. Schmidt

Northern Electric Company
150 Montreal-Toronto Blvd.
Lachine, PQ
CANADA
Attn: R. Iyengar

Northrop Corporation
1 Research Park
Palos Verdes Peninsula, CA 90274
Attn: H. Q. North

Northrop Corporation
3401 W. Broadway Avenue
Hawthorne, CA 90250
Attn: K. Chin

Oak Ridge National Laboratories
Oak Ridge, TN 37830
Attn: E. Sonder
R. Weeks

Office of Naval Research
Branch Office
1030 E. Green Street
Pasadena, CA 91106
Attn: R. E. Behringer

Oklahoma State University
Stillwater, OK
Attn: W. A. Sibley

Opto-Logic Corporation
3450 E. Spring Street
Long Beach, CA 90806
Attn: R. O. Jackson

Owens-Illinois, Inc.
Advanced Displays and Optics
P. O. Box 1035
Toledo, OH 43666
Attn: E. A. Oster, R&D Director

Pacific Sierra Research Corporation
1456 Cloverfield Blvd.
Santa Monica, CA 90404
Attn: A. R. Shapiro

Philco Ford
3939 Fabian Way
Palo Alto, CA 94303
Attn: R. Chapman

Poly-Optics Inc.
1815 East Carnegie
Santa Ana, CA 92705
Attn: A. C. Menadier

RCA Astro-Electronics
P. O. Box 800
Princeton, NJ 08540
Attn: L. Hellzeg
H. Kressei
D. Longcoy
R. O'Hanian
C. Staloff

Radiation, Inc.
Electronic Systems Division
P. O. Box 37
Melbourne, FL 32904

Rand Corporation
1700 Main Street
Santa Monica, CA 90406

Rank Precision Industries
411 Jarvis Avenue
Des Plaines, IL 60018
Attn: J. Reinhard
P. Stuart

R&D Associates
P. O. Box 9695
Marina Del Rey, CA 90291
Attn: R. Graham
S. C. Rogers
P. Schaefer

Rensselaer Polytechnical Institute
School of Engineering
Materials Dept.
Troy, NY 12181
Attn: R. H. Doremus

Rockwell International
Science Center
Thousand Oaks, CA 91301
Attn: F. Scholl

Rockwell International
Mail BB 35
L. A. International Airport
Los Angeles, CA 90009
Attn: E. Dahlke
W. L. Jackson, BB18

Rome Air Development Center
Code DCCW
Griffiss Air Force Base
Rome, NY 13441
Attn: A. E. Clough

SAI
P. O. Box 1458
Colorado Springs, CO 80901
Attn: O. Lopez

Schott Optical Glass
York Avenue
Duryea, PA 18642
Attn: J. Nimmerfroh

Science Application, Inc.
P. O. Box 2351
LaJolla, CA 92037
Attn: J. Leave

Space & Missile Systems
P. O. Box 92960
Worldway Postal Center
Los Angeles, CA 90009
Attn: Maj. C. Jund/DYGM
Lt. E. Landry, DYS
Lt. Col. Kennedy
Capt. J. Tucker

Spectronics, Inc.
830 E. Arapaho Road
Richardson, TX 75080
Attn: J. R. Baird

Sperry Research Center
100 North Road
Sudbury, MA 01776
Attn: R. A. Soref

Sperry Univac, M.S. 5293
P. O. Box 3525
St. Paul, MN 55165
Attn: M. S. Bergman

Stanford Research Institute
333 Ravenswood Avenue
Menlo Park, CA 84025
Attn: R. C. Adamo
H. E. Clifford
N. M. Johnson
D. Parker

State University of New York
Stonybrook, NY 11790
Attn: F. Y. Wang

Statham Instruments, Inc.
2230 Statham Blvd.
Oxnard, CA 93030
Attn: G. A. Raabe

Telecom, Inc.
2635 State Street, Suite 212
Las Vegas, NV
Attn: R. MacQuarrie

Tetra Tech, Inc.
3559 Kenyon Street
San Diego, CA 92110
Attn: R. C. Robinson

Texas Instruments, Inc.
P. O. Box 5936, M.S. 118
Dallas, TX 75222
Attn: F. A. Blum

TRW Systems Group
One Space Park
Redondo Beach, CA 90278
Attn: H. R. Huertas
F. Ridolphi
J. Z. Wilcox
A. A. Wiheles

U. S. Department of Commerce
OT/ITS, Boulder Laboratories
Boulder, CO 80302
Attn: R. L. Gallawa

U. S. Naval Avionics Facility
Code D813
5000 East 21st Street
Indianapolis, IN 46218
Attn: R. S. Katz

University of California
School of Engineering & Applied Science
Electrical Sciences & Engineering Dept.
Los Angeles, CA 90024
Attn: C. Yeh

University of California
Lawrence Livermore Laboratory
P. O. Box 808
Livermore, CA 94550
Attn: R. H. Barlett, L-24
G. A. Clough, L-525
A. Glass, L-547
F. K. Inami, L-151
H. Koehler, L-525
L. C. Loquist, L-154
W. J. Richards, L-540
R. A. Van Konyneburg, L-233
M. J. Weber, L-547

University of California
La Jolla, CA 92037
Attn: S. Lee

University of Illinois
Coordinates Science Lab
Urbana, IL 61801
Attn: W. D. Compton

University of North Carolina
Physics Department
Chapel Hill, NC 27514
Attn: J. H. Crawford, Jr.

University of Missouri
203 MRC
Rolla, MO 65401
Attn: C. A. Goben

University of Utah
Phys. Mechanical Engineering Dept.
Salt Lake City, UT
Attn: A. Sosin

University of Washington
Ceramic Engineering FB-10
Seattle, WA 98195
Attn: W. D. Scott

Valtec Fiberoptics
99 Hartwell Street
W. Boylston, MA 01583
Attn: Richard Cerny
Marshall C. Hudson

J. D. Kennedy, 1110; Attn: J. D. Plimpton, 1112
J. L. Benson, 1115
J. W. Wistor, 1116

G. E. Hansche, 1120

W. L. Stevens, 1230; Attn: S. D. Spray, 1232

J. W. Puariea, 1247

O. E. Jones, 1700

W. C. Myre, 1730

D. D. Robie, 2135

J. C. King, 2500

O. M. Stuetzer, 2540

R. L. Peurifoy, 4300

J. K. Galt, 5100; Attn: E. P. EerNisse, 5133

A. W. Snyder, 5400; Attn: J. V. Walker, 5420

J. G. Kelly, 5423

J. R. Brandon, 5442

R. G. Kepler, 5810; Attn: L. A. Harrah, 5811

R. C. Hughes, 5814

T. B. Cook, Jr., 8000; Attn: C. H. DeSelm, 8200

W. C. Scrivner, 8400

L. Gutierrez, 8100; Attn: A. N. Blackwell, 8110

W. E. Alzheimer, 8120

D. E. Gregson, 8150

R. D. Cozine, 8160

D. N. Tanner, 8159

L. M. Watkins, 8159

C. S. Selvage, 8180; Attn: R. J. Tockey, 8181

B. F. Murphey, 8300; Attn: D. B. Schuster, 8310

T. S. Gold, 8320

G. W. Anderson, Jr., 8330

J. F. Barham, 8360

R. L. Rinne, 8321; Attn: S. C. Keeton

P. L. Mattern, 8321
W. Bauer, 8334
J. Vitko, 8334
J. L. Wirth, 8340
W. D. Wilson, 8341
E. H. Barsis, 8342 (50)
C. M. Hartwig, 8342
R. W. Schmieder, 8342
C. D. Skoog, 8342 (25)
A. R. Willis, 8344
F. J. Murar, 8345
O. H. Schreiber, 8346
R. C. Wayne, 8365
R. A. Bice, 9000
M. Cowan, Jr., 9320
F. W. Neilson, 9350
Technical Publications and Art Division, 8265, for TIC (27)
F. J. Cupps, 8265/Technical Library Processes Division, 3141
Technical Library Processes Division, 3141 (2)
Library and Security Classification Division, 8266 (3)